AN INVESTIGATION OF THE RELATIONSHIP BETWEEN LOW CLOUD COVER AND LOWER TROPOSPHERIC STABILITY USING MISR

BY

BETHANY N. NORRIS

THESIS

Submitted in partial fulfillment of the requirements
for the degree of Master of Science in Atmospheric Sciences
in the Graduate College of the
University of Illinois at Urbana-Champaign, 2012

Urbana, Illinois

Adviser:

Professor Larry Di Girolamo

ABSTRACT

Marine boundary layer clouds account for a significant amount of uncertainty in future climate change projections from general circulation models (GCMs). To reduce the uncertainty of the role of clouds in GCMs, improved cloud parameterizations and evaluations of these parameterizations are often sought using satellite data. Several studies have shown that marine stratus cloud fraction is strongly correlated with stability of the lower troposphere. These results are verified using data from the Multiangle Imaging Spectroradiometer (MISR). The MISR data allow for improved cloud top height and cloud cover retrievals for low clouds compared to all other passive sensors. From MISR daily data, two-dimensional histograms of cloud fraction and cloud top height at 500 m vertical resolution are explored for the first time. The daily data are also used to study cloud fraction on sub-monthly time scales in order to better understand the processes affecting cloud cover on the order of days.

Average values of stability and low cloud fraction are compared at varying time scales to determine if known seasonal correlation holds for shorter time scales; as in previous work, no significant correlation was shown to exist on daily time scales based on an Eulerian view. To elucidate why this lack of correlation exists at shorter time scales, a Lagrangian view was examined by performing back trajectory analyses to determine if any time lag-correlation exists between the stability of the marine boundary layer and the cloud fraction at a given point for time lags up to 72 hours – no significant correlation was found. Using the MISR data, seasonal mean cloud fraction and various measures of stability had correlation coefficients on the order of 0.6 to 0.7. At monthly timescales, correlation coefficients are in the 0.7 to 0.8 range. At daily timescales, however, the correlation coefficients are nearly zero. The monthly analysis is also extended beyond marine stratus regions to other marine regions with low clouds, revealing areas of good correlation between low cloud and lower tropospheric stability where it was not expected, such as over the Gulf Stream in the western North Atlantic and east of China in the North Pacific. These results can then be compared with results from model-simulated

cloud cover and stability to evaluate and improve model parameterizations of cloud cover on a global scale.

ACKNOWLEDGMENTS

I would like to thank my advisor, Dr. Larry Di Girolamo, for his support and guidance as I undertook this project. I am grateful for his patience as I adjusted to the life and schedule of a graduate student. I would also like to acknowledge Dr. Guangyu Zhao for his invaluable assistance with the programming aspect of my research. This research was partially supported by a grant from the Jet Propulsion Laboratory (JPL) of the California Institute of Technology under contract 1260125. NCEP reanalysis data were obtained from the National Oceanic and Atmospheric Administration's Earth System Research Laboratory.

I would like to thank all the Department of Atmospheric Sciences graduate students for providing much needed moral support, camaraderie, and the occasional prank over the last two years. I would not be where I am today without them. A special thank you to all my family and friends, particularly Herb and Debbie Norris, Tyler Neyens, Tom Sturtevant, and Sarah Shannon, for their support and for providing me with a place to stay whenever I wanted to escape Champaign-Urbana.

TABLE OF CONTENTS

1. Introduction

1.1 Climatological Background

1.1.1 Marine Stratus Clouds and Climate

Clouds play an important role in the earth's energy balance. They can scatter incoming solar radiation so that less of it reaches the surface. Due to their colder temperatures relative to the surface, they also emit less thermal radiation than the surface. Low, optically thick clouds make a strong contribution to the planetary albedo (Manabe and Wetherald 1967); because they are close to the surface, there is little thermal difference between the clouds and the surface, so they do not have a significant effect on outgoing thermal radiation. Hartmann et al. (1992) estimate that these low clouds have a net cloud radiative forcing of about 15 W m^{-2}. Because of the substantial impacts of these clouds to the hydrologic and energy cycles at the surface, it is important to understand their formation as well as their spatial and temporal variability. These low, optically thick clouds can either be stratiform (common in the marine subtropics) or cumuliform (common in the trade wind regions). Due to their large horizontal extent, the marine stratiform clouds have a larger impact on the global radiation budget than the smaller trade wind cumulus.

Marine stratiform clouds typically form in the eastern subtropical oceans in the descending branch of the Hadley cell. A typical marine stratus deck off the coast of Southern California is shown in Figure 1.1. In the Hadley cell, air near the surface flows equatorward toward the Intertropical Convergence Zone (ITCZ). When the air converges at the ITCZ, it rises and moves poleward, where it eventually begins to subside to complete the circulation. As this air subsides, it warms, forming a thermal inversion in the lowest few kilometers of the troposphere (Klein 1997). In the marine boundary layer, uniformly cool sea surface temperatures (SSTs) create a cool, moist boundary layer. Since the boundary layer is effectively capped by the subsidence inversion, it continues to moisten through turbulent mixing until it becomes saturated. A schematic of this process is shown in Figure 1.2. Once

these marine stratus clouds form, they can cover thousands of square kilometers of the subtropical oceans. Because the marine boundary layer tends to be shallow (generally 4 km deep or less, but varies between regions), the vertical extent of marine stratus clouds is quite limited (Lin et al. 2009). Klein (1997) showed that for a marine stratus region in the Northwest Pacific, the subsidence inversion is located between 800 and 900 mb, i.e. the lowest few kilometers of the troposphere.

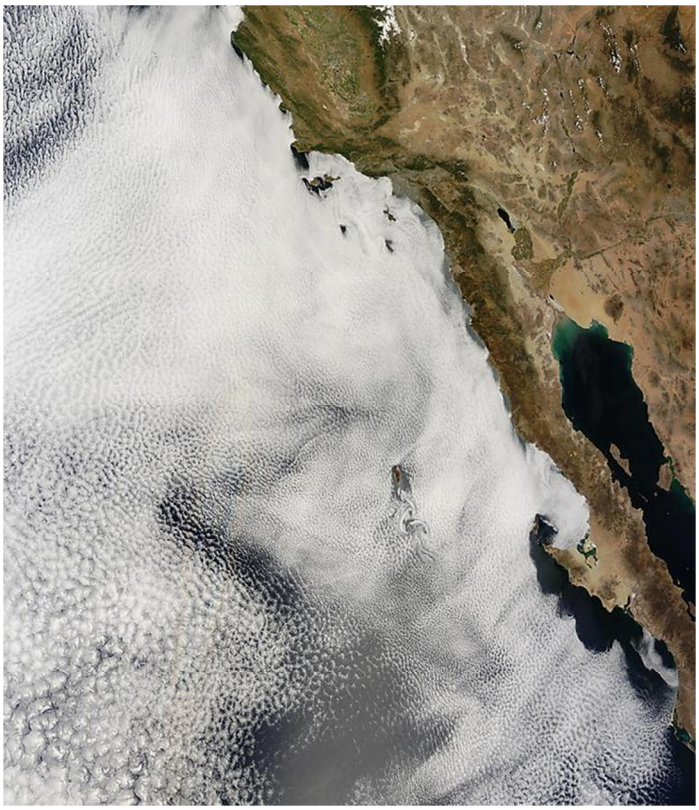

Figure 1.1: Marine stratiform clouds off the coast of southern California and Baja California. From MODIS Today (http://ge.ssec.wisc.edu/modis-today/), June 14, 2010.

In order to simulate past, present, and future climate states, clouds must be accurately accounted for in climate models (IPCC 2007). Due to computational expense and size relative to current general circulation model (GCM) grids, however, clouds are parameterized rather than explicitly modeled. Figure 1.3 shows zonal mean cloud cover as simulated by ten different GCMs from Zhang et al

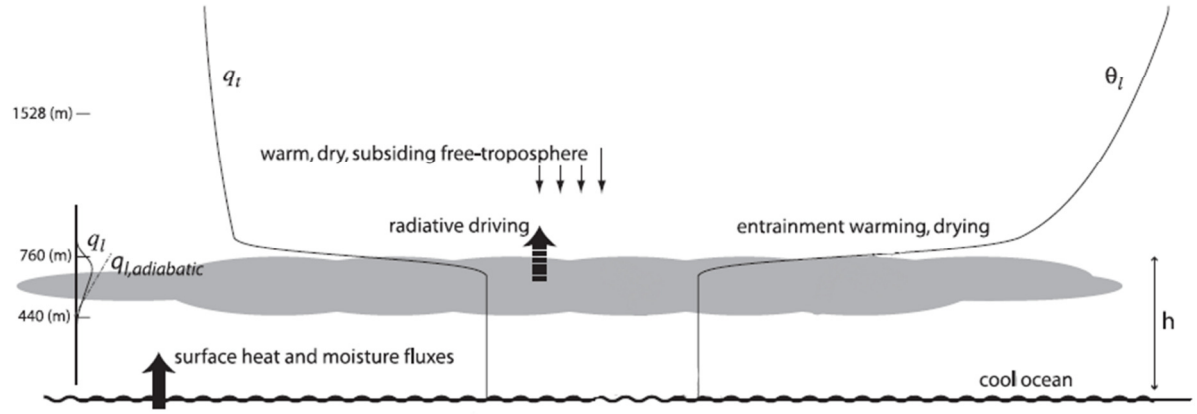

Figure 1.2: Schematic of a typical marine stratus deck. Temperature and humidity remain fairly constant throughout the well-mixed marine boundary layer. Above the MBL, the subsiding air is warm and dry, in contrast with the cool ocean surface. Adapted from Stevens et al. (2007).

(2005). The results from the various models frequently differ by 20% or more; model-generated cloud cover, then, is highly uncertain. In fact, clouds are one of the largest sources of uncertainty in climate models (IPCC 2007), and marine boundary layer clouds account for much of the uncertainty in tropical cloud radiative feedbacks (Bony and Dufresne 2005).

To improve model treatment of clouds, both parameterizations of cloud cover and evaluation of model results must be improved. This study seeks to improve the evaluation of model cloud cover using data from the Multiangle Imaging SpectroRadiometer (MISR) instrument on NASA's Terra platform as well as reanalysis data from the National Centers for Environmental Prediction/National Center for Atmospheric Research (NCEP/NCAR; Kalnay et al. 1996). This goal will be accomplished by investigating the relationship between low cloud cover and lower tropospheric stability (LTS); LTS is a good predictor of marine stratiform cloud cover on the seasonal and interannual time scales (Klein and Hartmann 1993, hereafter KH93). Statistics on cloud cover in marine stratiform regions using MISR's unique cloud top height retrieval algorithm will be presented. The dependence of the stability-low cloud cover relationship on temporal resolution will be assessed. The combination of the reanalysis data with MISR's high resolution cloud top height detection will help elucidate the relationship between the

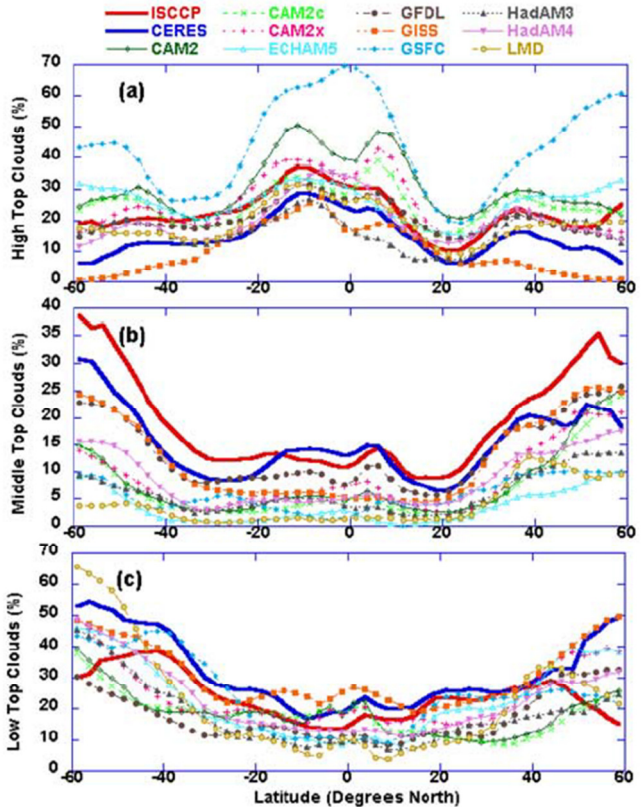

Figure 1.3: "(a) High top clouds, (b) middle top clouds, and (c) low top clouds in the DJF from satellite measurements and from the models. ISCCP data are from year 2000, CERES data are from two seasons of 2001 and 2002. Model results are from one year simulations with most of them forced with prescribed monthly sea-surface temperature of year 2000." From Zhang et al. (2005).

meteorological properties of the marine boundary layer and cloud coverage, as well as provide insight for other parts of the globe.

1.1.2 Influences on Marine Stratus Variability

With the goal of improving model cloud cover in mind, numerous studies have attempted to understand the causes of regional and seasonal variability in marine stratocumulus. One of the first such studies was undertaken by KH93, who used cloud data from the cloud atlas of Warren and Hahn

(2007), surface observations from the Comprehensive Ocean-Atmosphere Data Source (COADS; Woodruff et al. 1987), and upper-air observations from the European Center for Medium-Range Weather Forecasting (ECMWF). They found that for marine subtropical stratocumulus, the seasonal and interannual cycles of cloud amount and static stability are closely tied. Cloud amount was not well related to other factors, such as strength of the subtropical high (defined as the sea level pressure) or divergence of surface trade winds (KH93). The static stability, or lower tropospheric stability (LTS), is defined here as the inversion strength:

$$\mathrm{LTS} = \theta_{700\mathrm{hPa}} - \theta_{\mathrm{surface}} \tag{1.1}$$

where $\theta_{700\mathrm{hPa}}$ and $\theta_{\mathrm{surface}}$ are the potential temperatures at 700 hPa and the surface, respectively. The 700 hPa level was chosen because the inversion height varies from around 900 hPa in the poleward regions of the subtropics to around 750 hPa in the equatorward regions. A high LTS value represents a large difference between the surface and 700 hPa potential temperature, i.e. a more stable lower troposphere. Using seasonally averaged cloud cover and LTS for six different regions, stratocumulus cloud amount and LTS were found to be well correlated, with r = 0.94.

Building on KH93 results, Wood and Bretherton (2006, hereafter WB06) developed a new index of stability called the estimated inversion strength (EIS). EIS is calculated as

$$\mathrm{EIS} = \mathrm{LTS} - \Gamma_m^{850}(z_{700} - \mathrm{LCL}) \tag{1.2}$$

where LTS is the lower tropospheric stability, Γ_m^{850} is the moist adiabatic potential temperature gradient at 850 hPa, z_{700} is the height of the 700 hPa surface in meters, and LCL is the height of the lifting condensation level in meters. The EIS was developed as a more versatile alternative to LTS that appropriately characterizes stability in a wider range of temperatures and regions. Using this measure, EIS and low cloud fraction (again taken from the Warren and Hahn (2007) cloud atlas) were shown by WB06 to be strongly correlated, with an r value of 0.922 over the same regions as KH93.

Kubar et al. (2011) developed yet another measure of stability and its relationship to cloud cover using data from CloudSat, the Cloud-Aerosol Lidar and Infrared Pathfinder Satellite Observations (CALIPSO), and the Moderate Resolution Imaging Spectrometer (MODIS) on NASA's Terra satellite. The moist static energy (MSE) is defined as follows:

$$\text{MSE} = c_p T + gz + Lq \tag{1.3}$$

where c_p is the specific heat of air at constant pressure, L is the latent heat of vaporization at 0°C, and q is the mixing ratio of water vapor. The stability index, then is

$$\Delta\text{MSE} = \text{MSE}_{inv} - \text{MSE}_{sfc} \tag{1.4}$$

Here, MSE_{inv} is the moist static energy at 700 hPa, or at the midpoint of a low-level inversion below 700 hPa if the ECMWF data indicate that one is present. Like LTS and EIS, ΔMSE also correlates well with low cloud cover; for the CloudSat/CALIPSO cloud dataset, an r value of 0.938 was found (Kubar et al. 2011) over a transect of the North Pacific extending from the California coast to the deep convective regions of the tropics.

1.2 MISR

1.2.1 Instrument Overview

The large domains covered by marine stratus clouds make remote sensing from space an ideal way to study them. For this study, cloud fraction and cloud top height information will be taken from the MISR dataset. MISR is on NASA's Terra platform, a polar orbiter with a descending node equator crossing time of around 10:30 am LST. With a swath width of around 380 km, MISR is able to achieve global coverage in nine days. Details can be found in Diner et al. (1998).

MISR (shown in Figure 1.4) contains nine separate cameras, each at a different viewing angle. One camera points at nadir, four point in the along-track direction, and four point in the aft direction. Each camera contains four spectral channels centered at the following wavelengths: 446 nm (blue), 558

nm (green), 672 nm (red), and 866 nm (near infrared). The horizontal resolution of MISR varies from 250 m to 1100 m, depending on camera and spectral channel.

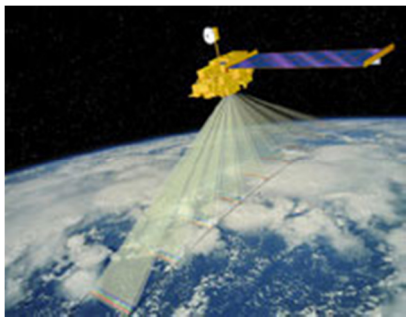

Figure 1.4: Computer generated image of MISR.
(http://www-misr.jpl.nasa.gov/Mission/)

Because of its multiple viewing angles, MISR can detect cloud top heights to within 562 m using a stereoscopic technique (Moroney et al. 2002). It takes about 7 minutes for each camera to view the same scene, during which time any clouds in the scene may have moved; as a result, a cloud motion correction is needed. MISR's stereoscopic technique, then, relies on high quality wind measurements to make this correction for cloud motion.

The advantage in using MISR for this study over other satellite datasets lies in its excellent ability to retrieve both cloud top height of marine stratocumulus (e.g. Garay et al. 2008; Harshvardhan et al. 2009) and their coverage (e.g. Zhao and Di Girolamo 2004).

1.2.2 The Cloud Fraction by Altitude Product

The MISR Cloud Fraction by Altitude (CFbA) product is a global, two-dimensional histogram of cloud fraction and cloud top height. For a full description of the product, see Di Girolamo et al. (2010). The CFbA product has a horizontal resolution of 0.5° by 0.5° latitude/longitude and a vertical resolution of 500 m.

Cloud fraction is reported for heights ranging from -500 m to 20 km. Cloud top heights are registered to the WGS84 ellipsoid (Di Girolamo et al. 2010), so it is possible to have negative heights if the surface is below the WGS84 ellipsoid value. Cloud fraction is also reported for height values less than -500 m, values greater than 20 km, and for the "no height retrieval" cases. The total cloud fraction is also included in the product. To reduce any potential systematic biases in the statistics due to pixels with no height retrieval, cloud top heights with the nearest neighbor algorithm applied are included as well.

Lack of a valid height retrieval can occur when the scene has very low contrast or highly variable wind conditions, since high quality wind measurements are needed to correct for cloud motion in the stereoscopic height retrieval technique. When this occurs, a nearest-neighbor algorithm is implemented in which the nearest pixel with a valid height retrieval within 200 km will be assigned to the pixel with the missing height. If not valid height retrieval within 200 km is found, the pixel is flagged as no retrieval, i.e. no cloud top height is assigned to that pixel.

Cloud fraction in the CFbA product is defined as the ratio of cloudy pixels to the total number of clear and cloudy pixels within a region. Over ice-free oceans, the CFbA cloud fraction is calculated using MISR's radiometric camera-by-camera cloud mask (RCCM). The RCCM is generated using radiometric information collected by each camera; thus, for a given scene, there are 9 RCCMs (Zhao and Di Girolamo 2004). The RCCM contains a glitter flag that indicates when a given pixel is likely to be contaminated by sun glitter. The CFbA processing algorithm starts with the nadir camera (designated An); if the An RCCM glitter flag indicates that the pixel is likely contaminated, it moves through the remaining cameras in order of increasing view angle until one is found that is not contaminated. Once a non-glint contaminated camera is found, that camera's RCCM is used as the cloud fraction input (Di Girolamo et al. 2010). The cloud fraction values are then normalized such that the total cloud fraction across all height bins is equal to the cloud fraction reported in the total cloud fraction bin.

2. CFbA Climatology

This chapter presents a cloud climatology using the MISR CFbA product. Here global, regional, and local climatologies are shown; the seasonal and interannual variations of cloud fraction and cloud top height in marine stratus regimes are explored. Lastly, cloud cover characteristics at a specific point in the Peruvian marine stratus regime are discussed in depth.

2.1. Global Climatology

Figure 2.1 shows a comparison of low (0-4 km cloud top height) to total cloud fraction from the CFbA product. Examining the northeastern Pacific marine stratus deck in JUN-AUG, the season of maximum low cloud fraction in this region, the low cloud cover and total cloud cover appear to be nearly identical. This would imply that very few middle or high clouds occur over this region during the Northern Hemisphere summer. The same is true for the southeastern Pacific in both JUN-AUG and SEP-NOV; the latter is the season in which the annual maximum low cloud fraction occurs in this region. The apparent lack of middle and high clouds in these regions, coinciding with the maximum in low cloud cover, could be due to an increase in subsidence; this could potentially cause the simultaneous increase in stability (since stronger subsidence enhances the temperature difference between the free troposphere and the boundary layer) and the associated increase in low cloud fraction.

2.2 Regional Climatology

Because of the high vertical resolution afforded by MISR, cloud cover features can be seen that, until now, were only visible using active spaceborne remote sensing instruments such as radars and lidars. Figure 2.2 shows cross sections of cloud fraction through the Northeast Pacific and Southeast Pacific stratus regions; in both cases, the coastline is near the right edge of the cross section. Note the

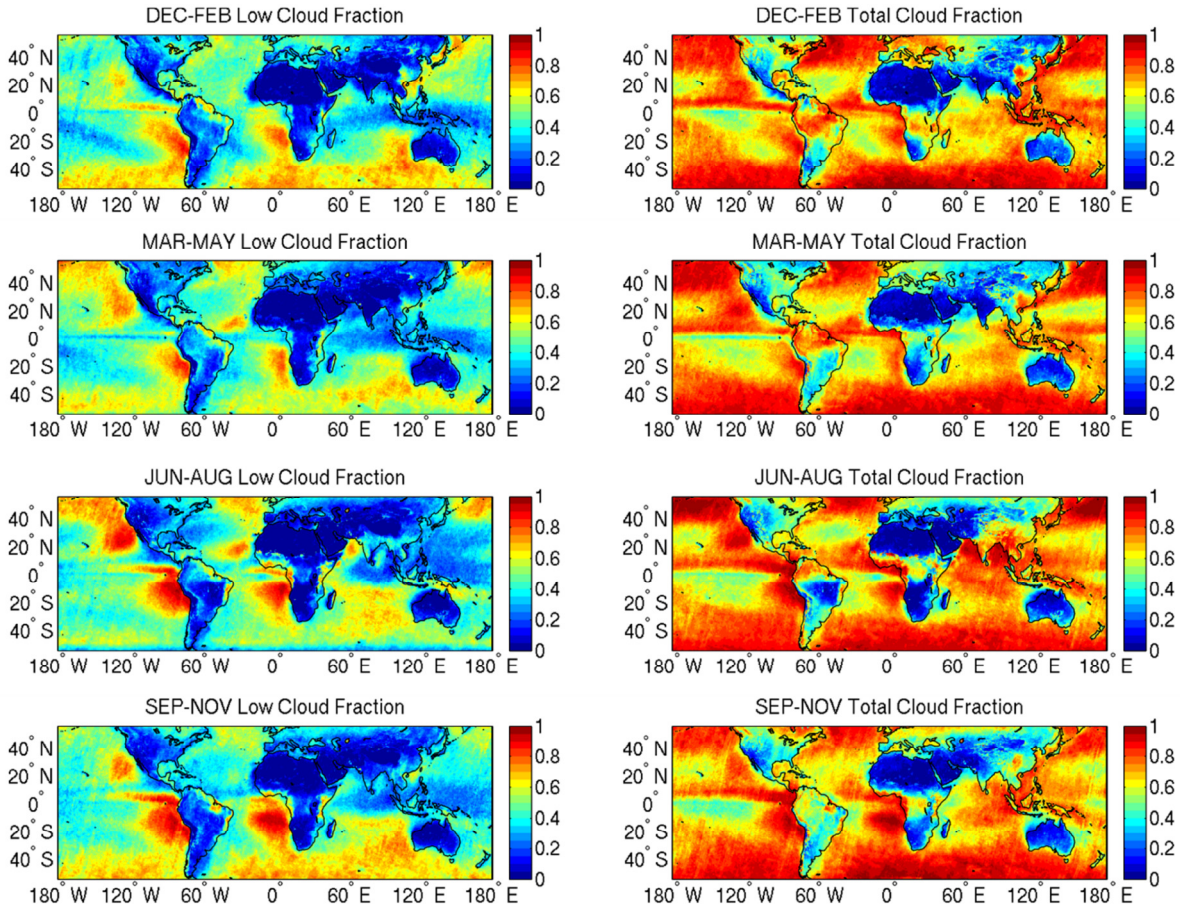

Figure 2.1: Maps of low cloud fraction (left) and total cloud fraction (right) for each season. Low cloud fraction consists of all clouds with cloud top height between 0 and 4 km from the CFbA dataset. Data are from 2001-2010.

lack of high cloud and the westward decrease in total cloud cover. The increase in cloud top height (and thus boundary layer depth) moving westward away from the continent is clearly evident for both cases. This increase in boundary layer depth was observed during the Variability of the American Monsoons (VAMOS) Ocean Cloud Atmosphere Land Study (VOCALS) field campaign (Bretherton et al. 2010). The cloud top height increases are on the order of 1 to 1.5 km, so a dataset with high vertical resolution is required to observe them.

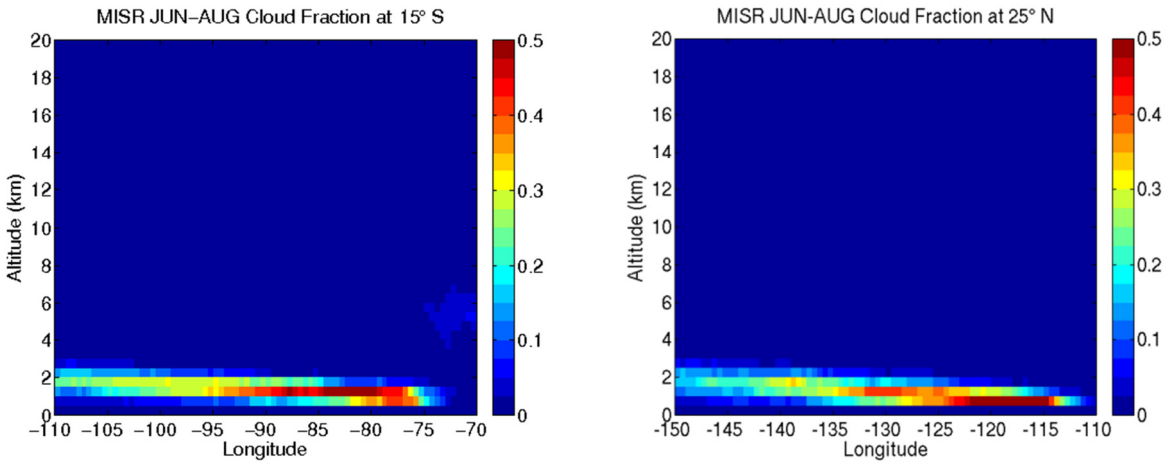

Figure 2.2: Vertical cross sections of cloud fraction along latitude lines passing through two marine stratus regimes (Northeast Pacific and Southeast Pacific). The season with the maximum low cloud fraction for each region is shown.

2.3 Local Climatology

CFbA data can also be used to track features such as seasonal cycles in cloud top height. Since cloud fraction is provided in height bins of 500 m, the daily mean cloud top height can be computed by summing the altitude bin center of all the height bins, weighted by the cloud fraction in that altitude bin, then dividing by the total cloud fraction. An example calculation is given in Eq. 2.1 using the data in Table 2.1.

Height bin	Height bin center	Cloud Fraction
500-1000 m	750 m	0
1000-1500 m	1250 m	0.4
1500-2000 m	1750 m	0.5

Table 2.1: Example CFbA data.

The calculation for low cloud fraction, then, is as follows:

$$\text{Daily Mean Height} = \frac{\Sigma_0^{4\text{km}} \text{Altitude Bin Center} \times \text{Cloud Fraction}}{\text{Total Cloud Fraction}} \quad (2.1)$$

$$\text{Daily Mean Height} = \frac{(750\ \text{m} \times 0) + (1250\ \text{m} \times 0.4) + (1750\ \text{m} \times 0.5)}{0 + 0.4 + 0.5} = 1528\ \text{m}$$

This is an effective method of estimating mean cloud height in marine stratiform regions because in regions covered by low stratiform cloud, frequently the cloud fraction is distributed over two or more contiguous height bins, much like the example above.

Figure 2.3 displays the normalized frequency of a particular cloud top height and cloud fraction for a location off the coast of California for a given month. The heights used are the daily mean heights described above. The seasonal cycle in cloud amount and cloud top height can be clearly seen, with the maximum heights in July in the 500-1000 m height range, and in the 1000-1500 m range for all other months shown. In addition, the frequency of occurrence of cloud fractions less than 0.8 becomes almost zero in July, with virtually all of the cloud top heights between 500 and 2000 m. This is not true of the other months shown, which have higher frequencies of lower cloud fractions and more variability in cloud top height.

2.4 Climatology at 20°S, 85°W

2.4.1 History of Southeast Pacific Marine Stratus Studies

In the last decade, numerous field campaigns (e.g. Bretherton et al. 2004, Wood et al. 2011) have been executed to better understand the climatology of and processes driving marine stratus formation and maintenance. One such field campaign was the Eastern Pacific Investigation of Climate Processes in the Coupled Ocean-Atmosphere System (EPIC; Bretherton et al. 2004), which improved understanding of the vertical structure of the marine boundary layer as well as processes governing cloud albedo, heat, and moisture fluxes. As part of EPIC, the Woods Hole Oceanographic Institute(WHOI) placed an Ocean Reference Station (Stratus ORS) at 20°S, 85°W; this is near the annual maximum of stratus cloud cover in the Southeast Pacific marine stratus regime. This extensive and

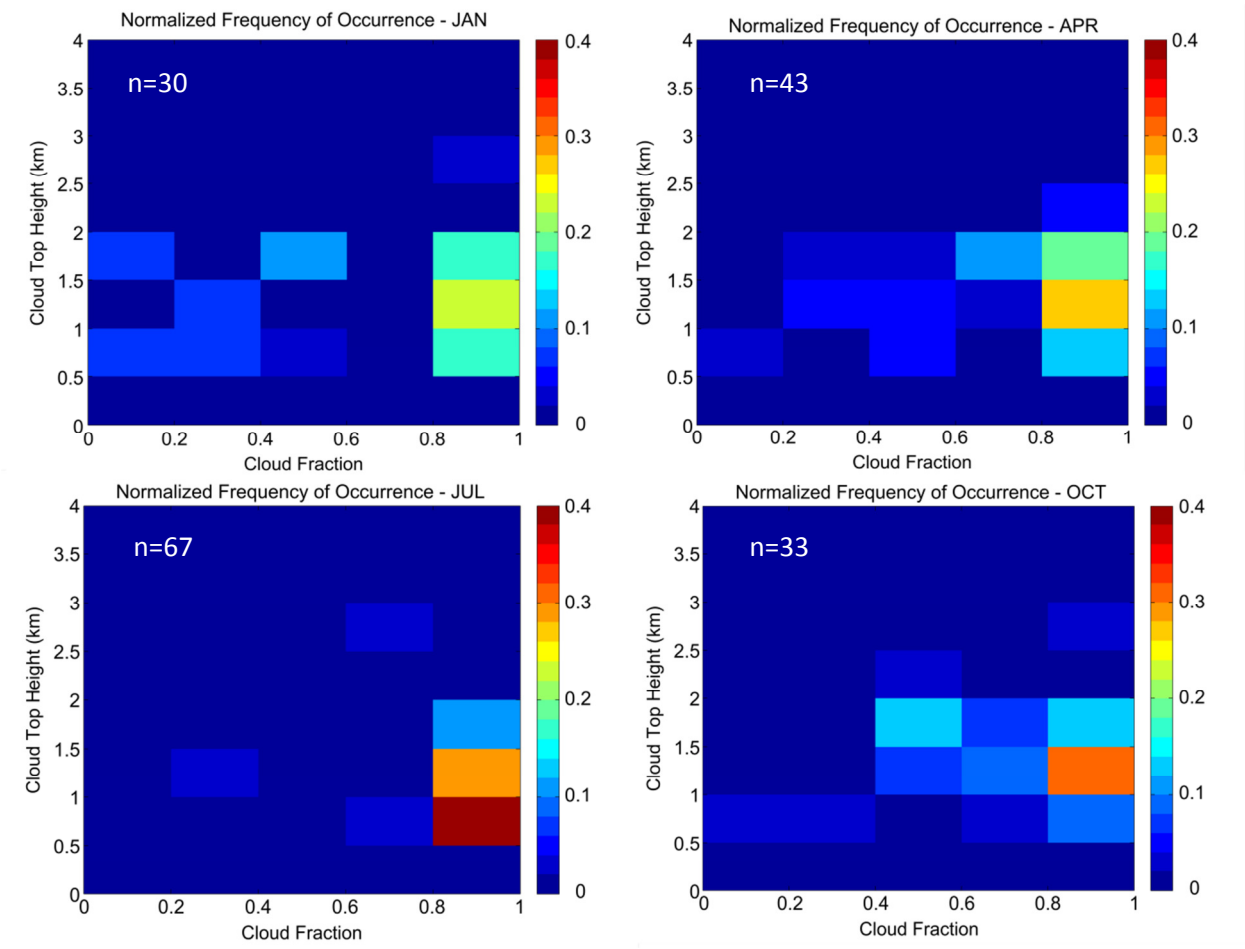

Figure 2.3: Histograms of cloud fraction vs. cloud top height for selected months. Cloud top height is calculated from CFbA data from 2001-2010 using the daily mean height calculation described in Section 2.3. Number of samples is indicated in the upper left corner of each plot (days where low cloud fraction = 0 are excluded). Location 25°N, 125°W (the center of the California stratus region in KH93).

persistent marine stratus regime influences El Niño-Southern Oscillation (ENSO) as well as the continent (Ghate et al. 2009); it therefore influences meteorological and climatic phenomena around the world. The Stratus ORS has taken observations of radiative fluxes and surface meteorology continuously since its launch in October 2000; Ghate et al. (2009) present an overview of the climatology of this region using data from this location. Here, the MISR cloud climatology for this location will be explored and evaluated against data from the Stratus ORS.

2.4.2 Stability and Cloud Cover

Low cloud fraction and stability have distinct seasonal cycles. Monthly time series from the MISR, NCEP/NCAR reanalysis , and Stratus ORS datasets are shown in Figure 2.4. Both low cloud fraction and stability peak around September and have a minimum around May. This marine stratus deck is present year round, with the lowest monthly cloud fraction value just over 60%. At its maximum, monthly cloud fraction approaches 90%. This is approximately 10% higher than the maximum shown in Ghate et al. (2009). There, cloud fraction is estimated using downwelling longwave radiative flux as measured from Stratus ORS and modeled estimates of cloud-emitted longwave radiation and clear-sky longwave radiation. The relation is given by

$$\mathrm{LWD} = \mathrm{CF} \times \mathrm{LW}_{\mathrm{cld}} + (1 - \mathrm{CF}) \times \mathrm{LW}_{\mathrm{clr}}, \tag{2.2}$$

where LWD is downwelling longwave radiative flux, $\mathrm{LW}_{\mathrm{cld}}$ is cloud-emitted longwave radiation, and $\mathrm{LW}_{\mathrm{clr}}$ is clear-sky longwave radiation. So while differences can be attributed to methods, the broad seasonality between the two is captured.

Because marine stratus clouds form in regions of large scale subsidence, middle and high clouds are uncommon (see Figure 2.2). This is particularly true in the season of maximum LTS and low cloud fraction. Monthly mean low cloud top height for all days, as well as only for those days in which MISR reported no high clouds (defined as clouds above 10 km), is shown in Figure 2.5; the two lines are the same or nearly the same throughout the year. However, when the lines are separate, mean cloud top height with cirrus filtered out is consistently lower than mean cloud top height with cirrus included(note that cirrus are not included in the mean cloud top height calculation). A potential explanation for this could be that cirrus clouds can only be maintained on days with relatively weak subsidence; this weak subsidence allows the turbulent mixing in the boundary layer to raise the height of the boundary layer top. Since marine stratus form at the top of the marine boundary layer (Lin et al. 2009), an increase in depth of the boundary layer results in an increase in cloud top height.

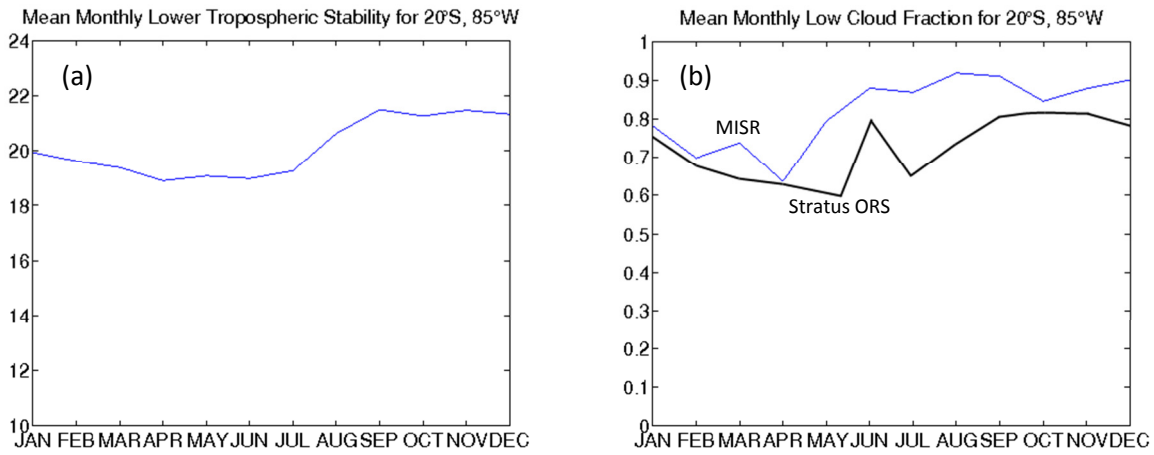

Figure 2.4: a) Lower tropospheric stability (LTS), and b) low cloud fraction from both MISR and the Stratus ORS for the Stratus ORS location. Low cloud is defined as cloud tops between 0 and 4 km using MISR data. LTS was calculated using NCEP/NCAR reanalysis data. MISR data are from 2001-2010; Stratus ORS data are from 2001-2005.

2.4.3 Cloud Top Height

Because the CFbA product has 500 m vertical resolution, it can be used to observe variations in cloud top height on a much finer scale than other passive satellite instruments. Figure 2.5 shows that mean low cloud top height (calculated using Eq. 2.1) for all days decreases by about 450 meters between the maximum in February and the minimum in August. Comparing Figure 2.5 with Figure 2.4, the minimum in low cloud top height occurs at around the same time as the maximum LTS and cloud fraction. Figure 2.6 shows a histogram, using daily data, for the Stratus ORS location for each month. A decrease in cloud top height from May through October is clearly evident from this perspective as well. Figure 2.6 also shows that the lifting condensation level (LCL) from Stratus ORS data varies between 625 m and about 720 m, while the mean monthly cloud top height (simply the monthly mean of the daily mean heights calculated using Eq. 2.1) varies between about 1.3 km and 1.8 km. The geometric thickness of clouds, then, also has a distinct seasonal cycle; clouds are geometrically thicker when cloud top heights are higher, and geometrically thinner when cloud top heights are lower. Since the cloud top

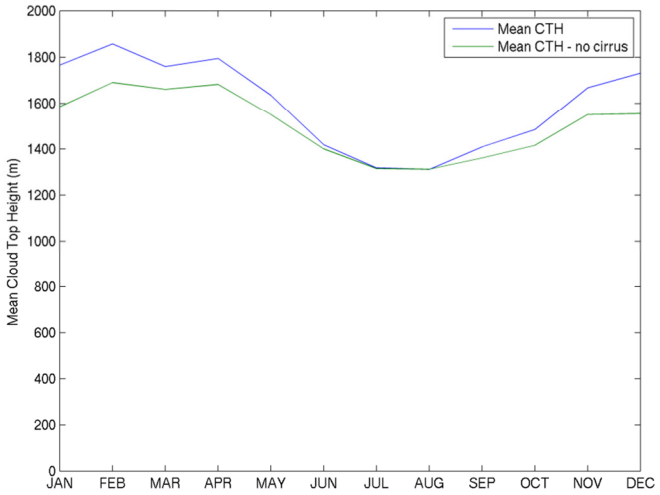

Figure 2.5: Time series of cloud top height at the Stratus ORS location. Mean cloud top height is shown here only for low (0-4 km cloud top height) clouds, as well as low cloud top height only on days with no high clouds (cloud top height > 10 km) present. Data are from 2001-2010.

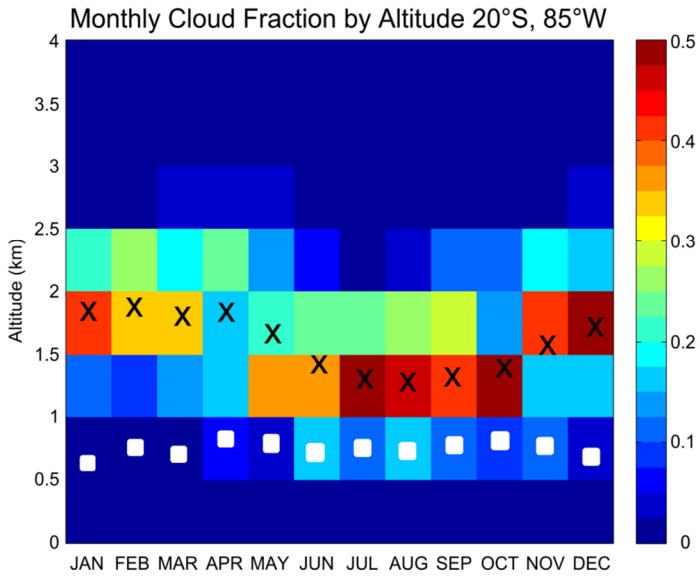

Figure 2.6: Histogram of cloud top height values by month for 2001-2010 for the Stratus ORS location. Data are normalized by the total number of data points for a given month. White squares represent the monthly mean LCL height from the Stratus ORS; black Xs represent the monthly mean cloud top height from MISR (Ghate et al. 2009).

height varies much more than the LCL, the seasonal cycle of cloud geometric thickness mirrors that of cloud top height. Here, the LCL height is calculated using surface temperature and moisture data from Stratus ORS. Since LCL height is approximately equivalent to cloud base, it can be used as a proxy for cloud base height. Ghate et al. (2009) calculateLCL height after Bolton (1980).

Despite the differences in determination of cloud fraction from Stratus ORS data and MISR data, the monthly mean cloud fraction values agree to within about 10% from JAN-APR and SEP-DEC. The differences in the MAY-AUG season are larger, on the order of 20%. For all months, the Stratus ORS monthly mean cloud fraction is lower than, or nearly the same as, that observed by MISR. The LCL heights, used here as a proxy for cloud base height, correspond closely with the heights of the lowest clouds observed by MISR.

2.5 Limitations

Like any data product, the CFbA dataset has its own set of limitations. For instance, due to the nature of passive remote sensing, optically thick high clouds may obscure lower clouds, preventing these lower clouds from being observed by MISR. This can be a particular problem in tropical deep convective regimes, where cirrus clouds associated with this convection are frequent. However, if multilayered clouds are present (such as cirrus over cumulus), unbiased cloud top heights may be retrieved for the lower cloud layer if the upper level clouds are optically thin enough. In addition, the MISR RCCM, which is used to derive the CFbA data, is a clear-conservative cloud mask. That is, if there is any cloud present in a pixel, the RCCM will designate the entire pixel as cloudy. Cloud fraction derived from a clear-conservative cloud mask will be the upper boundary of the range of possible cloud fraction values for a given scene. This can cause overestimation of cloud fraction in areas populated by small sub-pixel clouds (such as boundary layer cumulus), since the many partially filled pixels will be designated cloudy (Zhao and Di Girolamo 2006).

3. Stability and Low Cloud Cover

This chapter describes the relationship between stability of the marine boundary layer and marine stratus cloud coverage. The results of past stability-marine stratus studies are shown and discussed. Finally, the results of a similar investigation of the relationship between stability and marine stratus using the MISR dataset are presented.

3.1 History of Marine Stratus – Atmosphere Relationship Studies

3.1.1 LTS

As stated in the introduction, stability and low cloud fraction in marine stratus regions are strongly positively correlated, as shown by various studies (e.g KH93; WB06; Kubar et al. 2011). KH93 examined the seasonal cycles of sea surface temperature (SST), 700 hPa temperature, air temperature, stability, divergence of surface winds (which indicates strong subsidence aloft), and strength of the subtropical high to determine which if any of these exhibited a seasonal cycle similar to that of marine stratiform low cloud cover. For the California region (defined as 20°N-30°N and 120°W-130°W), only seasonal cycles of stability and strength of the subtropical high are similar to that of low cloud cover (see Figure 3.1). However, for other regions such as the Namibian stratus region, only stability has a seasonal cycle similar to that of cloud cover (see Figure 3.2). Stability, then, is the only atmospheric variable examined that has a similar seasonal cycle to that of low cloud cover in multiple marine stratus regimes.

Stability here is defined as the lower tropospheric stability (LTS; see Eq. 1.1). To discover a correlation between cloud fraction and stability, seasonal mean LTS in several different marine stratus regions was plotted against stratus cloud fraction in those regions (Figure 3.3). Using these seasonal means, LTS was found to explain over 60% of the variance in low stratiform cloud cover in the regions dominated by marine stratus (KH93).

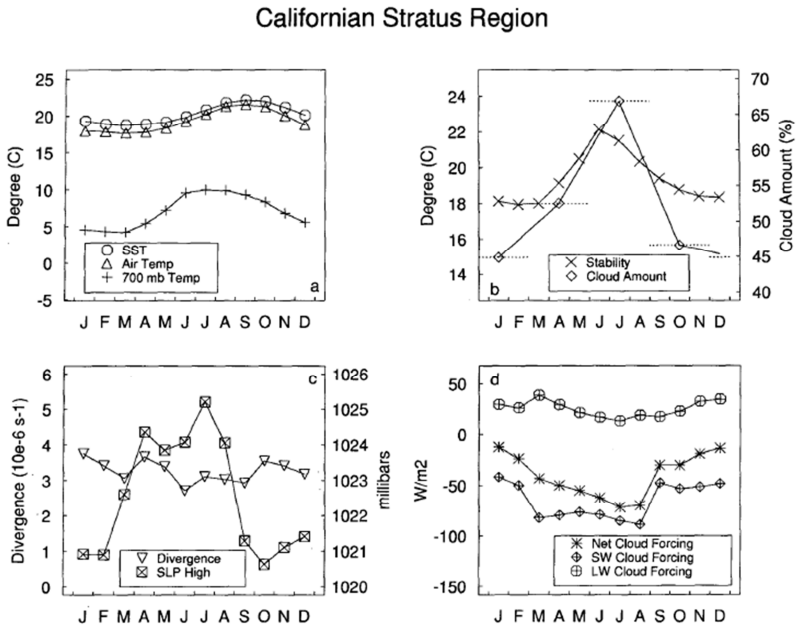

Figure 3.1: Seasonal cycles for the California stratus region of (a) sea surface temperature, air temperature, and 700 mb temperature; (b) stability and low cloud amount; (c) divergence of surface wind and strength of the subtropical high; (d) net, shortwave, and longwave cloud forcing. From KH93.

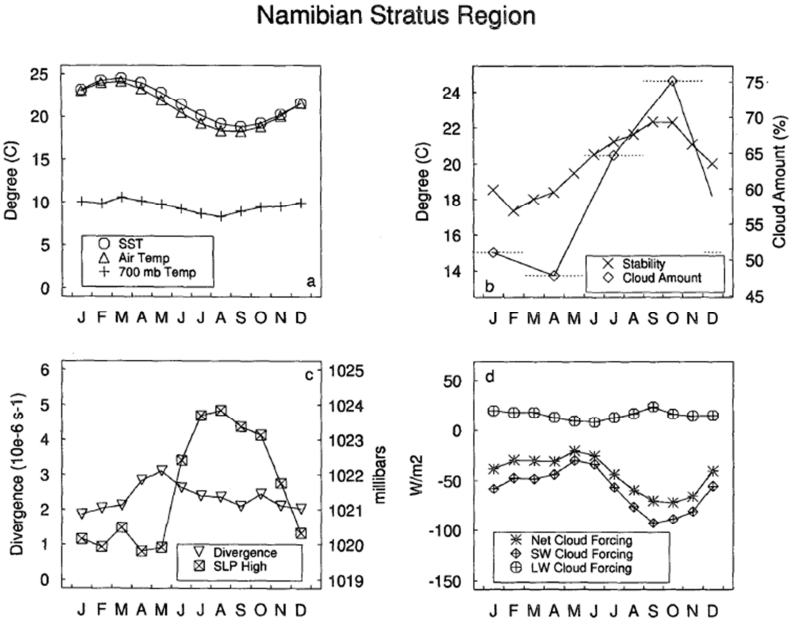

Figure 3.2: Seasonal cycles for the California stratus region of (a) sea surface temperature, air temperature, and 700 mb temperature; (b) stability and low cloud amount; (c) divergence of surface wind and strength of the subtropical high; (d) net, shortwave, and longwave cloud forcing. From KH93.

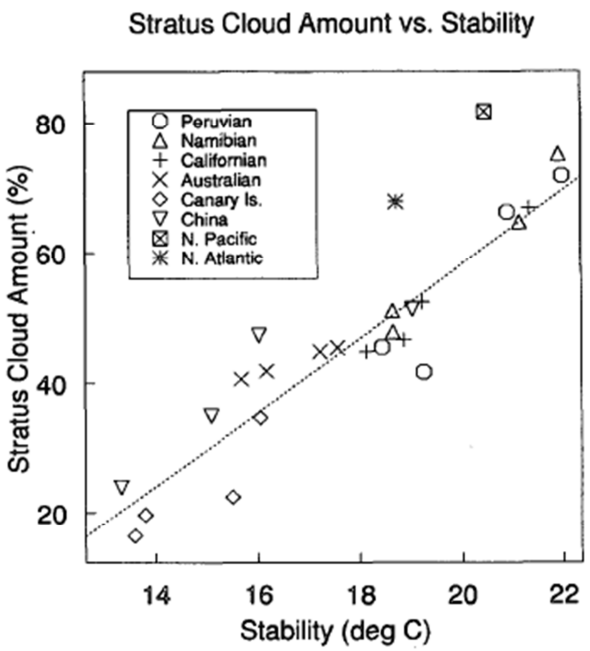

Figure 3.3: Seasonal mean stratus cloud amount vs. seasonal mean LTS for different marine stratus regimes (see Table 3.1 and Figure 3.6 for region boundaries). Adapted from KH93.

3.1.2 EIS

The estimated inversion strength (EIS) stability index was developed by WB06 to account for possible future changes in the climate state in which the LTS-low cloud cover relationship may not hold. The EIS takes not only the LTS into account, but also the thermodynamic profile of the lower troposphere and surface conditions. As a result, it is a more versatile measure of the marine boundary layer conditions in a given region. When a regression is performed using seasonal mean EIS and seasonal mean low cloud cover for the same regions used by KH93, over 80% of the variance in low cloud cover can be explained by changes in EIS (WB06).

Since LTS and EIS appear to be correlated with cloud cover, at least as demonstrated for marine stratus, we would expect global maps of stability to contain similar features to a global map of cloud cover. Figure 3.4 shows a comparison of 0-4 km cloud fraction, LTS, EIS, and ΔMSE, averaged over JJA.

In marine stratus regimes such as those near California, Peru, and Namibia, the stability maps show many of the same features as the cloud fraction map. This provides visual confirmation that large stability values and large cloud fractions tend to occur in the same locations in the same time interval.

3.1.3 Issues With Data Sources

Both the KH93 study and the WB06 study used data from the Warren and Hahn (2007) cloud atlas. Separate atlases exist for land and ocean; both consist of surface observations of cloud cover; over oceans, these are ship observations. The data are available at 5 degree and 10 degree spatial resolution; for the 5 degree data, the highest temporal resolution available is a seasonal (3 month) mean; for the 10 degree data, monthly means are available. For the best spatial resolution, then, temporal resolution must be sacrificed. This is why seasonal means were used in the calculations; at the time of the original Klein and Hartmann study, the Warren cloud atlas was the most frequently used cloud dataset and had the best spatial and temporal resolution available at the time. WB06 used the same data, despite having higher resolution climatologies available, in order to accurately compare their EIS to the KH93 LTS.

Because the Warren cloud atlas for oceans relies on observations from ships, large regions of the oceans may be sparsely, if at all, sampled. For these points, then, the data may not be truly representative of the cloud cover characteristics at that location. An example of the Warren cloud atlas data is shown in Figure 3.5. In addition, since these are surface observations, cloud height (and thus cloud type) is assigned by cloud base height. This can cause difficulties when comparing with satellite climatologies or model cloud cover, both of which assign cloud altitude using height of the cloud top rather than cloud base.

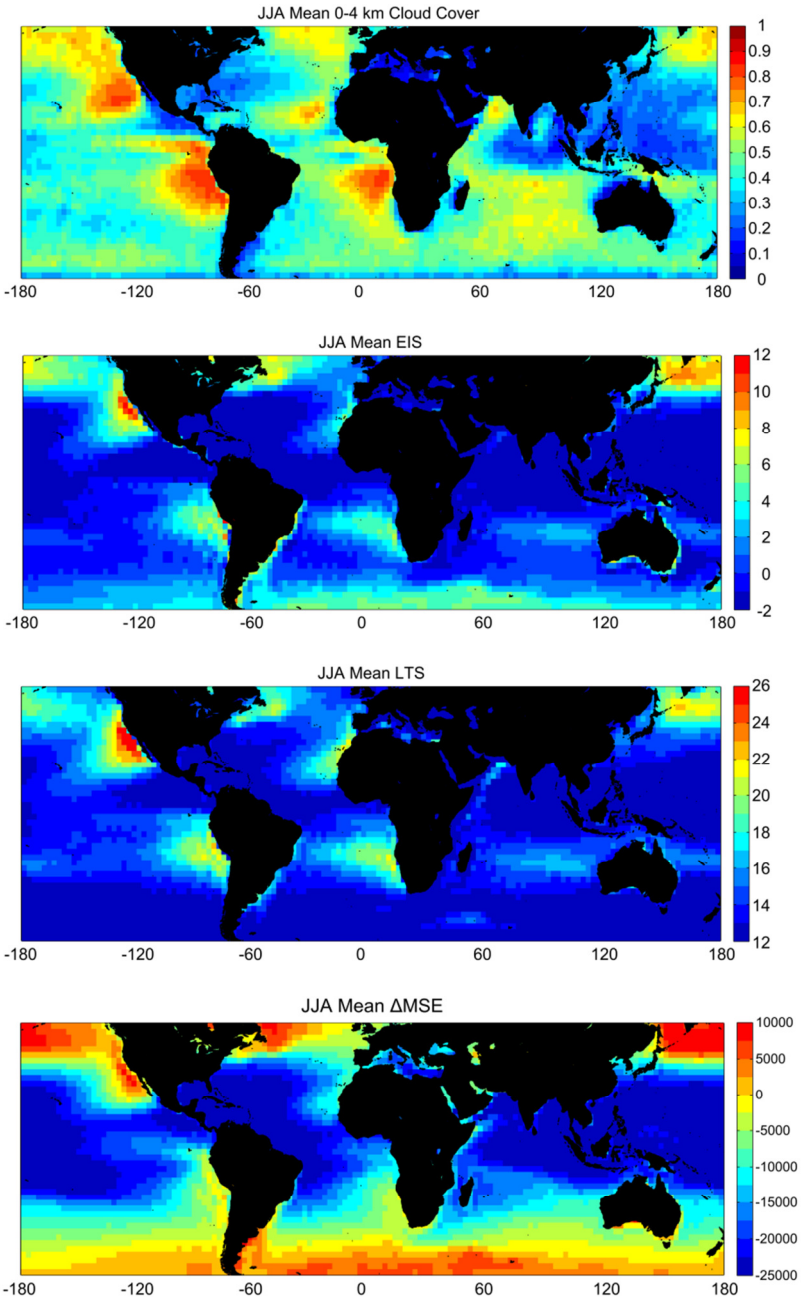

Figure 3.4: Global maps of low cloud fraction (top), LTS (middle), and EIS (bottom). Low cloud fraction is calculated from MISR CFbA monthly mean cloud fraction; LTS and EIS are calculated after KH93 and WB06 respectively, using monthly means from NCEP/NCAR reanalysis data. Data are from 2001-2010.

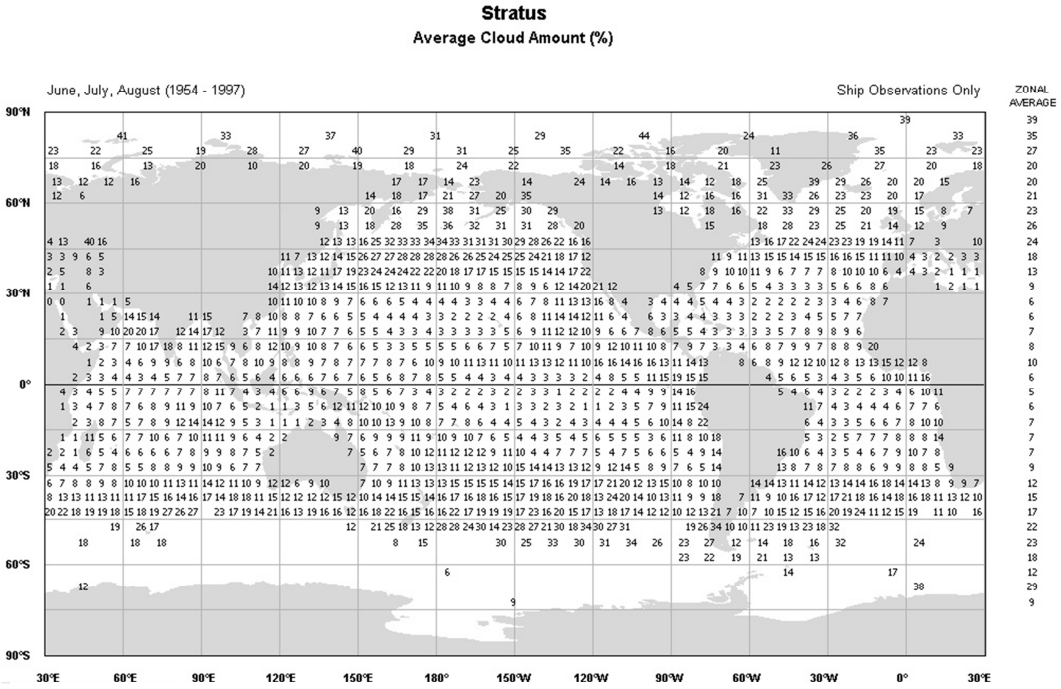

Figure 3.5: Image showing data from the Warren and Hahn (2007) cloud atlas. Shown here is stratus cloud cover for JJA over oceans.

3.1.4 ΔMSE

To improve on the previously developed measures of stability in marine stratus regimes, Kubar et al. (2011) developed a new measure of stability: the change in Moist Static Energy, ΔMSE (see Eqs. 1.3 and 1.4) between the subsidence inversion level (or 700 hPa if an inversion level is not identified) and the surface. Instead of studying multiple regions, this study focused on one region in the Northeast Pacific. Rather than using surface cloud observations, this study used cloud height and fraction data from CloudSat, a spaceborne cloud radar (Stephens et al. 2002), the CALIPSO Cloud-Aerosol Lidar with Orthogonal Polarization (CALIOP, also known as CALIPSO; Winker et al. 2010), and the Moderate Resolution Imaging Spectrometer (MODIS) on NASA's Aqua platform. The sensitivity of CloudSat is reduced for low clouds below 1.2 km (a large percentage of marine stratus), but CALIPSO can detect these low clouds accurately. MSE includes three terms: sensible, latent, and potential energy. It increases with height in a stably stratified atmosphere, so higher values of ΔMSE indicate a more stable

boundary layer. The relationship between ΔMSE and cloud cover has a strong seasonal cycle, with r values greater than 0.9 for MAM, JJA, and SON, but less than 0.7 for DJF. A regression was also performed using both MODIS cloud information and the CloudSat/CALIPSO dataset against LTS and EIS for the JJA season; as expected, the correlation was quite high, with r values around 0.94. This result is difficult to compare against the KH93 and WB06 regression lines, however, since it only accounts for one year of data for one location.

3.2 Results Using MISR

Because of the issues inherent in using the Warren cloud atlas, or any other surface observation dataset, for determining the cloud fraction for a given region, the analysis of KH93 and WB06 was repeated using cloud fraction and cloud top height from the MISR Cloud Fraction by Altitude product. Because virtually all of the boundary layer clouds in marine stratus regions are in the lowest 4 km of the troposphere, 4 km was chosen as the threshold for low clouds. In this analysis, the marine stratus regions listed in Table 3.1 and shown in Figure 3.6 were used; these regions are a subset of the regions used to develop the LTS-low cloud cover relationship in KH93.

Region	Location
California	20°-30°N, 120°-130°W
Peru	10°-20°S, 80°-90°W
Canary Islands	15°-25°N, 25°-35°W
China	20°-30°N, 105°-120°E
Namibia	10°-20°S, 0°-10°E
Australia	25°-35°S, 95°-105°E

Table 3.1: The regions used in KH93 to determine the relationship between low cloud cover and LTS.

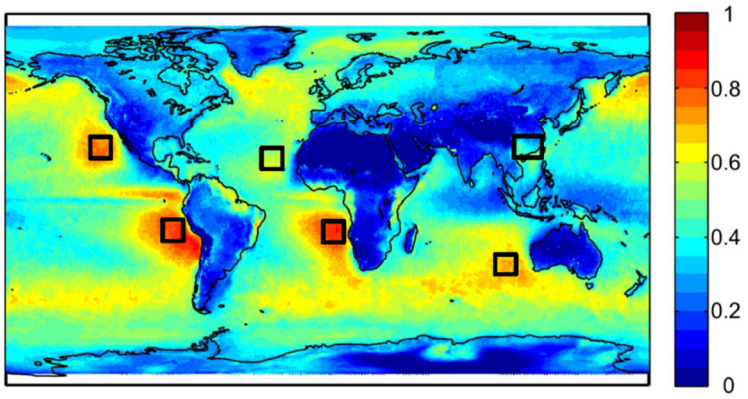

Figure 3.6: MISR annual 0-4 km cloud fraction map with boxes highlighting regions shown in Table 3.1.

Figure 3.7 shows that the cloud fractions on average are higher when using the MISR dataset than for the original analysis using the Warren cloud atlas. There are several reasons why this could be the case; one such reason is the larger field of view from a satellite instrument when compared to surface observations; with a smaller field of view, a surface observer is more likely to observe mesoscale variations in cloud cover and thus report a cloud fraction that is not representative of a larger area. Depending on spatial resolution, a satellite instrument may not observe these variations and may designate the whole scene as cloudy. The clear conservative cloud mask used by MISR, which provides an upper boundary on the true cloud fraction, may also be responsible for the higher cloud fractions since it will flag as cloudy any cloud edge pixels. Additionally, both KH93 and WB06 investigated a time period from 1951-1981, while the MISR data used here cover 2001-2010; this difference in time period being studied may be partly responsible for the difference. Lastly, the definitions of what constitutes "low cloud" differ substantially between the original KH93/WB06 analysis and the analysis presented here using the MISR dataset. In the Warren cloud atlas, low clouds are divided into three types: cumulonimbus, cumulus, and stratus (the latter includes variants such as stratocumulus and sky-obscuring fog); low clouds in KH93 are only those classified as stratus in the Warren cloud atlas. In contrast, "low cloud" in the MISR analysis is strictly those clouds with cloud top heights between 0 and

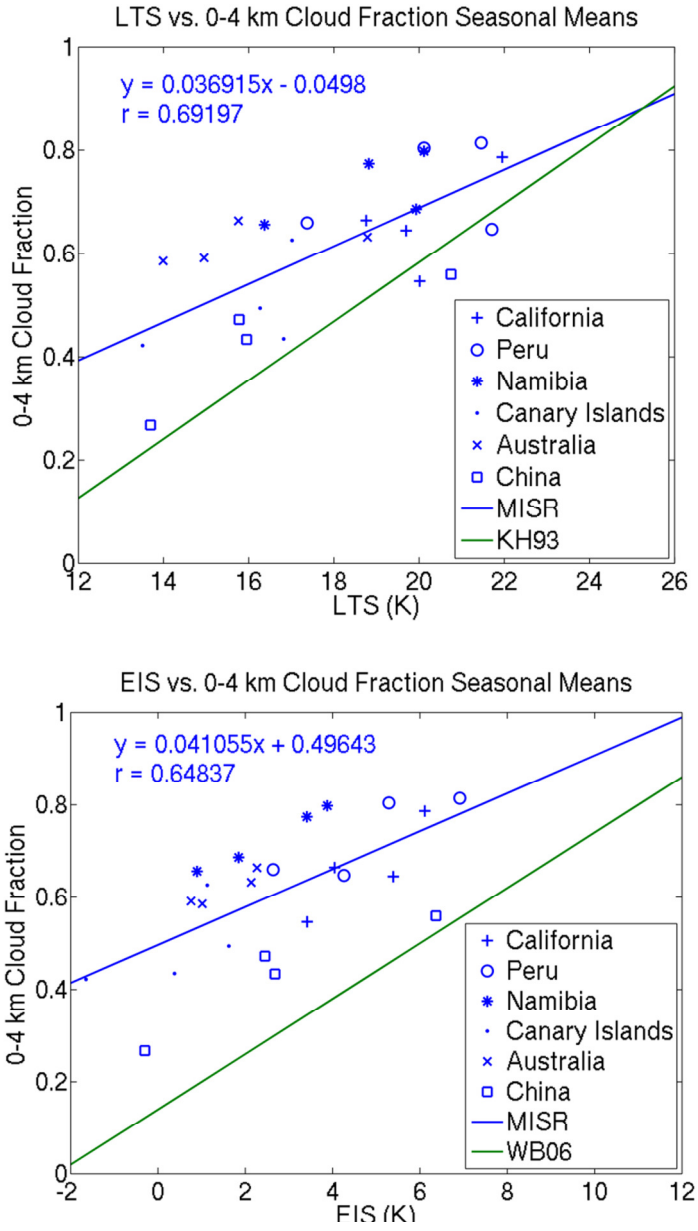

Figure 3.7: (top) Seasonal mean LTS vs. 0-4 km cloud fraction as in KH93. Blue line indicates regression using MISR data, green line indicates the original KH93 regression. (bottom) Seasonal mean EIS vs. 0-4 km cloud fraction as in WB06. Blue line indicates regression using MISR data, green line indicates the original WB06 regression.

4 km. MISR will then include some low cloud which may be classified as cumulus or other low cloud types in the Warren cloud atlas.

The same analysis was performed using using the ΔMSE parameter and MISR data. Since the Kubar et al. (2011) study focused only on one region, the analysis was expanded to the other regions shown in Table 3.1 and Figure 3.6 for an accurate comparison with the LTS and EIS regression lines; Figure 3.8 shows the results of this analysis. When it is done in this way, the DJF points have much higher values of ΔMSE than all other seasons. With DJF included, the correlation drops to 0.22;

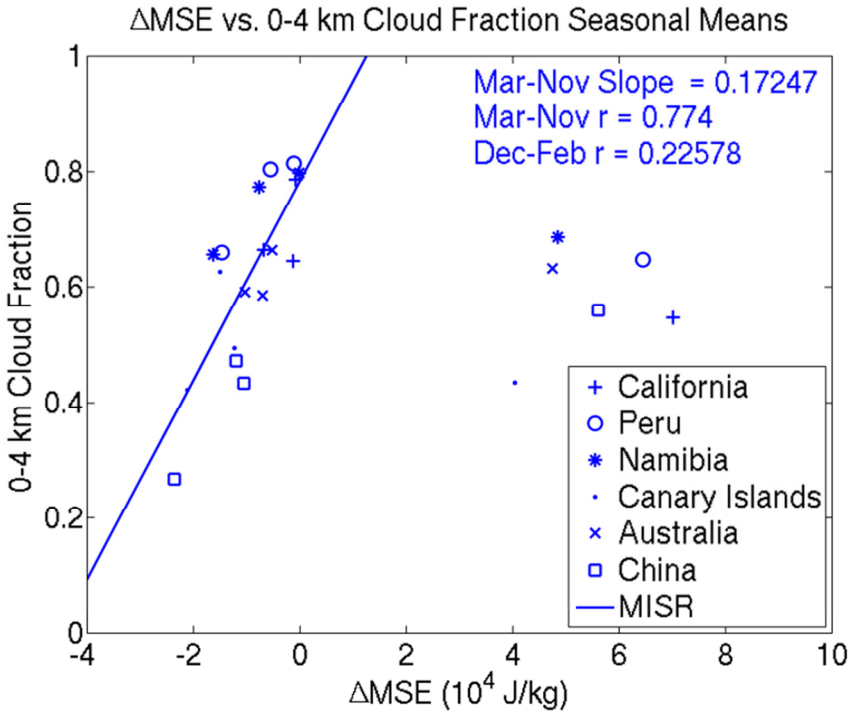

Figure 3.8: As in Figure 3.7, but using the ΔMSE parameter from Kubar et al. (2011). Blue line indicates the regression line using the MISR dataset.

however, since all the DJF points are clustered apart from the rest of the data, they were removed from the correlation calculation to get a better sense of the relationship during the other seasons. Excluding DJF, the correlation is quite good, with r = 0.77. However, as previously stated, there is a strong seasonal cycle to ΔMSE; the correlation coefficient for the DJF season is only 0.23. Only part of this

difference is due to the seasonal cycle; the method in which ΔMSE is calculated may have impacted this result as well. Kubar et al. (2011) used reanalysis data from the European Center for Medium Range Weather Forecasting (ECMWF), which has 91 vertical levels and can discern layers in which an inversion is present. For this comparison, NCEP/NCAR reanalysis data were used; this dataset has 17 vertical levels and thus cannot accurately pinpoint inversion layers, which tend to be rather shallow. To calculate ΔMSE, MSE_{700} was used rather than MSE_{inv}, as suggested by the original study. This could also bias the results.

4. Effects of Varying Temporal and Spatial Resolution

This chapter presents an investigation of how the stability-marine stratus relationship changes when the spatial and/or temporal resolution is varied. Monthly and daily relationships for specific regions are examined and discussed. A temporal lag is then applied to the daily relationship to determine if upstream conditions affect marine stratus cloud coverage on a daily time scale. Lastly, a probabilistic approach is presented in which the statistical likelihood of a given set of conditions is determined.

4.1 Monthly Analysis

Both the LTS vs. low cloud fraction and EIS vs. low cloud fraction relationships were obtained from seasonal means of stability and cloud cover by combining the different marine stratus regimes defined in Table 3.1. The correlations, as previously shown, are quite strong. However, from a climate modeling perspective, it would be useful to examine each region individually and see if the correlation continues to hold in one region. This regional perspective will allow climate models to be evaluated on a regional basis, which is important for cloud parameterization evaluation and improvement. Regional analysis would be difficult to do using seasonal means since there would only be four data points, so monthly means were calculated and used instead of the seasonal mean values. Figure 4.1 shows the monthly mean low cloud fraction plotted against LTS for the Stratus ORS location off the coast of Peru and the California stratus region. The correlations increase compared to the seasonal plot of several regions (e.g. Figure 3.7) when individual regions are examined on a monthly time scale.

The low cloud fraction vs. stability plots in marine stratus regimes have two dominant characteristics. First, they tend to have a strongly positive correlation coefficient. Second, the slope of the best fit line is always positive (see Figures 3.7 and 3.8). These characteristics, however, may not be

unique to marine stratus regimes; to investigate this, linear slope and correlation of monthly mean low cloud fraction vs. stability were calculated for every point on the globe, at 2.5° by 2.5° horizontal

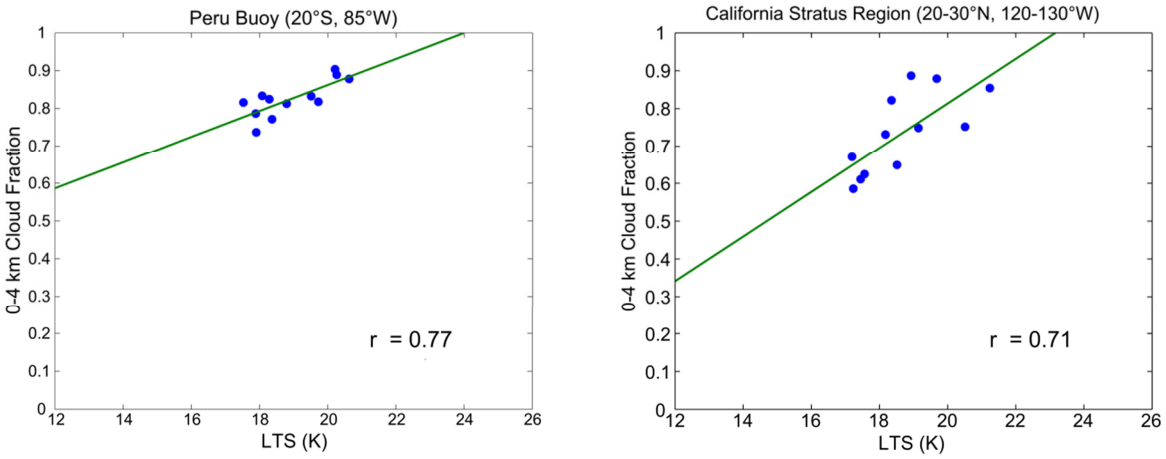

Figure 4.1: Monthly mean LTS vs. 0-4 km cloud fraction for two marine stratus regions: (left) the Stratus ORS location off the coast of Peru (see Chapter 2) and (right) the California stratus region from KH93.

resolution, between 55°N and 55°S (these boundaries were chosen to avoid issues relating to MISR cloud detection over ice). The results are shown in Figure 4.2.

Large slope and correlation coefficient values occur in the expected regions (i.e. the areas dominated by marine stratus), but large values of slope and/or correlation coefficient can also be found in other regions, most notably in the western North Atlantic near the location of the Gulf Stream current and off the Chinese coast. Marine stratus in these regions form when cold air flows over the warm ocean current; the resulting strong heat and moisture fluxes produce convection that deepens the marine boundary layer (KH93). Also note the strong correlations with negative slopes. The reasons for these are not explored here, though it is an interesting area for future study. Maps such as these can aid in efforts to evaluate the output generated by GCMs, particularly since they show the relationship between stability and low cloud cover not just for one specific region, but on a global scale. If maps like these are produced using model output stability and cloud cover, regions in which the models perform well (and poorly) can be identified and cloud parameterizations can be adjusted accordingly.

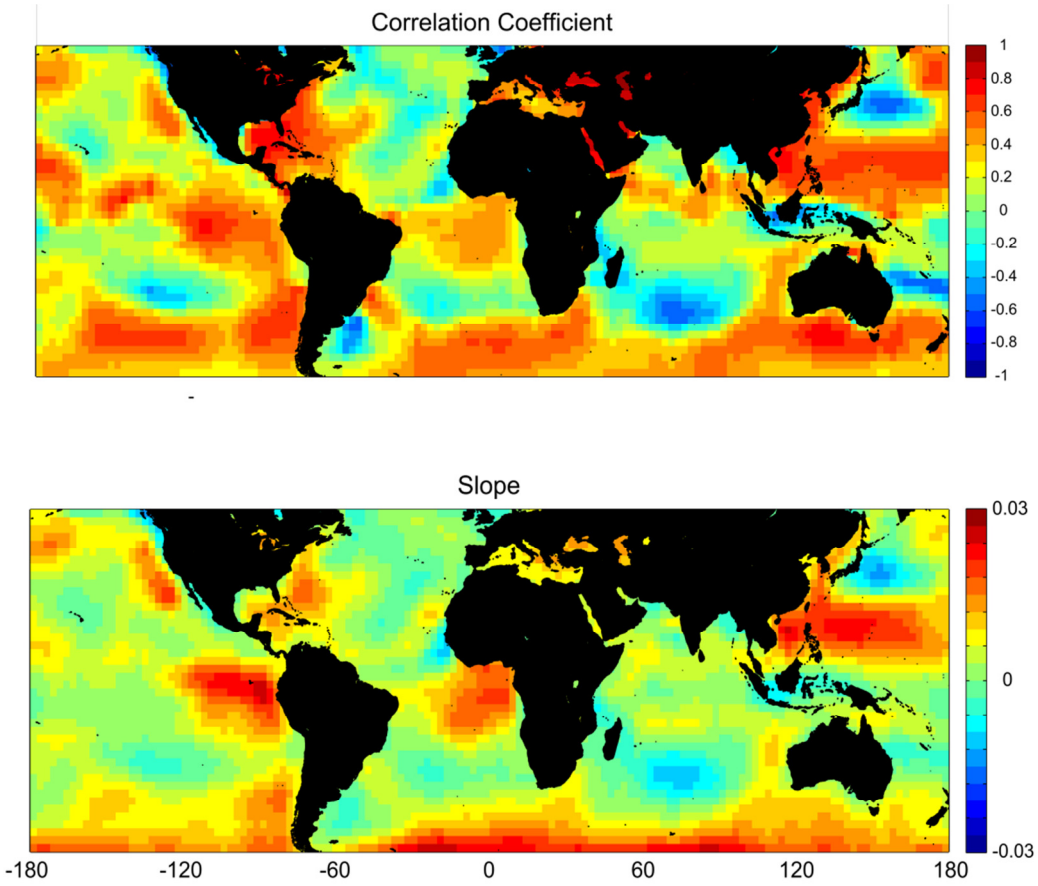

Figure 4.2: Maps of slope and correlation coefficient for the monthly mean LTS vs. low cloud fraction relationship.

4.2 Daily Analysis

4.2.1 Background

The strong relationship between low cloud cover and stability on monthly and seasonal time scales has already been shown. It might be expected, then, that the relationship would hold on the daily time scale as well. However, the relationship falls apart on the daily scale (KH93; Klein 1997; Zhang et al. 2009). Albrecht (1991) showed that low cloud cover was not correlated with cloud top entrainment instability (CTEI) or the mixing line slope proposed by Betts and Boers (1990), both of which are daily varying parameters. Klein (1997) examined data from ocean weather station November, located at

30°N, 140°W. Surface observations were taken every 3 hours and radiosondes were launched every 12 hours between 1949 and 1974, resulting in an extensive climatology with high temporal resolution. When comparing daily values of stability and low cloud fraction, the fraction of variance explained was quite low, less than 0.2. If averaging time is increased, however, the fraction of variance explained steadily increases to almost 0.6 for an averaging interval of 25 days. Figure 4.3 shows the change in r^2 with increasing averaging time obtained by Klein (1997).

This increase in r^2 raises an obvious question: why do the daily data points, which do not by themselves have any kind of correlation, form such a strong relationship when averaged over times approaching one month? One hypothesis is that there is a lag between the atmospheric conditions and cloud cover at a given point; numerous studies such as Klein et al. 1995, Klein 1997 (summertime Northeast Pacific), and Mauger and Norris (2010) (summertime Northeast Atlantic) have explored potential time lag relationships between boundary layer meteorological variables and low cloud cover. It is worth noting that both Klein et al. (1995) and Klein (1997) are focusing on data from the Ocean Weather Station November, which is located at 30°N, 140°W. This location is outside of the maximum in summertime low cloud fraction (see Fig. 2.1 and Fig. 3.6), so the effects of stability in this location may not be as strong as in areas closer to the cloud fraction maximum. The Northeast Atlantic region examined in Mauger and Norris 2010 (defined as 24°-40°N and 35°-10°W) has only a weak correlation between low cloud fraction and LTS (Fig. 4.2). They found that increases in LTS, as well as decreases in SST, are associated with increases in low cloud cover 24-48 hours downwind; however, the correlation coefficients are still weak, ranging from about -0.3 to 0.3. Klein (1997) found a similar association, on the order of 24-30 hours, but the r^2 values are very small and the variations with lag are not statistically significant at the 99% confidence level.

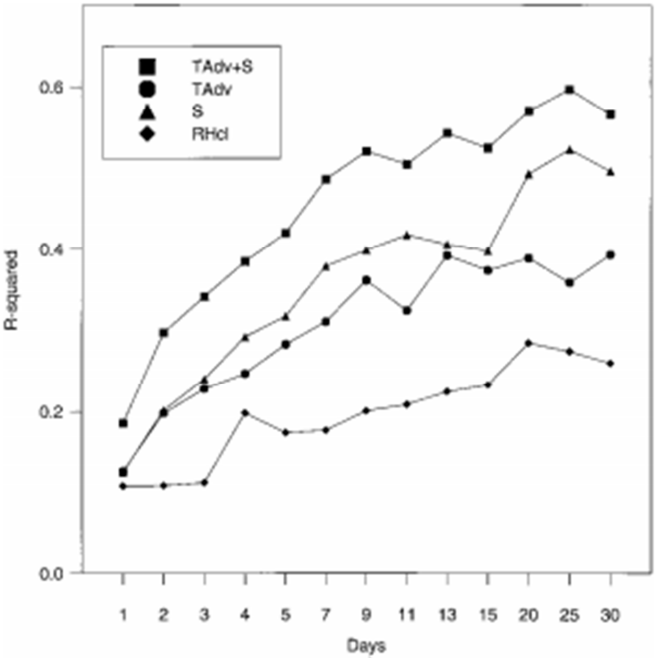

Figure 4.3: Fraction of variance explained for various predictors of low cloud cover as a function of averaging time. Squares represent temperature advection combined with stability, circles represent temperature advection by itself, triangles represent stability by itself, and diamonds represent the relative humidity of the cloud layer. From Klein (1997).

4.2.2 MISR Test

Using the daily MISR data, this lack of a relationship between daily stability and low cloud cover was sought. Since Terra is in a sun synchronous orbit, the cloud cover data is retrieved at the same time for every day. Rather than using the daily mean stability, then, the closest data time to the MISR overpass time from the NCEP/NCAR reanalysis dataset was chosen. This ensures that the observations are as close to coincident as possible. The results, shown in Figure 4.4, are in line with the other studies that have documented this lack of a daily relationship.

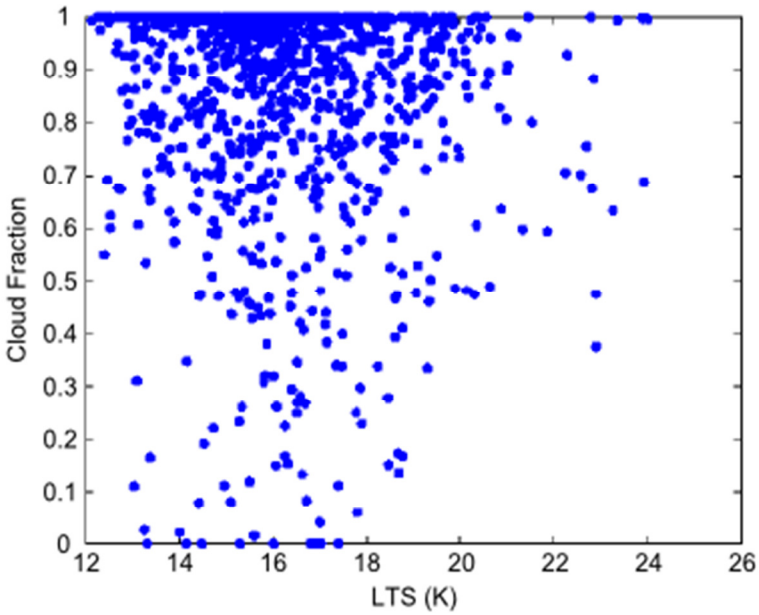

Figure 4.4: Daily LTS vs. low cloud fraction for the Stratus ORS location.

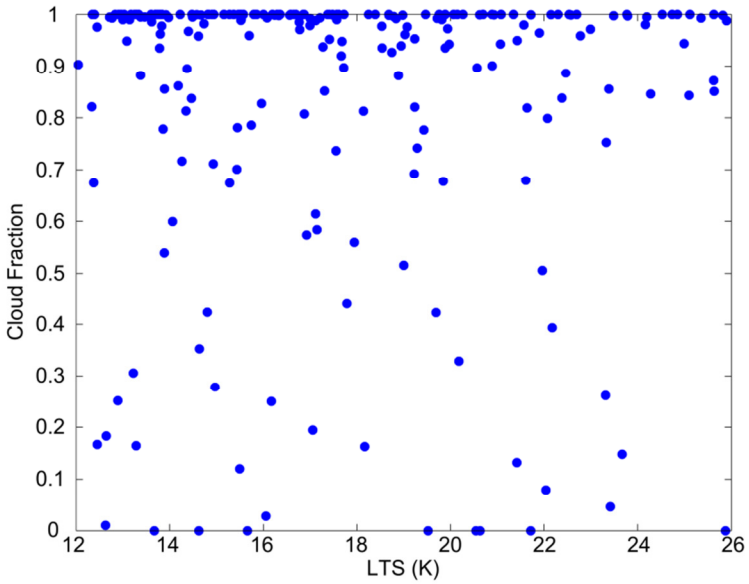

Figure 4.5: Daily LTS vs. low cloud fraction for the California stratus region (see Table 3.1) with a 36 hour time lag.

4.2.3 Lagrangian Analysis

To further investigate the lag relationships discussed in Section 4.2.1, a Lagrangian analysis was performed using the MISR low cloud fraction data and NCEP/NCAR reanalysis low-level wind to track the parcel back in time. 925 hPa wind was chosen since it is the closest of the 17 vertical levels in the reanalysis data to the level at which marine stratus clouds typically occur. Using these wind data, back trajectories were calculated in six-hourly intervals up to 72 hours back from the starting point. Figure 4.5 shows the daily LTS vs. low cloud fraction with a 36 hour time lag for the California region. Despite the promising results shown in earlier studies, no correlation was observed. Other regions, such as the Peruvian stratus, were also analyzed with similar results.

4.3 A Probabilistic Approach

4.3.1 Results

Perhaps a more informative approach for GCM cloud parameterization evaluation and development is a probabilistic approach; that is, determining the likelihood of certain conditions when other conditions are true. This approach is used to examine the relationships between cloud fraction, cloud top height, and stability using two different perspectives: looking at cloud top height as a function of stability (here LTS is used to quantify stability), and looking at cloud top height as a function of cloud fraction for a given range of LTS values. The results of the first perspective for a point within the KH93 California stratus region are shown in Figure 4.6. For this region, June and July are typically the months with highest stability and average cloud fraction. Figure 4.6 shows that these two months appear to have the smallest variation in the LTS and cloud top height (CTH) frequencies. This coincides with the minimum in cloud top height and the maximum in LTS (Figure 4.7). Once the subsidence inversion begins to weaken in August and September, LTS and CTH values appear to be distributed among a wider range of values, in accordance with the weakening of the thermal inversion at the top of the boundary

layer. The highest frequency LTS values also increase in the summer months, which is consistent with climatology as well. Another way of thinking of this is that in June, if the cloud fraction is above 90%, there is about a 20% chance that the LTS is between 24 and 26 and the cloud top height is

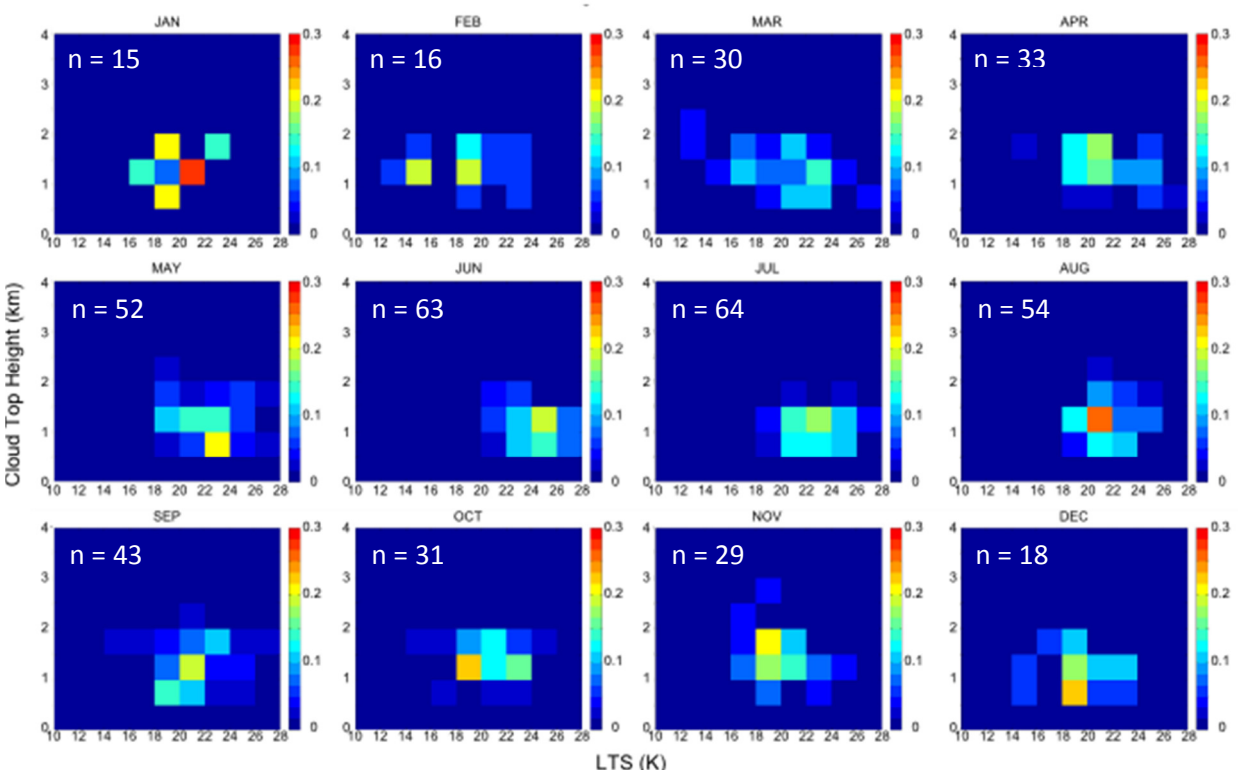

Figure 4.6: Monthly plots of LTS frequency (as computed from NCEP/NCAR reanalysis data) vs. cloud top height frequency (from MISR data) in the California stratus region (25°N, 125°W) on days with low cloud fraction >= 90%. Colors represent the normalized frequency of occurrence of a given LTS/cloud top height combination. Data are from 2001-2010. MISR data have been degraded to 2.5° by 2.5° horizontal resolution to match the reanalysis data. Number of samples indicated in the top left of each plot. See Appendix A for more results.

between 1 and 1.5 km. This perspective shows explicitly which conditions are most likely to occur with a given cloud fraction; in February, for instance, the LTS is most often between 14 and 20 K with a cloud top height of 1 to 1.5 km, while in November the LTS is most often between 18 and 22 K with a cloud top height of 1 to 2 km.

Another perspective relates cloud top height and cloud fraction (similar to Figure 2.3) while constraining the LTS to be in a certain range. Figure 4.8 shows this perspective for July, the annual peak

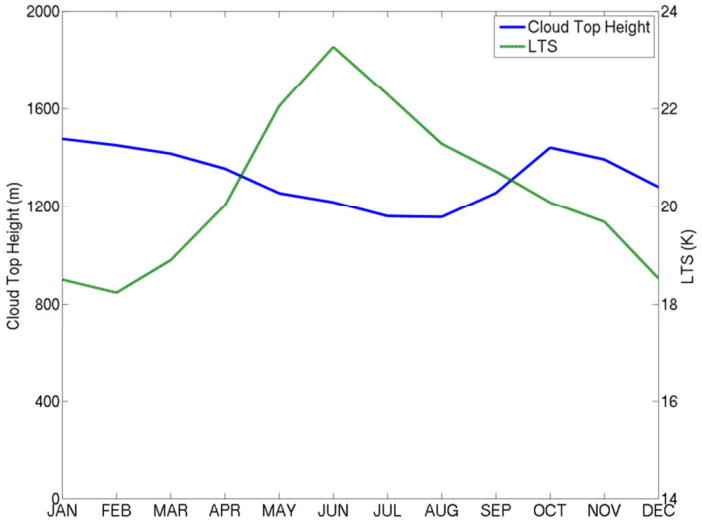

Figure 4.7: Monthly mean cloud top height and LTS time series for a point in the California stratus. Mean cloud top height is calculated the MISR CFbA product using all days when clouds are present; LTS is calculated using reanalysis data. Data are from 2001-2010.

in cloud fraction and stability in the California stratus region, for LTS values common to this season and region. The distribution is clearly dependent on the LTS. For instance, when LTS is between 20 and 22 K, around 45% of the samples have cloud fraction > 0.8 and CTH 0.5-1.5 km; the remaining 55% of samples are distributed among the remaining cloud fraction bins. When LTS increases to 22-24 K, the percentage of samples in the 0.5-1km height range and cloud fraction > 0.8 range increases to over 90% with no samples having a cloud fraction of less than 0.8. The number of samples does decrease by about 45% (27 samples in the 20-22 K LTS range compared to 15 in the 22-24 K range), but sampling here is still sufficient to observe the characteristics of the distribution. This perspective – cloud fraction and cloud top height as a function of LTS – could be useful to modelers looking to parameterize marine stratus using boundary layer conditions, since LTS is relatively easily simulated in GCMs.

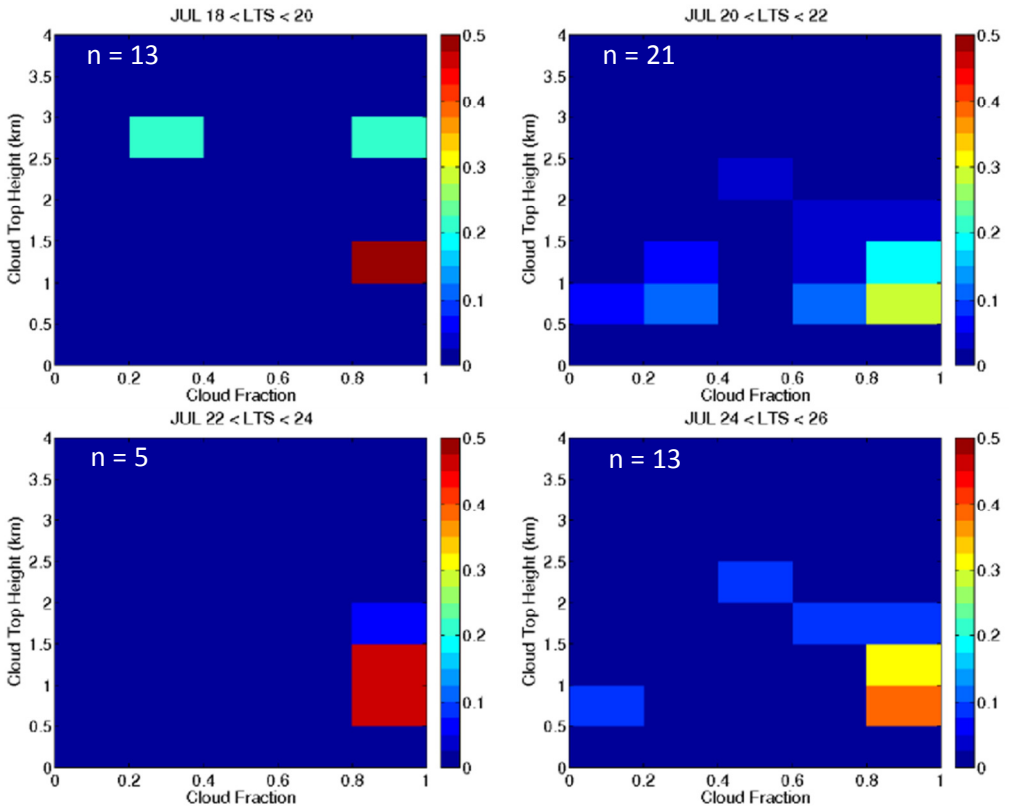

Figure 4.8: Histograms of cloud top height and cloud fraction from MISR with LTS within a given range. Data are shown for July for 25°N, 125°S (California stratus region) from 2001-2010. Colors represent normalized frequency of occurrence for a given cloud fraction and cloud top height (similar to Figure 2.3). Number of samples is indicated in the upper left of each plot. Only selected results are shown here; see Appendix B for more results.

4.3.2 Sampling Issues

While both perspectives may be useful for observing and predicting conditions in the subtropical marine boundary layer, sampling issues must be considered when interpreting these analyses. Figure 4.9 shows the average number of samples per month from the MISR data. Subtropical regions typically have between 6 and 10 samples per month; over the ten years of data discussed here, there will be approximately 60 to 100 samples for a given month (though this varies depending on the month). Once constraints are placed on the data, such as only showing days in which the LTS is in a given range, the number of samples may decrease dramatically depending on the constraint. For instance, in Figure 4.8,

the plot showing data for LTS between 18 and 20 (a relatively rare occurrence for that season) has five samples, while the plot showing LTS between 22 and 24 (a more common occurrence) has 15. Some of the results which describe uncommon conditions, then, are not reliable; the reliability of these results is not quantified here.

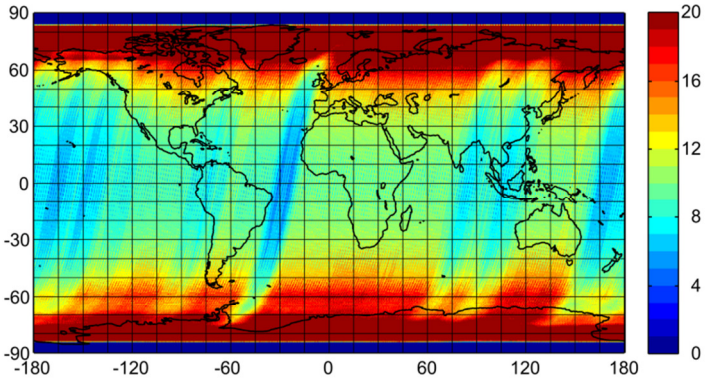

Figure 4.9: Average number of samples per month from MISR. Because MISR is on Terra, a sun synchronous platform, sampling is much higher in the polar regions than in the lower latitudes.

5. Summary and Conclusions

5.1 Summary

Clouds play a critical role in the global energy balance. They not only regulate the distribution of energy, but also those of precipitation and aerosols as well. The marine stratus clouds that occur in the eastern subtropical oceans account for a significant portion of these impacts due to their high albedo and large horizontal extent (hundreds of kilometers at times). As a result, it is important to be able to accurately model these clouds in general circulation models that predict future climate states. However, these models do not handle clouds well, resulting in a large spread in cloud cover between models; Bony and Dufresne (2005) showed that most of this spread is due to differences in marine boundary layer clouds. Past studies have determined that there is a strong relationship on seasonal and interannual time scales between subtropical marine stratus and the stability of the marine boundary layer; accurately reproducing relationships such as this from model output is a key element of model evaluation.

This study uses data from the MISR instrument to investigate this relationship between stability and cloud cover. With its nine camera angles and stereoscopic height retrieval technique, MISR allows for accurate determination of both cloud coverage and cloud top height for low, optically thick clouds. MISR, then, is ideal for studying subtropical marine stratus, which tend to be in the lowest 3 km of the troposphere. The 500 m vertical resolution of MISR's CFbA product allows for examination of relatively fine scale height variations for the first time using a passive instrument. The 10:30 am equator crossing time of the Terra platform is around the midpoint of the diurnal cycle of marine stratus cloud cover and cloud top height; data obtained at this time will represent the approximate mean of these quantities.

Numerous studies over the past two decades have attempted to describe the relationship between low cloud cover and boundary layer stability. Several indices have been developed to quantify stability: lower tropospheric stability (LTS), the difference in potential temperature between 700 hPa

and the surface (KH93); estimated inversion strength (EIS), an enhanced version of LTS that incorporates more information about the structure of the boundary layer (WB06); and ΔMSE, the change in moist static energy between the surface and the inversion level (Kubar et al. 2011). All of these indices show a strong correlation with low cloud fraction on seasonal time scales. Using the MISR dataset for low cloud fraction, these results still hold; the correlations are notably weaker, but still quite strong.

To investigate the relationship between stability and low cloud cover for individual regions, monthly mean stability and cloud fraction were plotted for several different regions. The correlation appeared to increase when this was done. Global maps of the slope and correlation coefficient of the monthly mean stability vs. monthly mean cloud fraction were then produced. While high slope and correlation coefficient appeared in the expected regions, these also showed up in unexpected regions such as over the Gulf Stream current. The analysis was then taken down to the daily time scale, where no correlation was found between stability and cloud fraction. While perhaps surprising, this lack of relationship has been documented in previous studies. A potential cause of this could be the existence of a time lag between the stability and cloud cover in a given region. While earlier studies have showed that stability may be weakly correlated with low cloud fraction 24-48 hours downwind, my analysis using the MISR data yielded no such relationship. Looking at the relationships using a probabilistic perspective involving stability, cloud top height, and cloud fraction, a seasonal cycle of LTS vs. cloud top height variability is clearly evident on days with high cloud fraction (above 90%).

5.2 Conclusions and Future Work

With a vertical resolution of 500 m, the MISR CFbA dataset reveals features that were, until recently, undetectable using passive instruments. Features such as the trimodal distribution of cloud cover in the tropics, interannual variations in marine stratus cloud top height, and frequency of cloud top fraction vs. cloud top height are now able to be observed and analyzed. Global maps of the slope

and correlation coefficient of the monthly mean stability vs. low cloud fraction relationship enable evaluation of model output on a regional basis; this could occur by comparing the model-generated stability parameters (e.g. LTS, EIS, ΔMSE) to model-generated cloud cover, producing global maps similar to the maps shown in Chapter 4, and comparing the sets of maps. Parameterizations of clouds could then be adjusted accordingly.

The relationship between daily low cloud fraction and stability is all but nonexistent when using daily MISR data and nearly coincident stability observations from reanalysis data. It is possible that there is a time lag between the stability conditions of the marine boundary layer and low cloud cover; that is, stability does not have an immediate impact on cloud cover. A few studies have hinted at this, and it is certainly an interesting area for further research. Another area of future work is the investigation of the relationship between correlation coefficient and averaging time, similar to Klein (1997). To perform this analysis, however, a cloud cover dataset with a higher sampling frequency than MISR (which has global coverage every 9 days) would be needed. Along with this, future research could explore the relationship between cloud cover and stability using other reanalysis datasets, such as the ECMWF reanalysis or NASA's Modern Era Retrospective-Analysis for Research and Applications (MERRA) dataset. Lastly, the causes of large slope and correlation coefficient that occur outside of subtropical marine stratus regions would be a worthy investigation.

References

Albrecht, B.A. (1991), Fractional cloudiness and cloud-top entrainment instability, J. Atmos. Sci., 48, 1519-1525.

Betts, A.K. and R. Boers (1990), A cloudiness transition in a marine boundary layer, J. Atmos. Sci., 47, 1480-1497.

Bolton, D. (1980), The computation of equivalent potential temperature, Mon. Wea. Rev., 108, 1046-1053.

Bony, S., and J.-L. Dufresne (2005), Marine boundary layer clouds at the heart of tropical cloud feedback uncertainties in climate models, Geophys. Res. Lett., 32, L20806, doi:10.1029/2005GL023851.

Bretherton, C.S. and Coauthors (2004), The EPIC 2001 stratocumulus study, Bull. Amer. Meteor. Soc., 85, 967-977.

Bretherton, C.S., R. Wood, R.C. George, D. Leon, G. Allen, and X. Zheng (2010), Southeast Pacific stratocumulus clouds, precipitation and boundary layer structure sampled along 20°S during VOCALS-Rex, Atmos. Chem. Phys., 10, 10639-10654.

Di Girolamo, L., A. Menzies, G. Zhao, K. Mueller, C. Moroney, and D.J. Diner (2010), MISR Level 3 cloud fraction by altitude algorithm theoretical basis. Jet Propulsion Laboratory, JPL D-62358, 18 pp. [Available online at http://eospso.gsfc.nasa.gov/eos_homepage/for_scientists/atbd/docs/MISR/MISR_CFBA_ATBD.pdf].

Diner, D. J., and Coauthors (1998), Multi-angle Imaging SpectroRadiometer (MISR) description and experiment overview. IEEE Trans. Geosci. Remote Sens., 36, 1072–1087.

Garay, M.J., S.P. de Szoeke, and C.M. Moroney (2008), Comparison of marine stratocumulus cloud top heights in the southeastern Pacific retrieved from satellites with coincident ship-based observations, J. Geophys. Res., 110, D18204, doi:10.1029/2008JD009975.

Ghate, V.P., B.A. Albrecht, C.W. Fairall, and R.A. Weller (2009), Climatology of Surface Meteorology, Surface Fluxes, Cloud Fraction, and Radiative Forcing over the Southeast Pacific from Buoy Observations, J. Clim., 22, 5527-5540.

Harshvardhan, G. Zhao, L. Di Girolamo, and R.N. Green (2009), Satellite-Observed Location of Stratocumulus Cloud-Top Heights in the Presence of Strong Inversions, Trans. Geosci. Rem. Sens., 47, 1421-1428.

Hartmann, D. L., M.E. Ockert-Bell, and M. L. Michelsen (1992), The effect of cloud type on Earth's energy balance: global analysis, J. Clim., 5, 1281-1304.

IPCC (2007), Climate Change 2007: The Physical Science Basis. Contribution of Working Group I to the Fourth Assessment Report of the Intergovernmental Panel on Climate Change [Solomon, S., D. Qin, M. Manning, Z. Chen, M. Marquis, K.B. Averyt, M. Tignor and H.L. Miller (eds.)]. Cambridge University Press, Cambridge, United Kingdom and New York, NY, USA, 996 pp.

Kalnay et al., The NCEP/NCAR 40-year reanalysis project, Bull. Amer. Meteor. Soc., 77, 437-470, 1996.

Klein, S.A. and D. L. Hartmann (1993), The seasonal cycle of low stratus clouds, J. Clim., 6, 1587-1606.

Klein, S.A., D.L. Hartmann, and J.R. Norris (1995), On the relationships among low-cloud structure, sea surface temperature, and atmospheric circulation in the summertime Northeast Pacific, J. Clim., 8, 1140-1155.

Klein, S. A. (1997), Synoptic variability of low-cloud properties and meteorological parameters in the subtropical trade wind boundary layer, J. Clim., 10, 2018-2039.

Kubar, T.L., D.E. Waliser, and J.-L Li (2011), Boundary layer and cloud structure controls on tropical low cloud cover using A-Train satellite data and ECMWF analyses, J. Clim., 24, 194-215.

Lin, W., M. Zhang, and N.G. Loeb (2009), Seasonal variation of the physical properties of marine boundary layer clouds off the California coast, J. Clim., 22, 2624-2638.

Manabe, S. and R.T. Wetherald (1967), Thermal equilibrium of the atmosphere with a given distribution of relative humidity, J. Atmos. Sci., 24, 241-259.

Mauger, G.S. and J.R. Norris (2010), Assessing the impact of meteorological history on subtropical cloud fraction, J. Clim., 23, 2926-2940.

Moroney, C., R. Davies, and J.-P. Muller (2002), Operational retrieval of cloud-top heights using MISR data, IEEE Trans. Geosci. Rem. Sens., 40, 1532-1540.

Stephens, G. L., and Coauthors (2002), The CloudSat mission and the A-Train—A new dimension of space based observations of clouds and precipitation, Bull. Amer. Meteor. Soc., 83, 1771–1790.

Stevens, B. and Coauthors (2007), On the Structure of the Lower Troposphere in the Summertime Stratocumulus Regime of the Northeast Pacific, Mon. Wea. Rev., 135, 985-1005.

Warren, S.G. and C.J. Hahn (2007), Climatic atlas of clouds over land and ocean [available online: http://www.atmos.washington.edu/CloudMap/WebO/index.html]

Winker, D. M., and Coauthors (2010), The CALIPSO mission: A global 3D view of aerosols and clouds, Bull. Amer. Meteor. Soc., 91, 1211–1229.

Wood, R. and C.S. Bretherton (2006), On the relationship between low cloud cover and lower-tropospheric stability, J. Clim., 19, 6425-6432.

Wood, R. and Coauthors (2011), The VAMOS Ocean-Cloud-Atmosphere-Land Study Regional Experiment (VOCALS-REx): goals, platforms, and field operations, Atmos. Chem. Phys., 11, 627-654.

Woodruff, S.D., R.J. Slutz, R.L. Jenne, and P.M. Steurer (1987), A comprehensive ocean-atmosphere data set, Bull. Amer. Meteor. Soc., 68, 1239-1250.

Zhang, M.H. and Coauthors (2005), Comparing clouds and their seasonal variations in 10 atmospheric general circulation models with satellite measurements, J. Geophys. Res., 110, D15802, doi:10.1029/2004JD005021

Zhang, Y., B. Stevens, B. Medeiros, and M. Ghil (2009), Low-cloud fraction, lower-tropospheric stability, and large-scale divergence. J. Clim., 22, 4827-4844.

Zhao, G. and L. Di Girolamo (2004), A Cloud Fraction versus View Angle Technique for Automatic In-Scene Evaluation of the MISR Cloud Mask, J. Appl. Meteorol., 43, 860-869.

Zhao, G. and L. Di Girolamo (2006), Cloud fraction errors for trade wind cumuli from EOS-Terra instruments, Geophys. Res. Lett., 33, L20802, doi:10.1029/2006GL027088.

Appendix A

These figures show monthly normalized 2-dimensional histograms at 25°N, 125°W of LTS and cloud top height for all days with cloud cover above a given threshold. LTS was calculated using NCEP/NCAR reanalysis data and cloud information was taken from the MISR CFbA product. The CFbA data were degraded to 2.5° by 2.5° horizontal resolution to match the reanalysis data resolution.

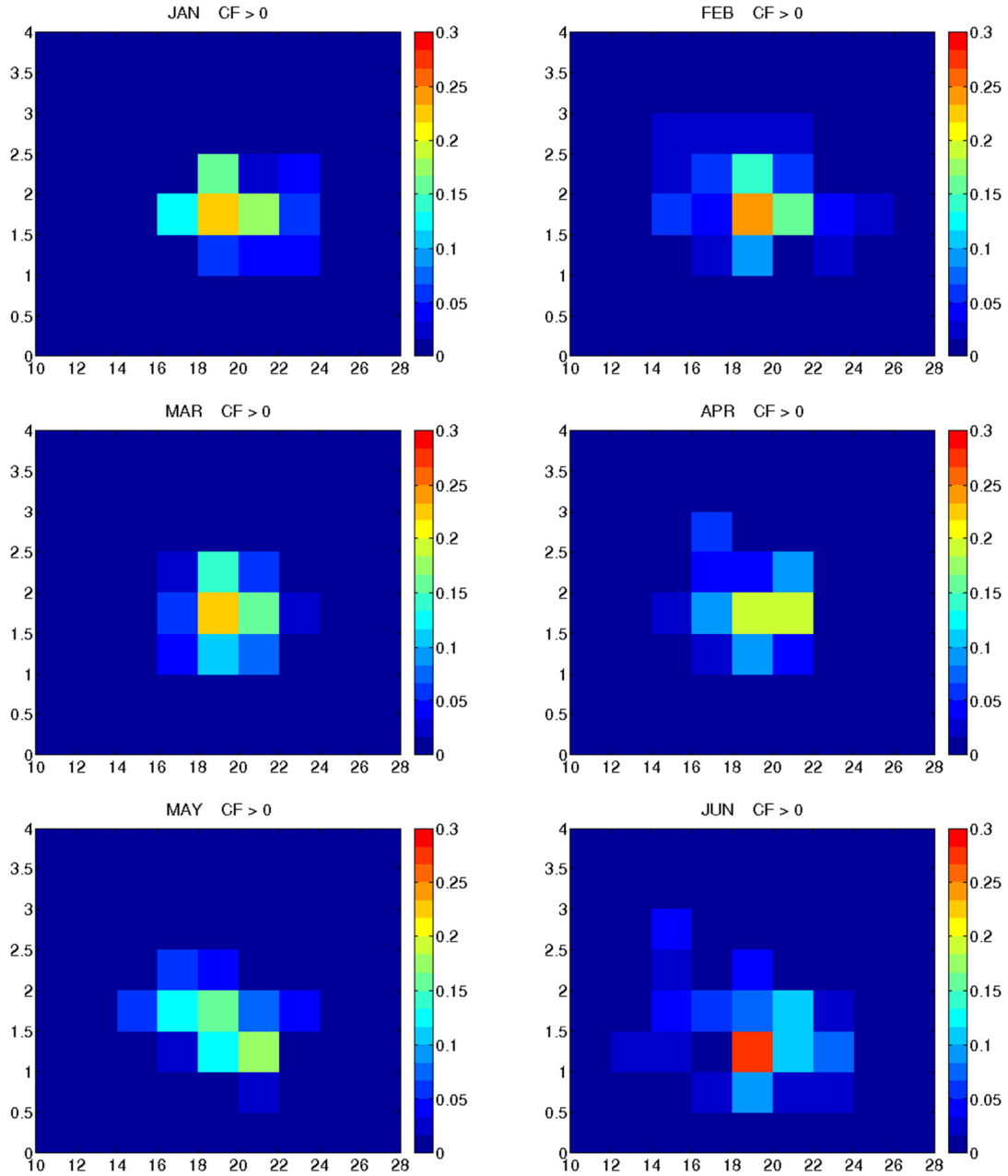

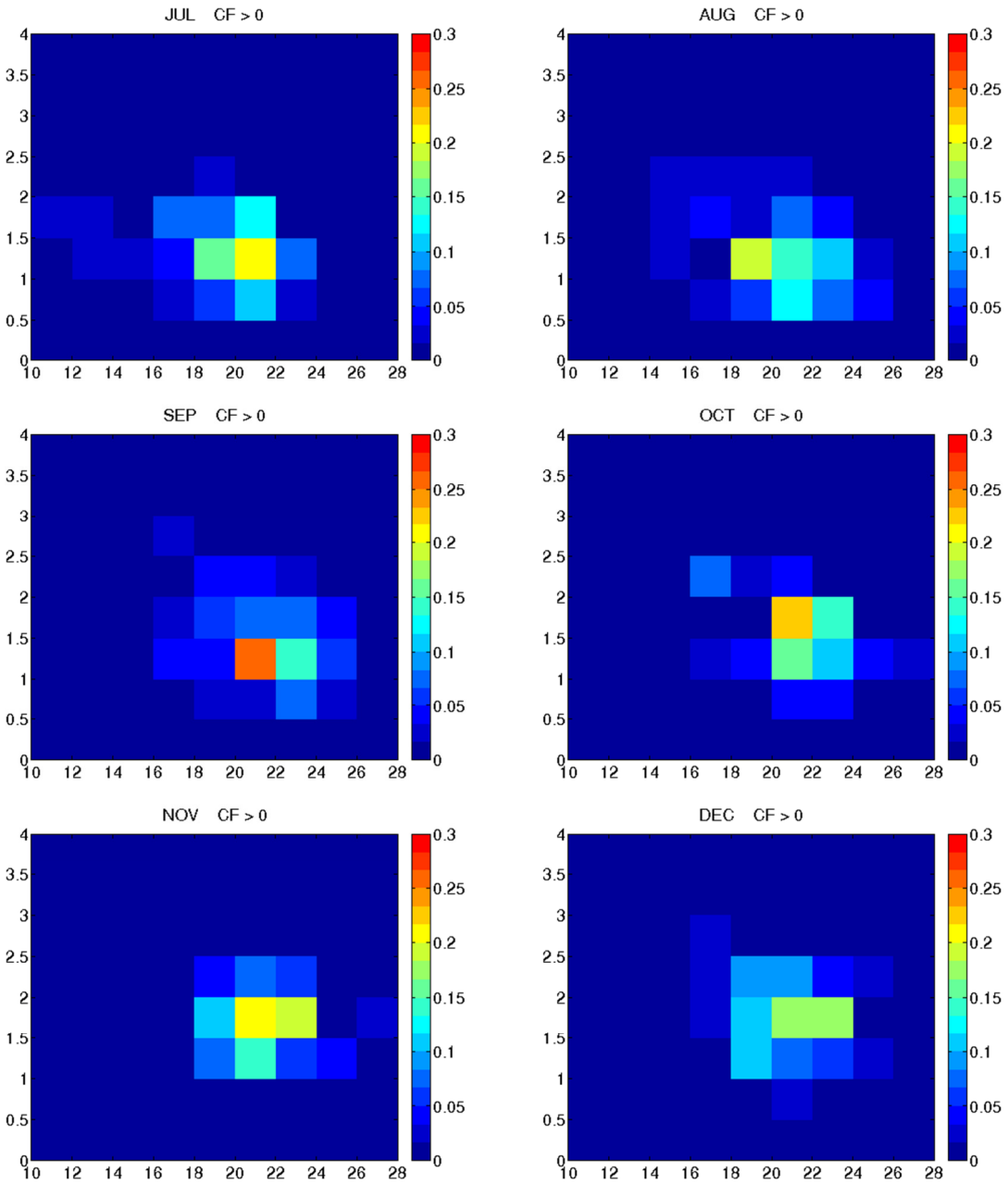
JUL CF > 0
AUG CF > 0
SEP CF > 0
OCT CF > 0
NOV CF > 0
DEC CF > 0

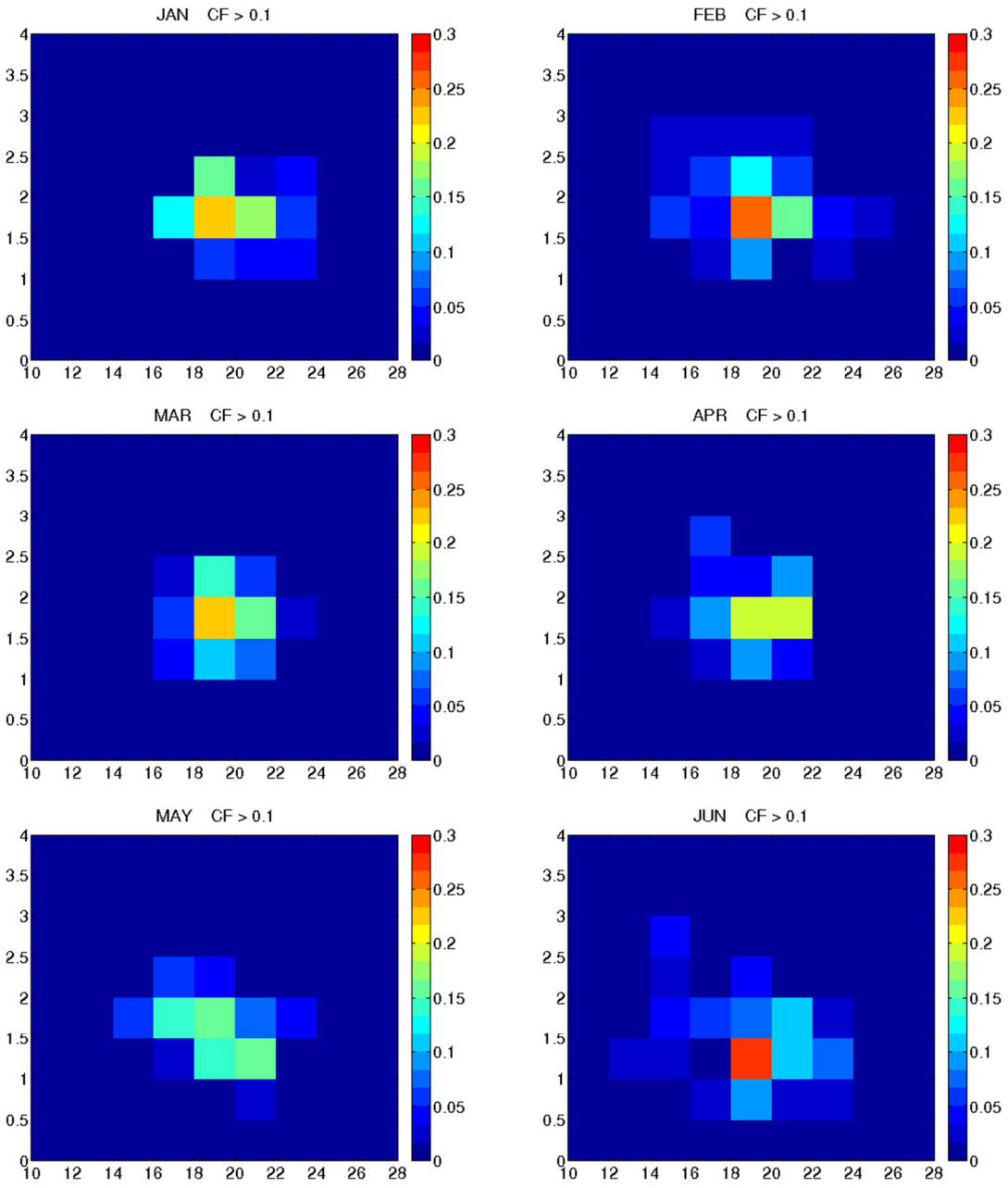
JAN CF > 0.1
FEB CF > 0.1
MAR CF > 0.1
APR CF > 0.1
MAY CF > 0.1
JUN CF > 0.1
0 0.5 1 1.5 2 2.5 3 3.5 4
10 12 14 16 18 20 22 24 26 28
0 0.05 0.1 0.15 0.2 0.25 0.3

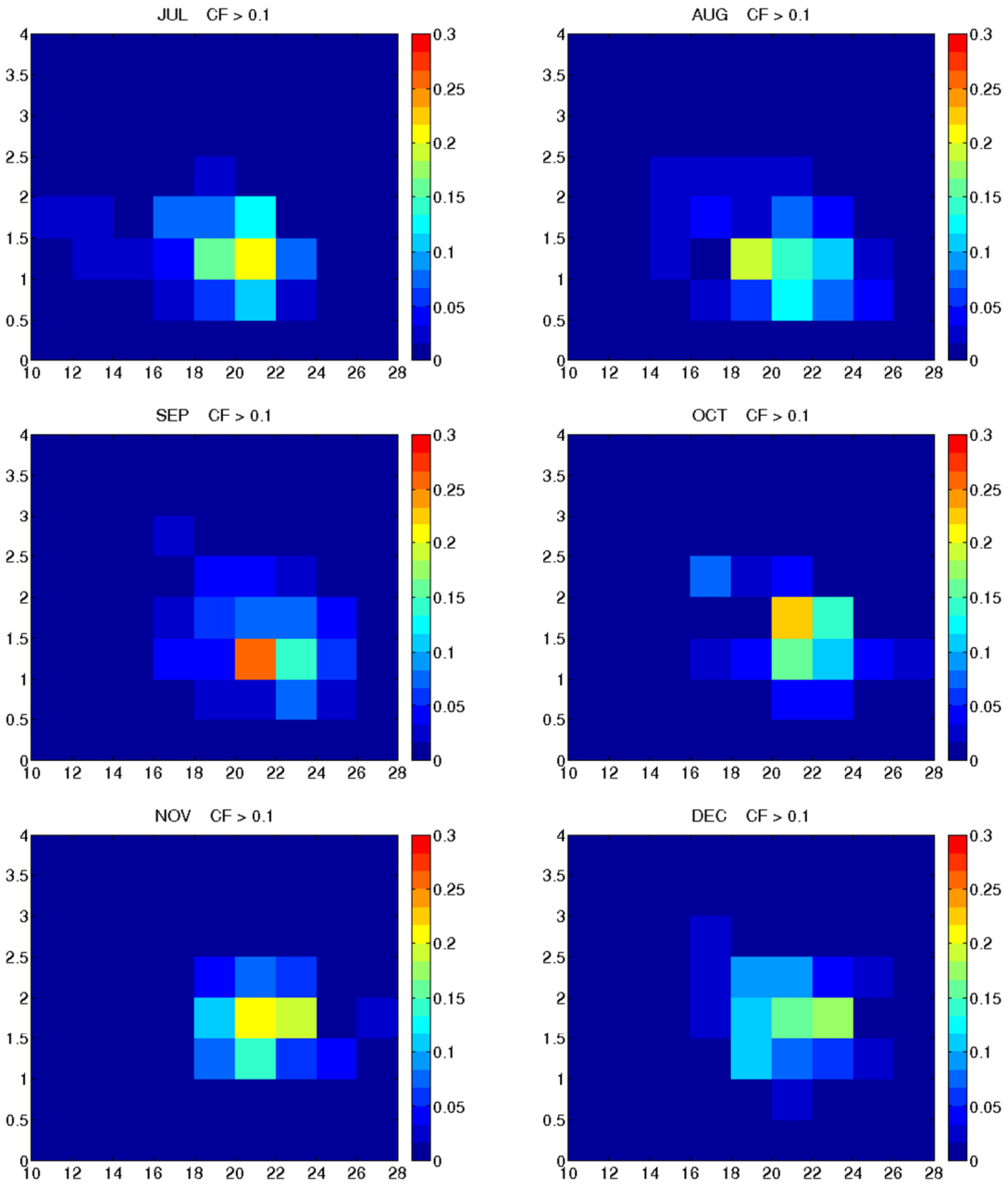
JUL CF > 0.1
AUG CF > 0.1
SEP CF > 0.1
OCT CF > 0.1
NOV CF > 0.1
DEC CF > 0.1
0 0.5 1 1.5 2 2.5 3 3.5 4
10 12 14 16 18 20 22 24 26 28
0 0.05 0.1 0.15 0.2 0.25 0.3

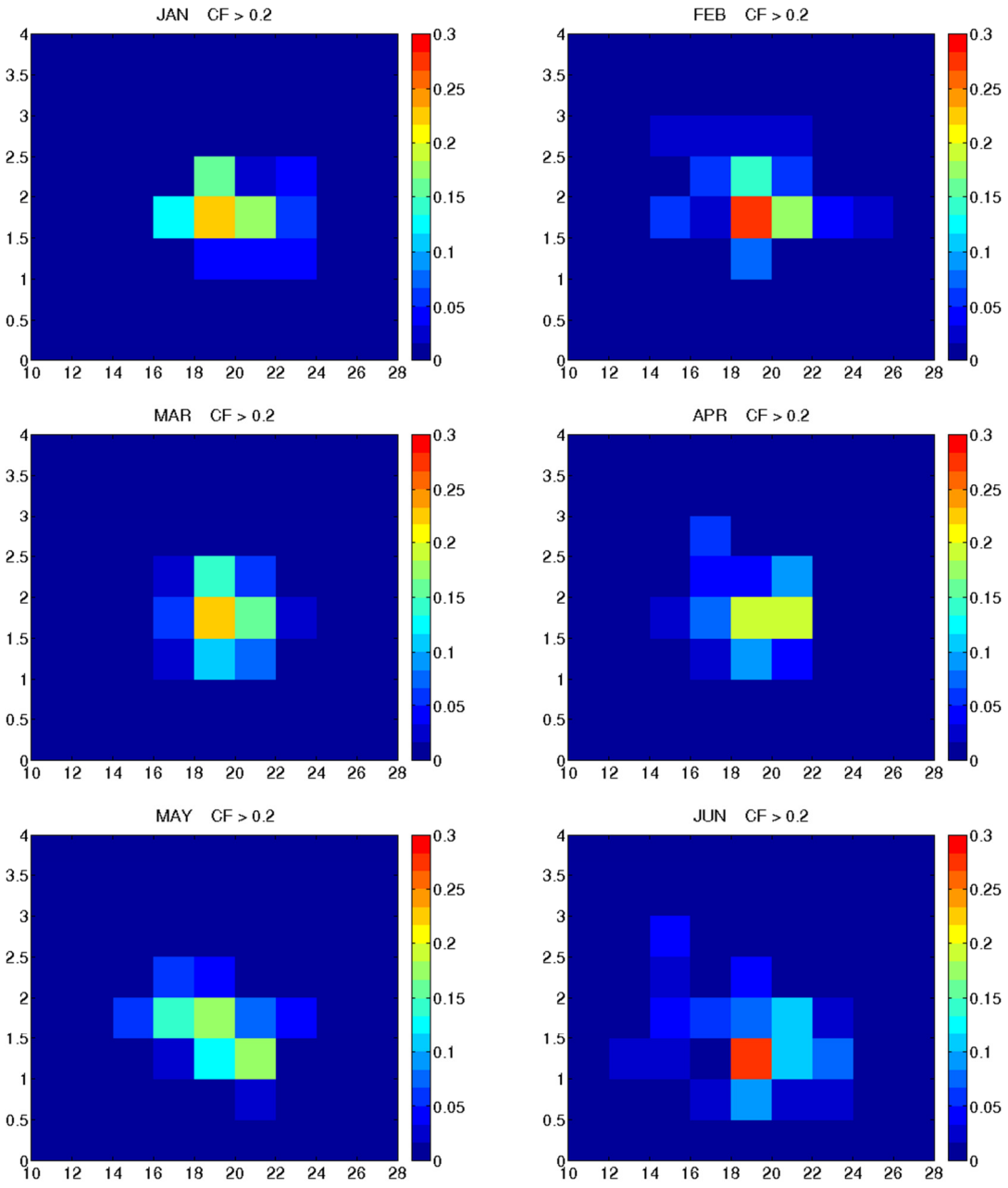
JAN CF > 0.2
FEB CF > 0.2
MAR CF > 0.2
APR CF > 0.2
MAY CF > 0.2
JUN CF > 0.2
0 0.5 1 1.5 2 2.5 3 3.5 4
10 12 14 16 18 20 22 24 26 28
0 0.05 0.1 0.15 0.2 0.25 0.3

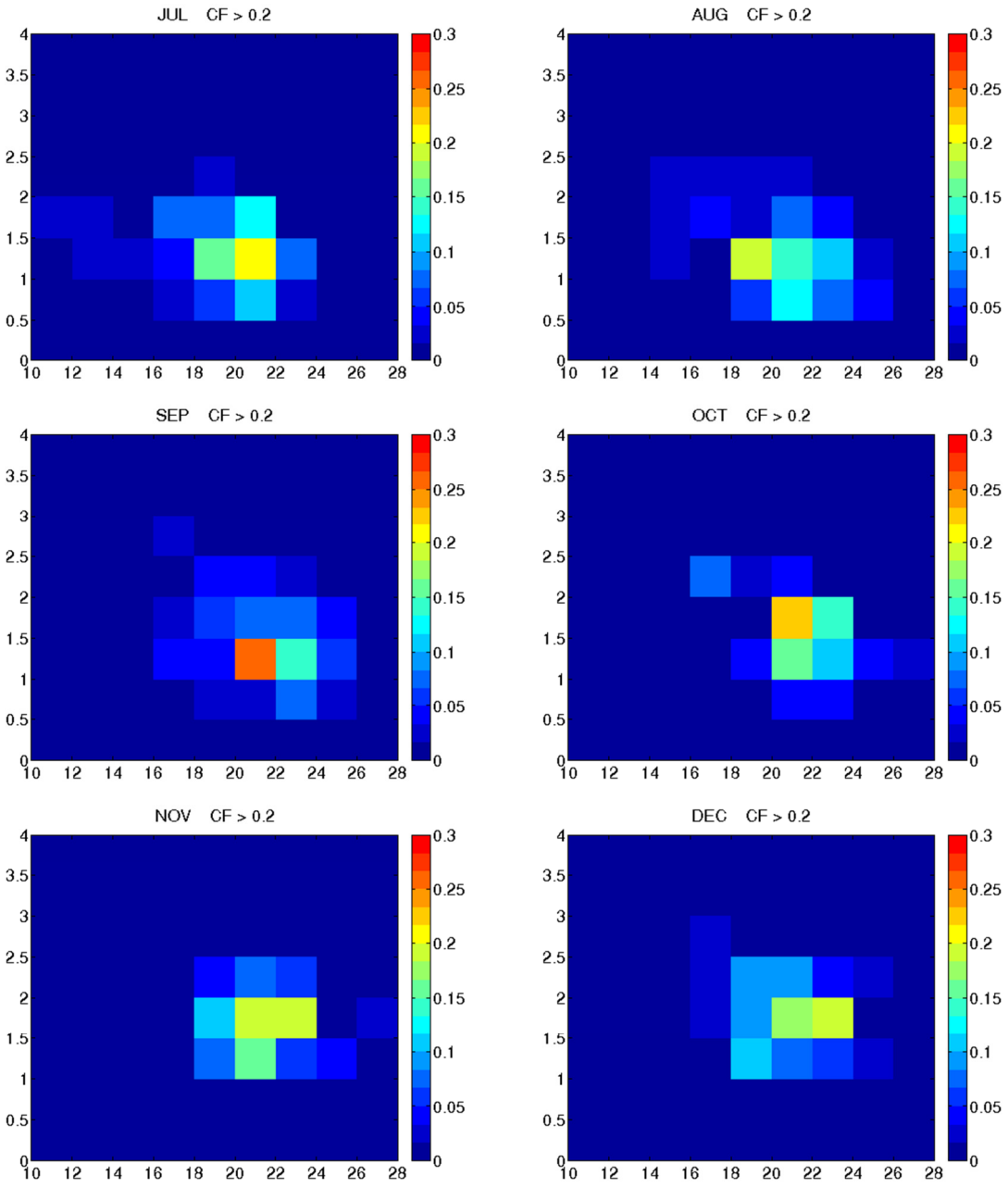
JUL CF > 0.2
AUG CF > 0.2
SEP CF > 0.2
OCT CF > 0.2
NOV CF > 0.2
DEC CF > 0.2
0 0.5 1 1.5 2 2.5 3 3.5 4
10 12 14 16 18 20 22 24 26 28
0 0.05 0.1 0.15 0.2 0.25 0.3

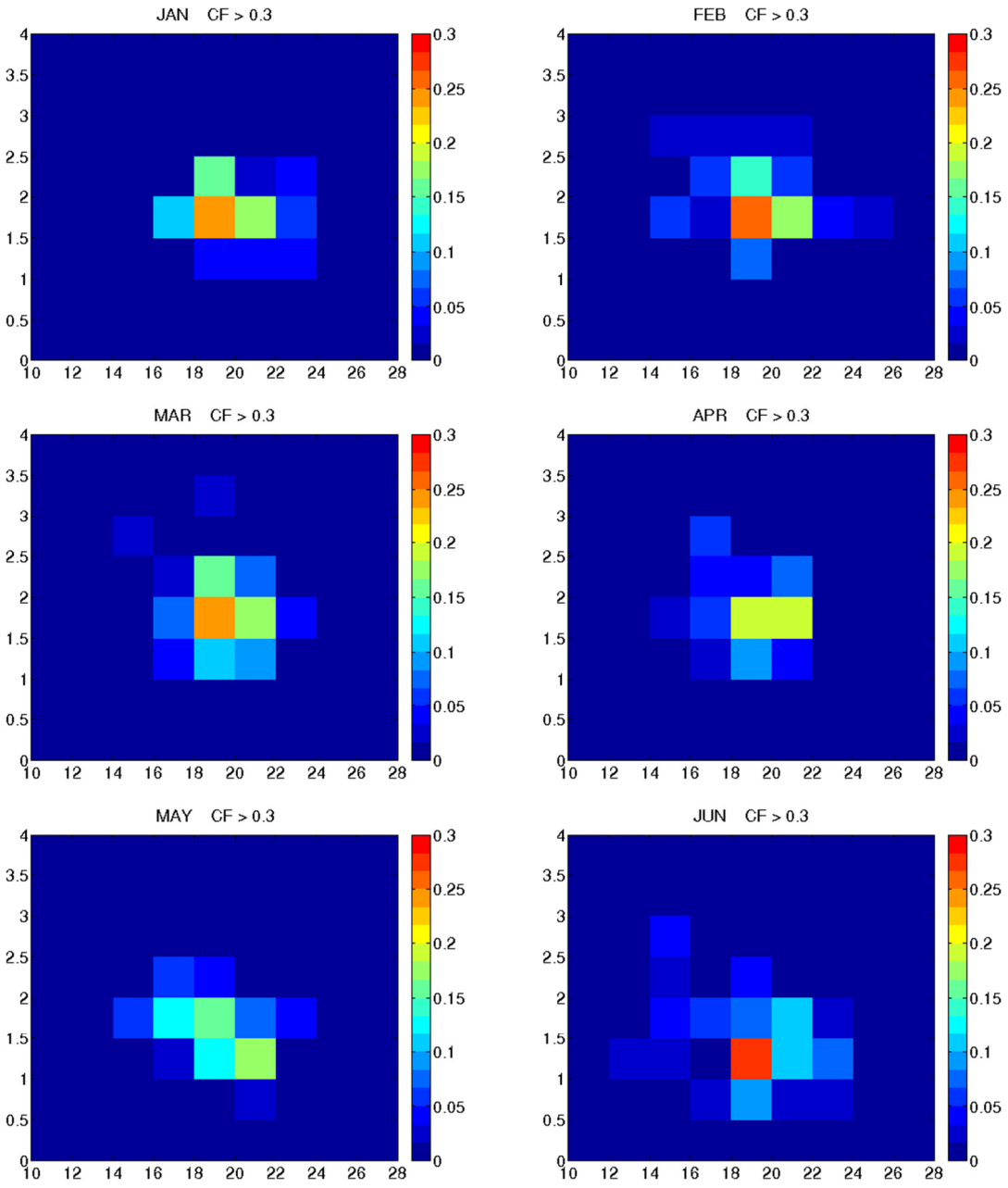
JAN CF > 0.3
FEB CF > 0.3
MAR CF > 0.3
APR CF > 0.3
MAY CF > 0.3
JUN CF > 0.3
0 0.5 1 1.5 2 2.5 3 3.5 4
10 12 14 16 18 20 22 24 26 28
0 0.05 0.1 0.15 0.2 0.25 0.3

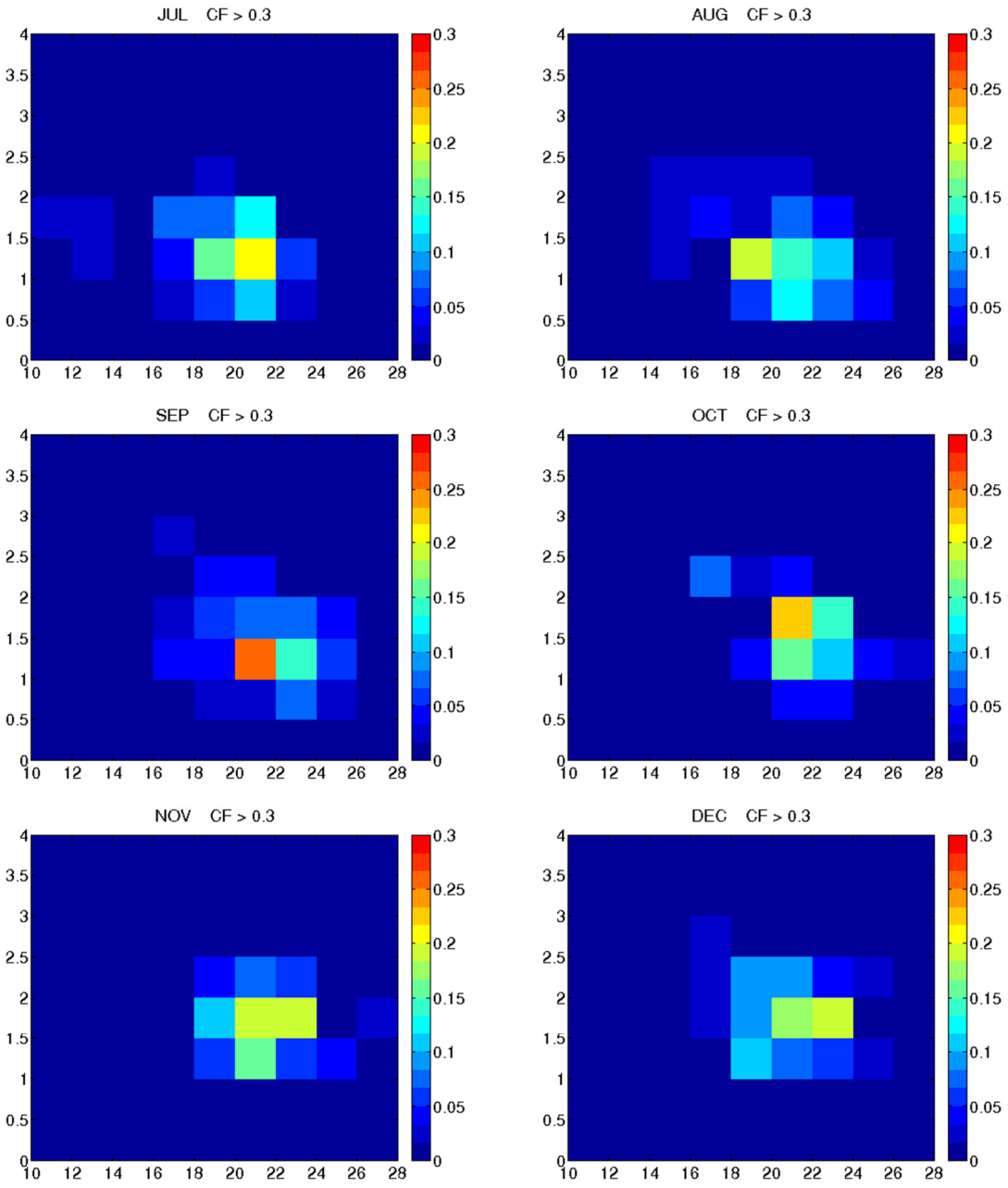
JUL CF > 0.3
AUG CF > 0.3
SEP CF > 0.3
OCT CF > 0.3
NOV CF > 0.3
DEC CF > 0.3
0 0.5 1 1.5 2 2.5 3 3.5 4
10 12 14 16 18 20 22 24 26 28
0 0.05 0.1 0.15 0.2 0.25 0.3

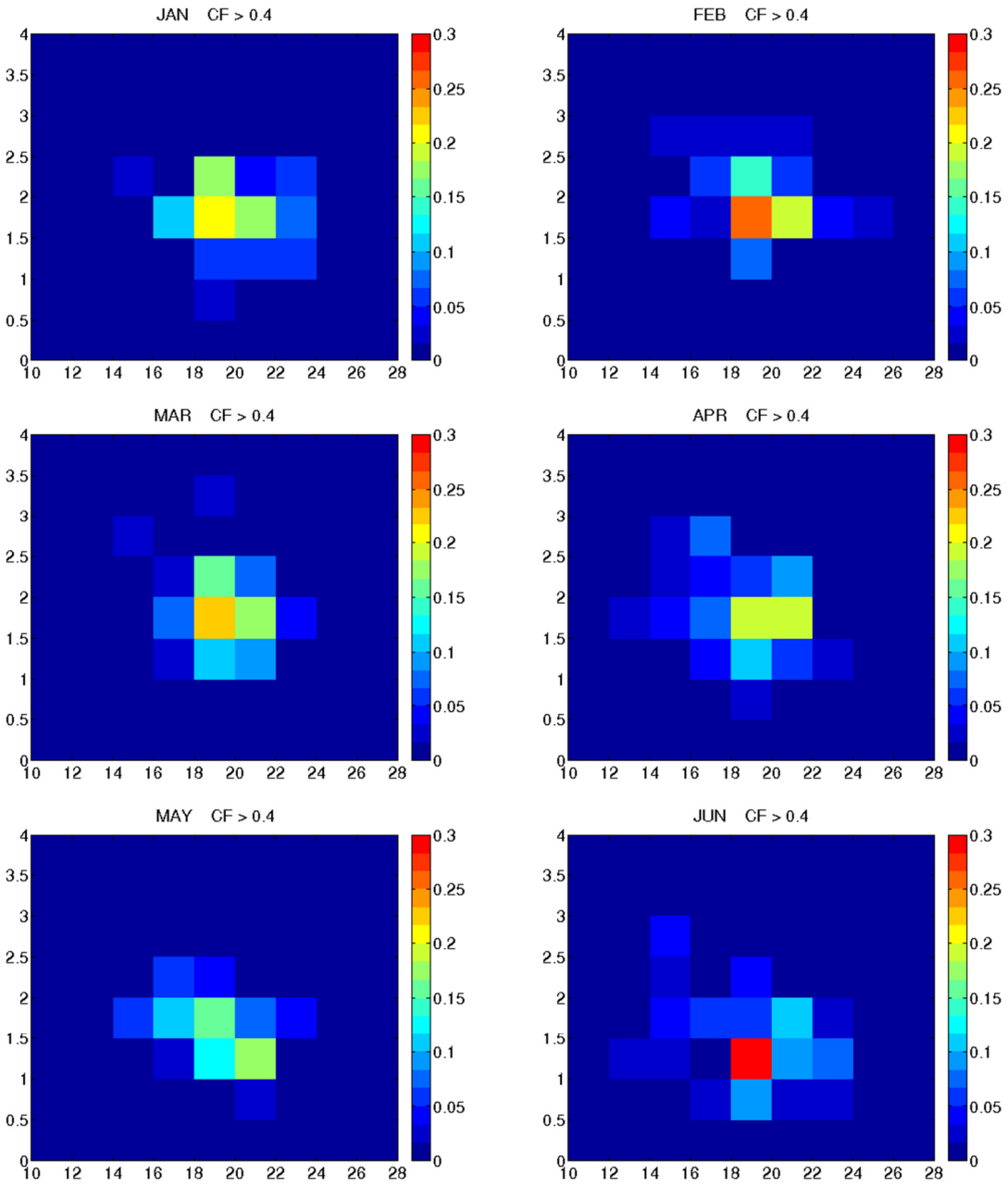
JAN CF > 0.4
FEB CF > 0.4
MAR CF > 0.4
APR CF > 0.4
MAY CF > 0.4
JUN CF > 0.4
0 0.5 1 1.5 2 2.5 3 3.5 4
10 12 14 16 18 20 22 24 26 28
0 0.05 0.1 0.15 0.2 0.25 0.3

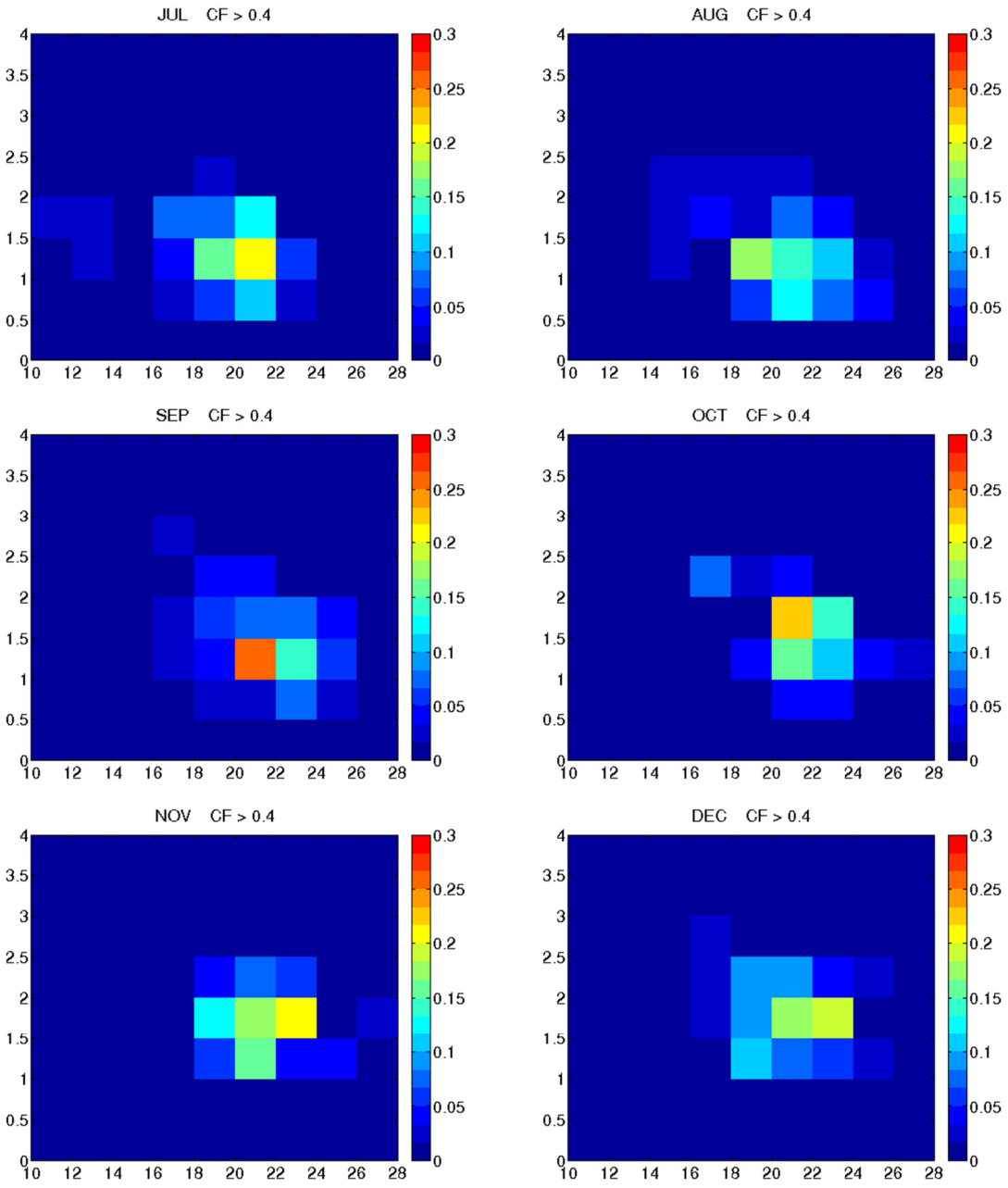
JUL CF > 0.4
AUG CF > 0.4
SEP CF > 0.4
OCT CF > 0.4
NOV CF > 0.4
DEC CF > 0.4
0 0.5 1 1.5 2 2.5 3 3.5 4
10 12 14 16 18 20 22 24 26 28
0 0.05 0.1 0.15 0.2 0.25 0.3

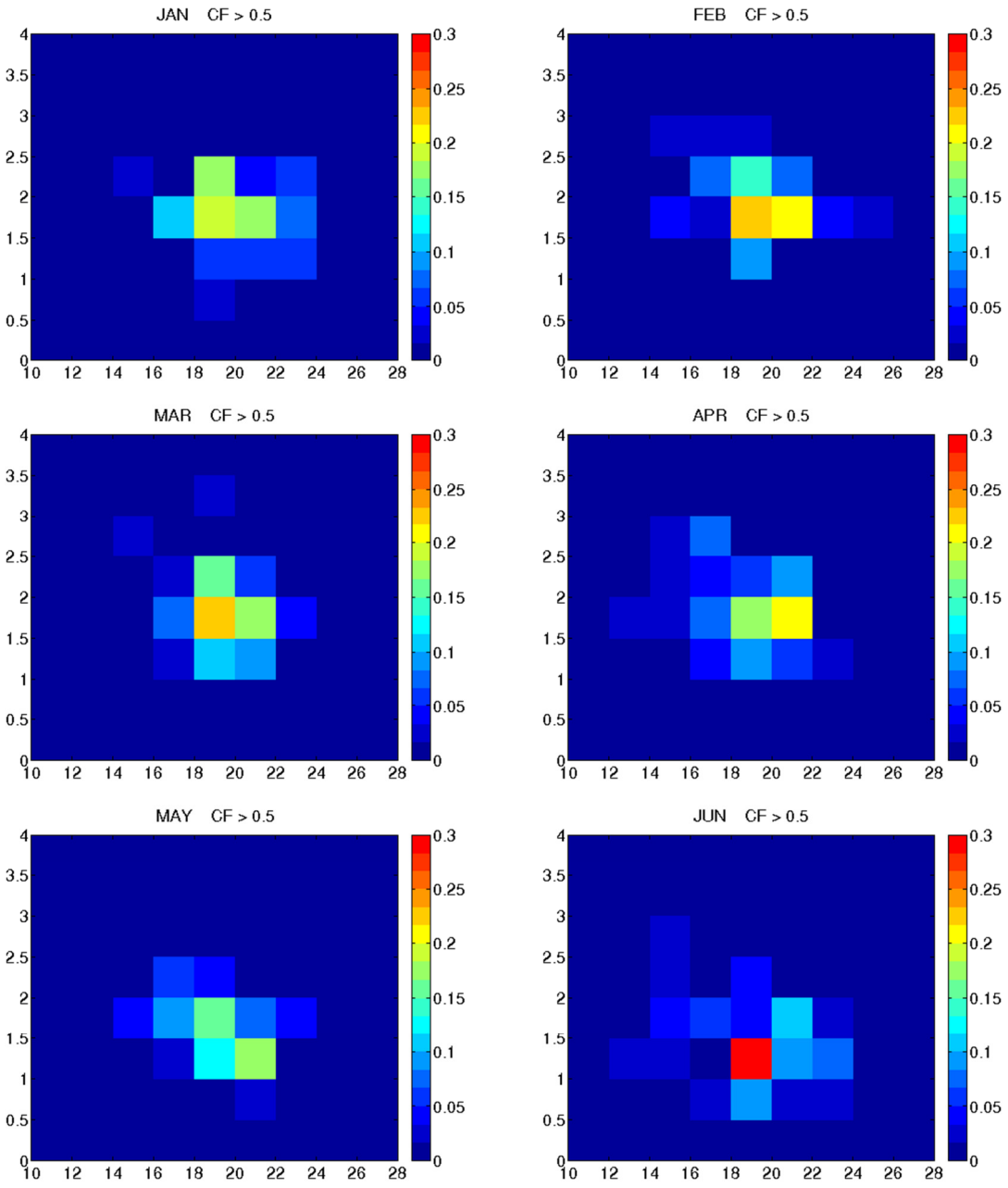
JAN CF > 0.5
FEB CF > 0.5
MAR CF > 0.5
APR CF > 0.5
MAY CF > 0.5
JUN CF > 0.5
0 0.5 1 1.5 2 2.5 3 3.5 4
10 12 14 16 18 20 22 24 26 28
0 0.05 0.1 0.15 0.2 0.25 0.3

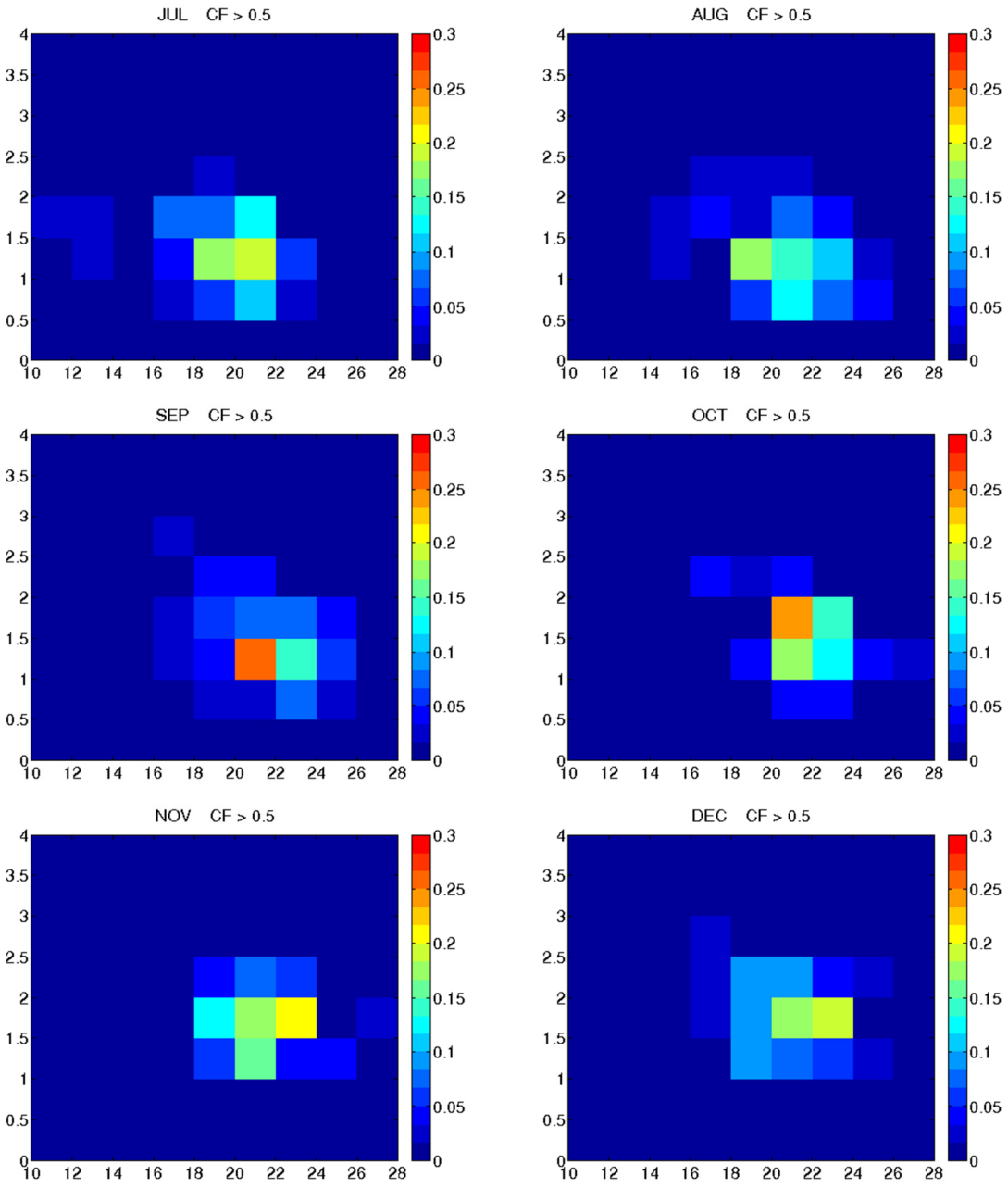
JUL CF > 0.5
AUG CF > 0.5
SEP CF > 0.5
OCT CF > 0.5
NOV CF > 0.5
DEC CF > 0.5
0 0.5 1 1.5 2 2.5 3 3.5 4
10 12 14 16 18 20 22 24 26 28
0 0.05 0.1 0.15 0.2 0.25 0.3

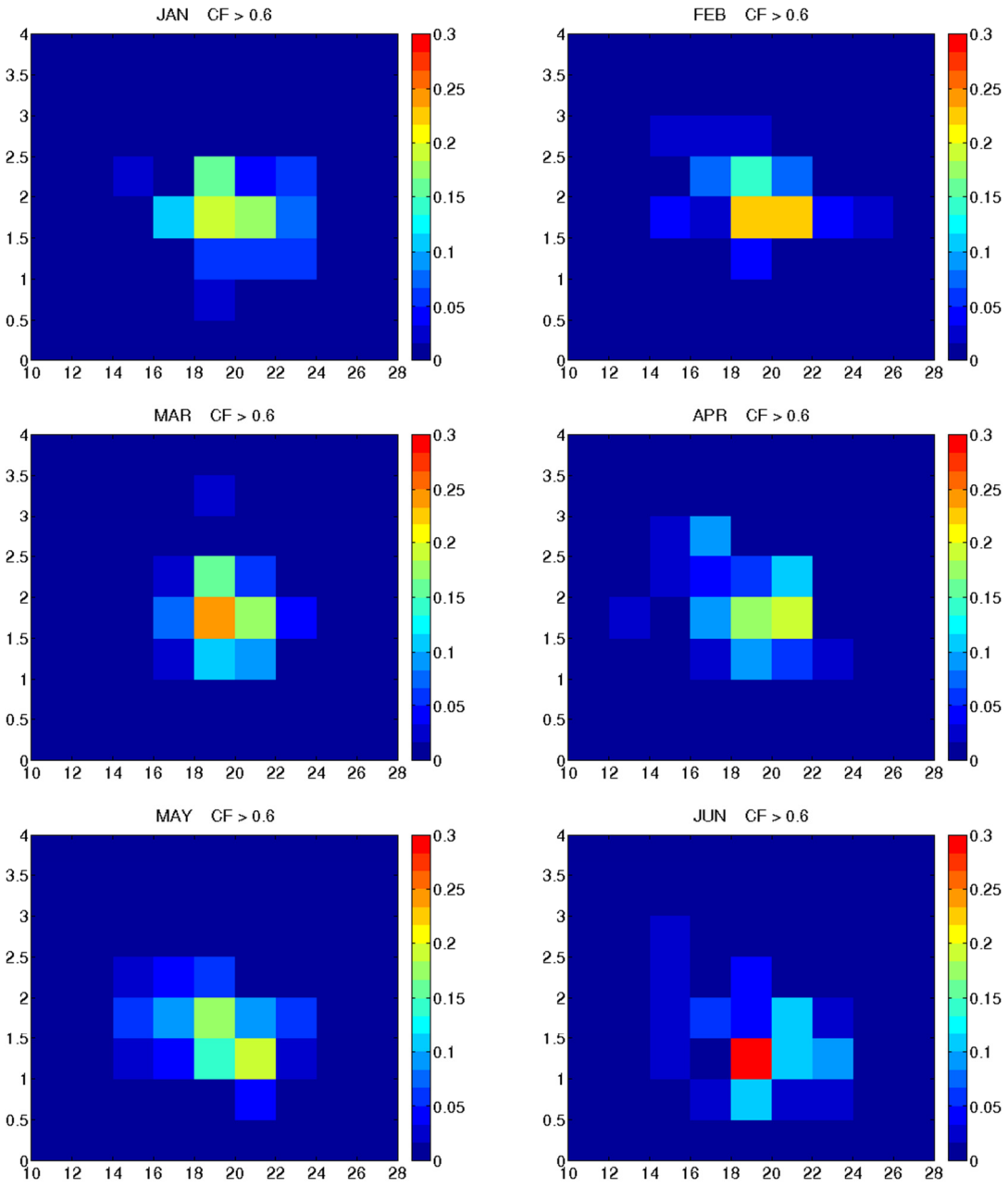
JAN CF > 0.6
FEB CF > 0.6
MAR CF > 0.6
APR CF > 0.6
MAY CF > 0.6
JUN CF > 0.6
0 0.5 1 1.5 2 2.5 3 3.5 4
10 12 14 16 18 20 22 24 26 28
0 0.05 0.1 0.15 0.2 0.25 0.3

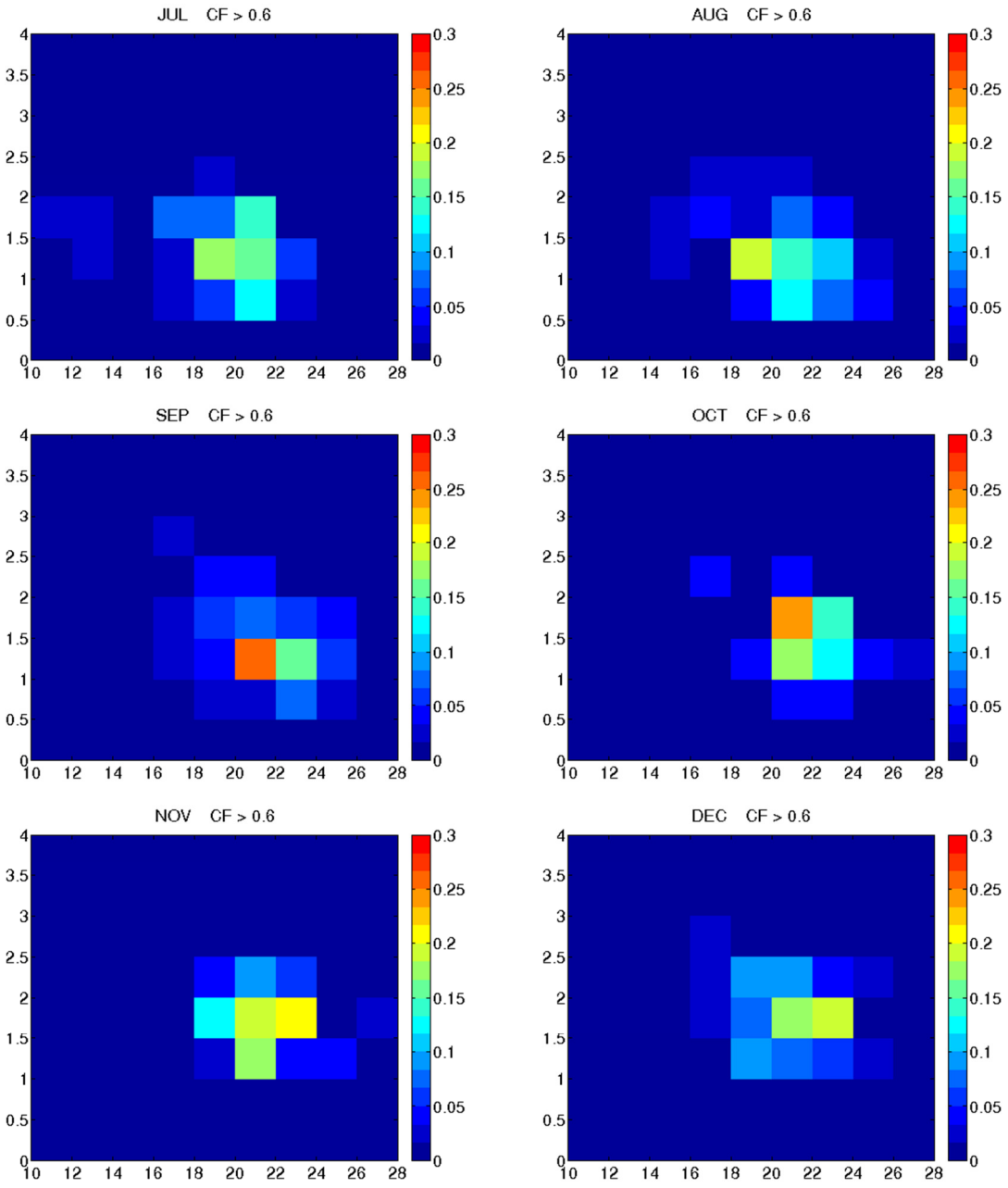
JUL CF > 0.6
AUG CF > 0.6
SEP CF > 0.6
OCT CF > 0.6
NOV CF > 0.6
DEC CF > 0.6
0 0.5 1 1.5 2 2.5 3 3.5 4
10 12 14 16 18 20 22 24 26 28
0 0.05 0.1 0.15 0.2 0.25 0.3

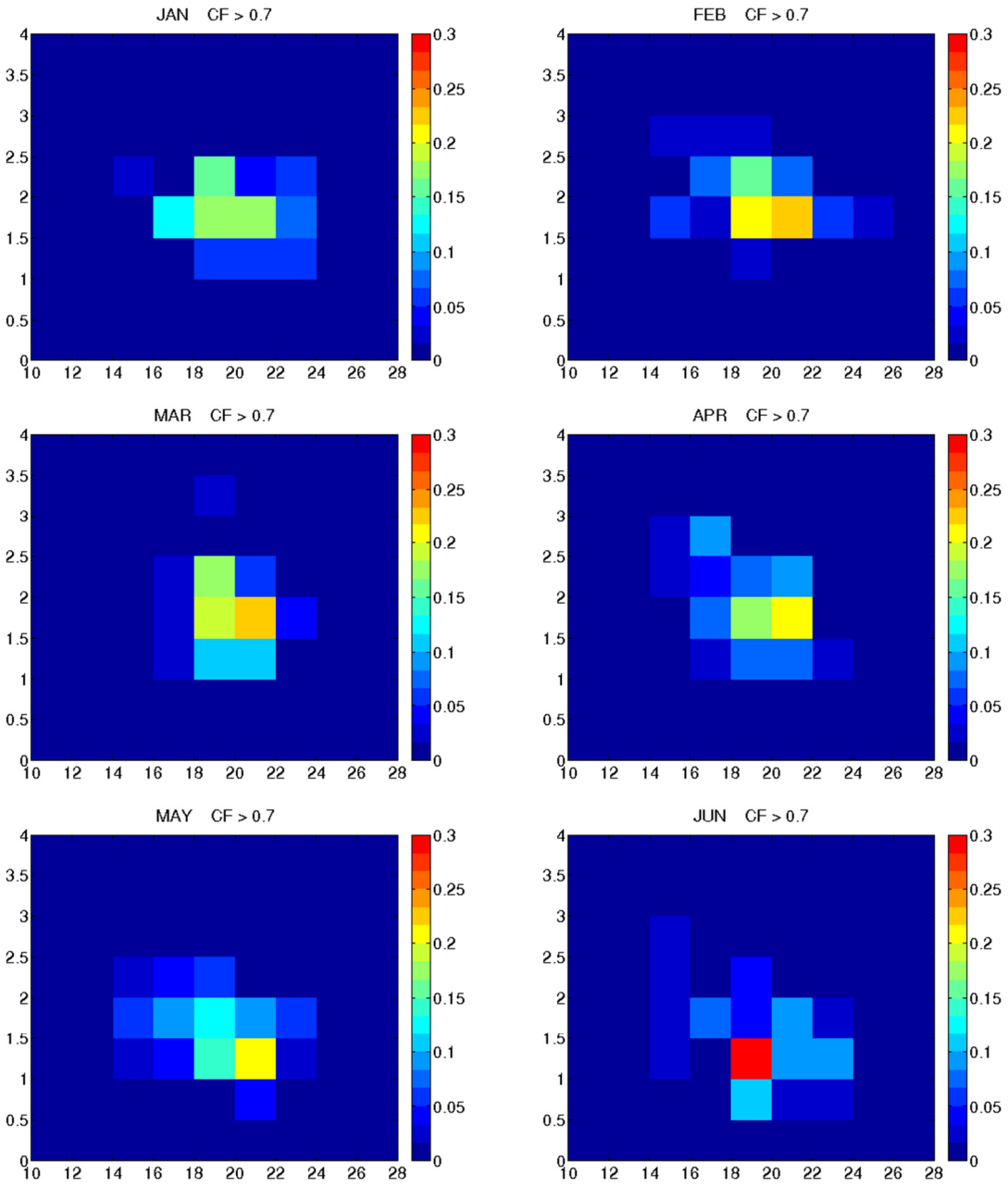
JAN CF > 0.7
FEB CF > 0.7
MAR CF > 0.7
APR CF > 0.7
MAY CF > 0.7
JUN CF > 0.7
0 0.5 1 1.5 2 2.5 3 3.5 4
10 12 14 16 18 20 22 24 26 28
0 0.05 0.1 0.15 0.2 0.25 0.3

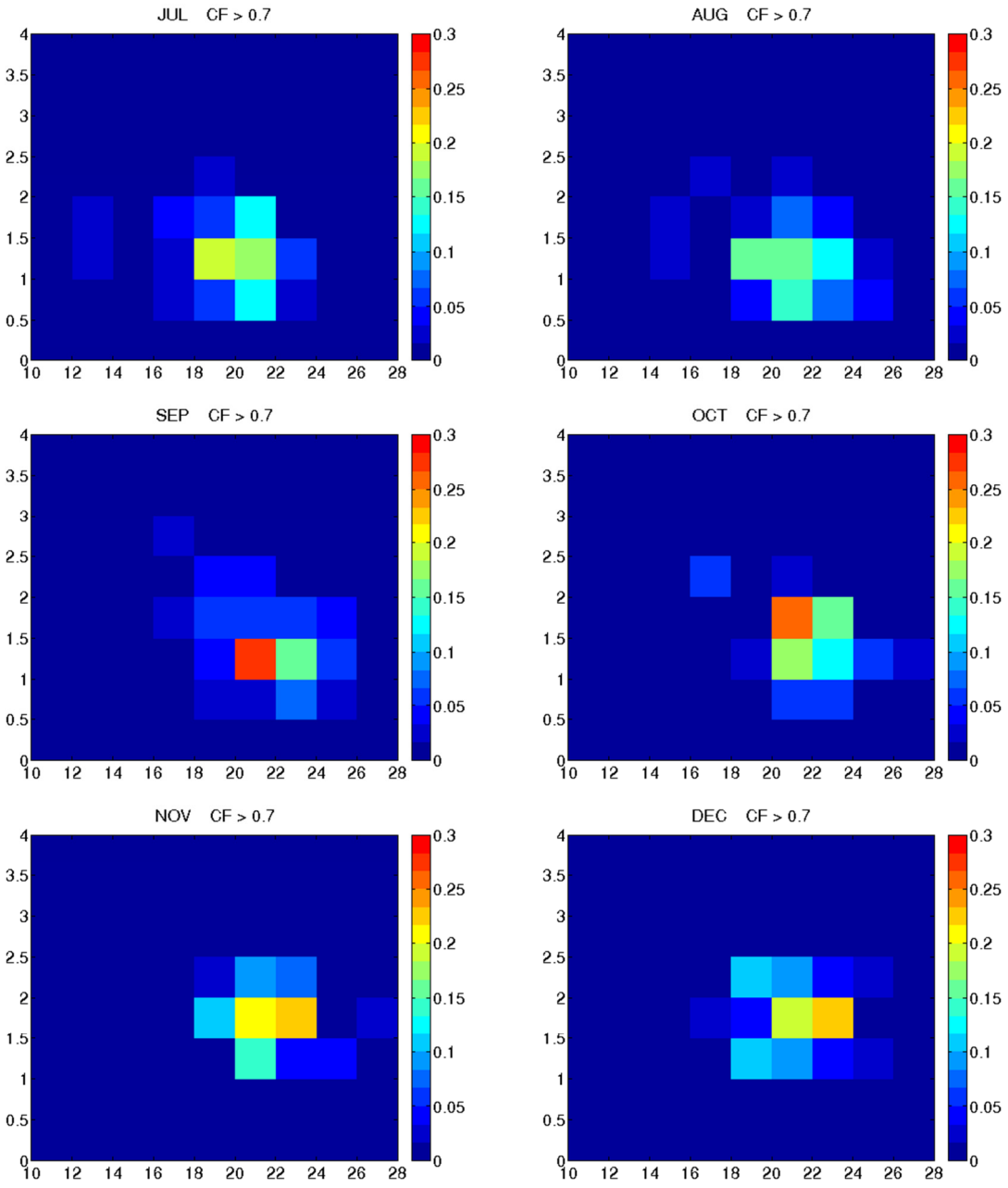
JUL CF > 0.7
AUG CF > 0.7
SEP CF > 0.7
OCT CF > 0.7
NOV CF > 0.7
DEC CF > 0.7
0 0.5 1 1.5 2 2.5 3 3.5 4
10 12 14 16 18 20 22 24 26 28
0 0.05 0.1 0.15 0.2 0.25 0.3

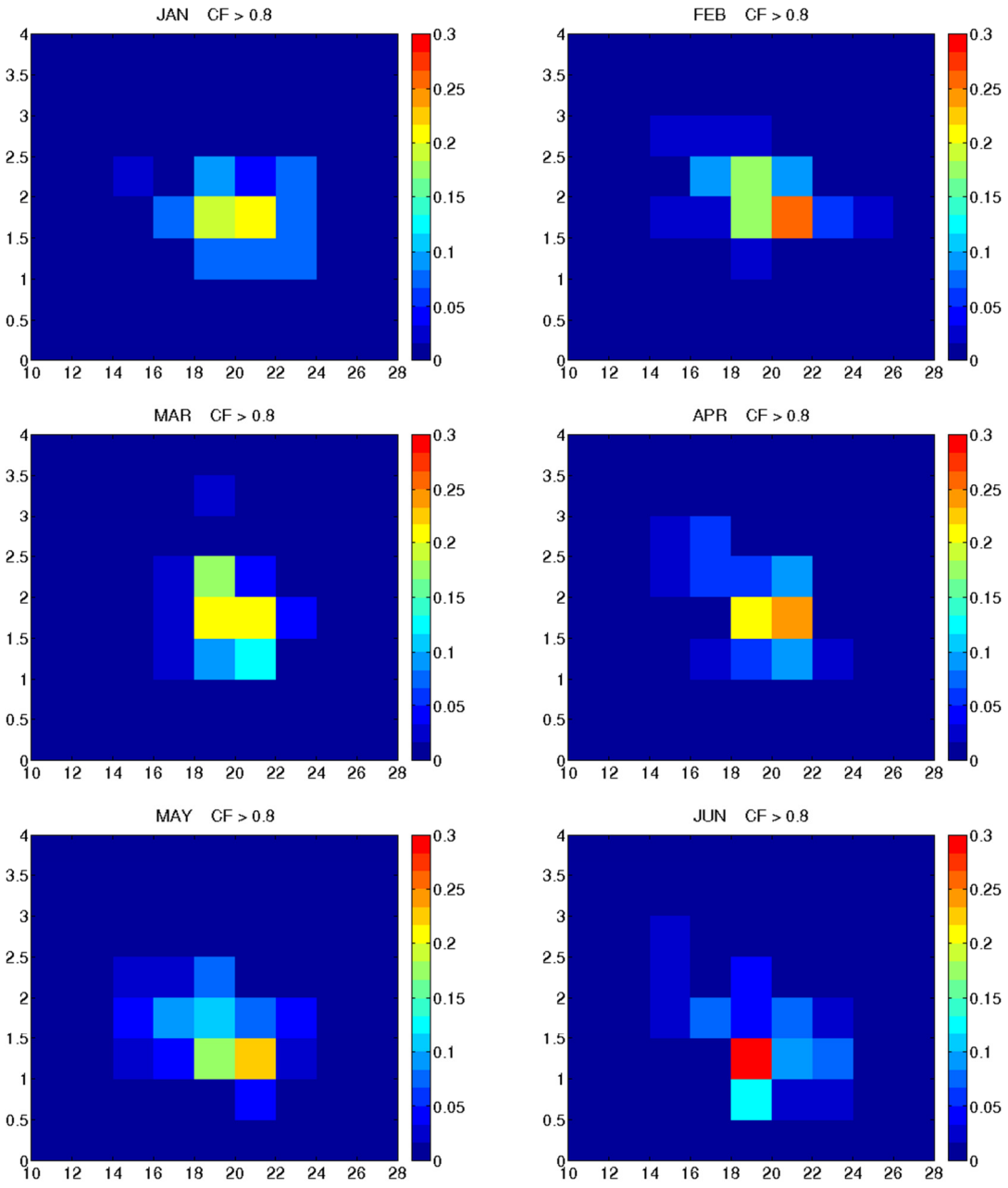
JAN CF > 0.8
FEB CF > 0.8
MAR CF > 0.8
APR CF > 0.8
MAY CF > 0.8
JUN CF > 0.8
0 0.5 1 1.5 2 2.5 3 3.5 4
10 12 14 16 18 20 22 24 26 28
0 0.05 0.1 0.15 0.2 0.25 0.3

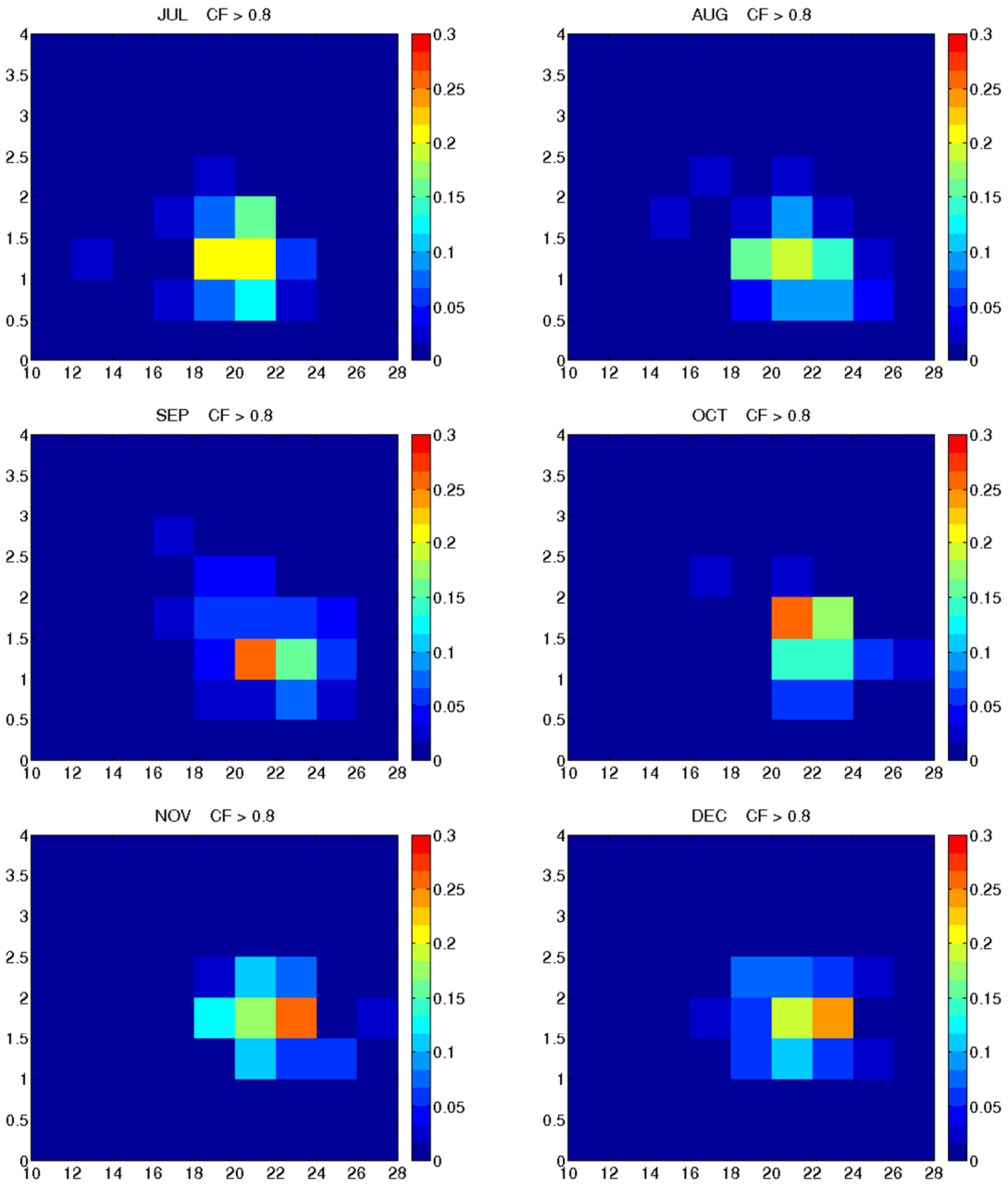
JUL CF > 0.8
AUG CF > 0.8
SEP CF > 0.8
OCT CF > 0.8
NOV CF > 0.8
DEC CF > 0.8
0 0.5 1 1.5 2 2.5 3 3.5 4
10 12 14 16 18 20 22 24 26 28
0 0.05 0.1 0.15 0.2 0.25 0.3

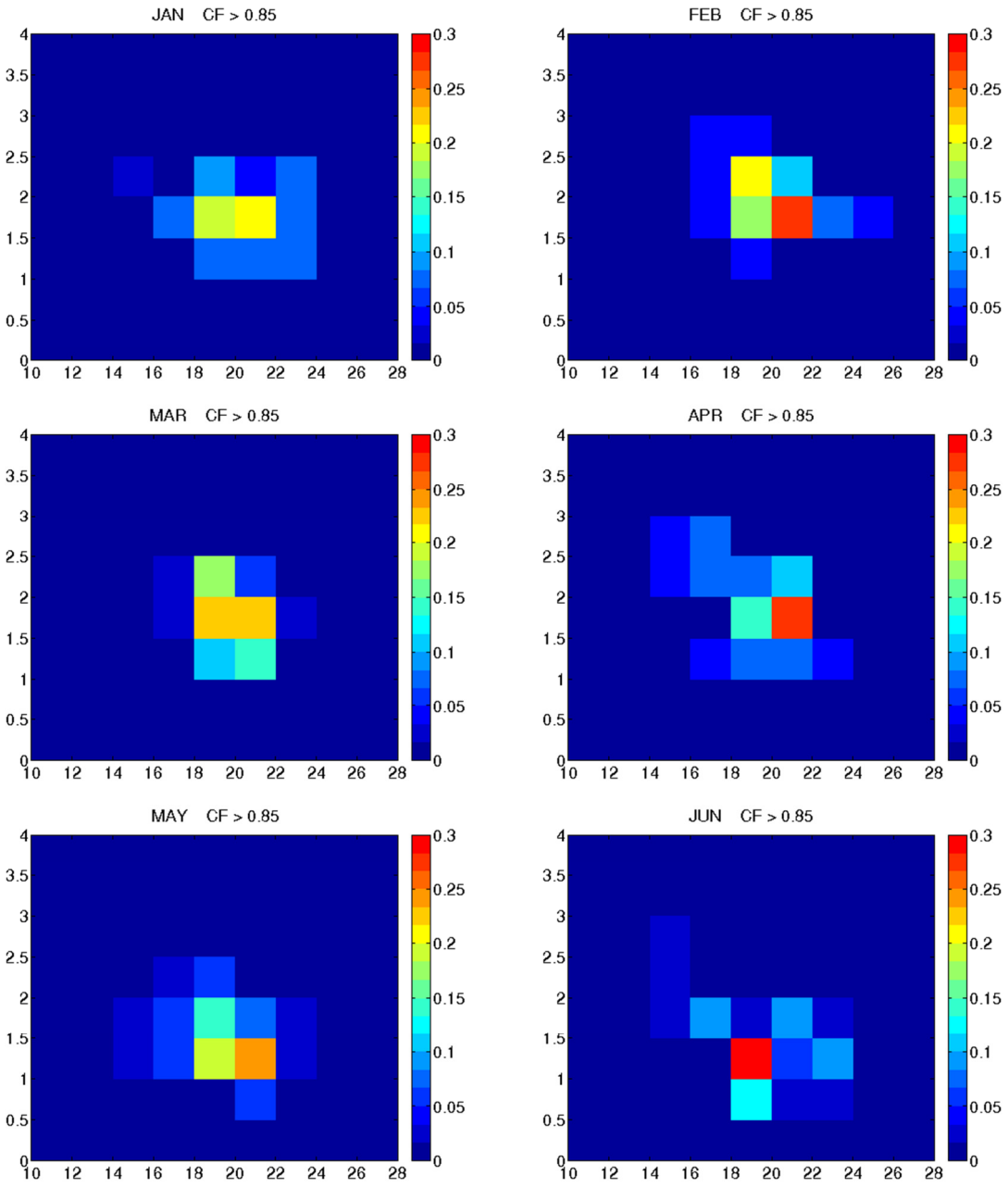
JAN CF > 0.85
FEB CF > 0.85
MAR CF > 0.85
APR CF > 0.85
MAY CF > 0.85
JUN CF > 0.85
0 0.5 1 1.5 2 2.5 3 3.5 4
10 12 14 16 18 20 22 24 26 28
0 0.05 0.1 0.15 0.2 0.25 0.3

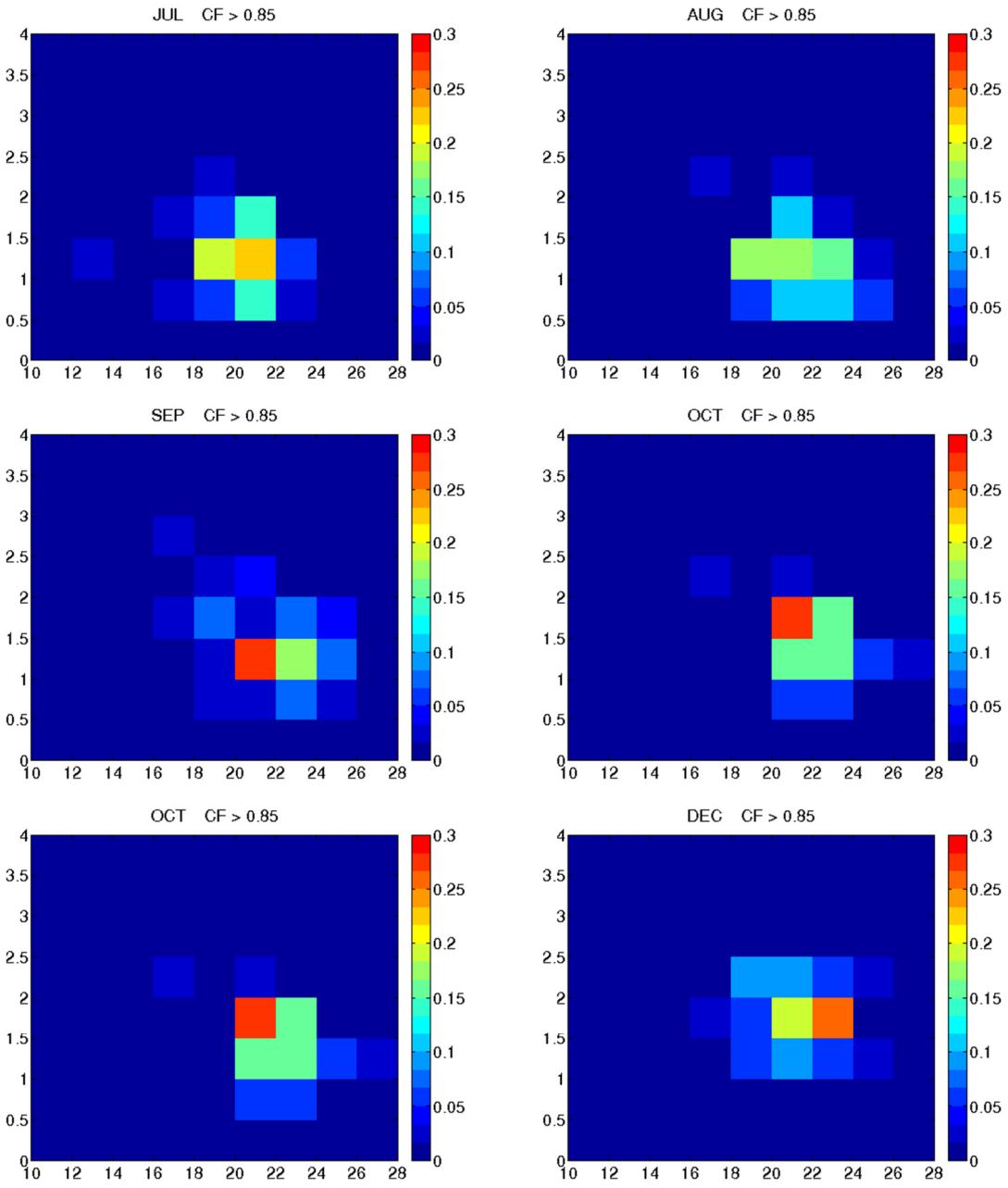
JUL CF > 0.85
AUG CF > 0.85
SEP CF > 0.85
OCT CF > 0.85
OCT CF > 0.85
DEC CF > 0.85

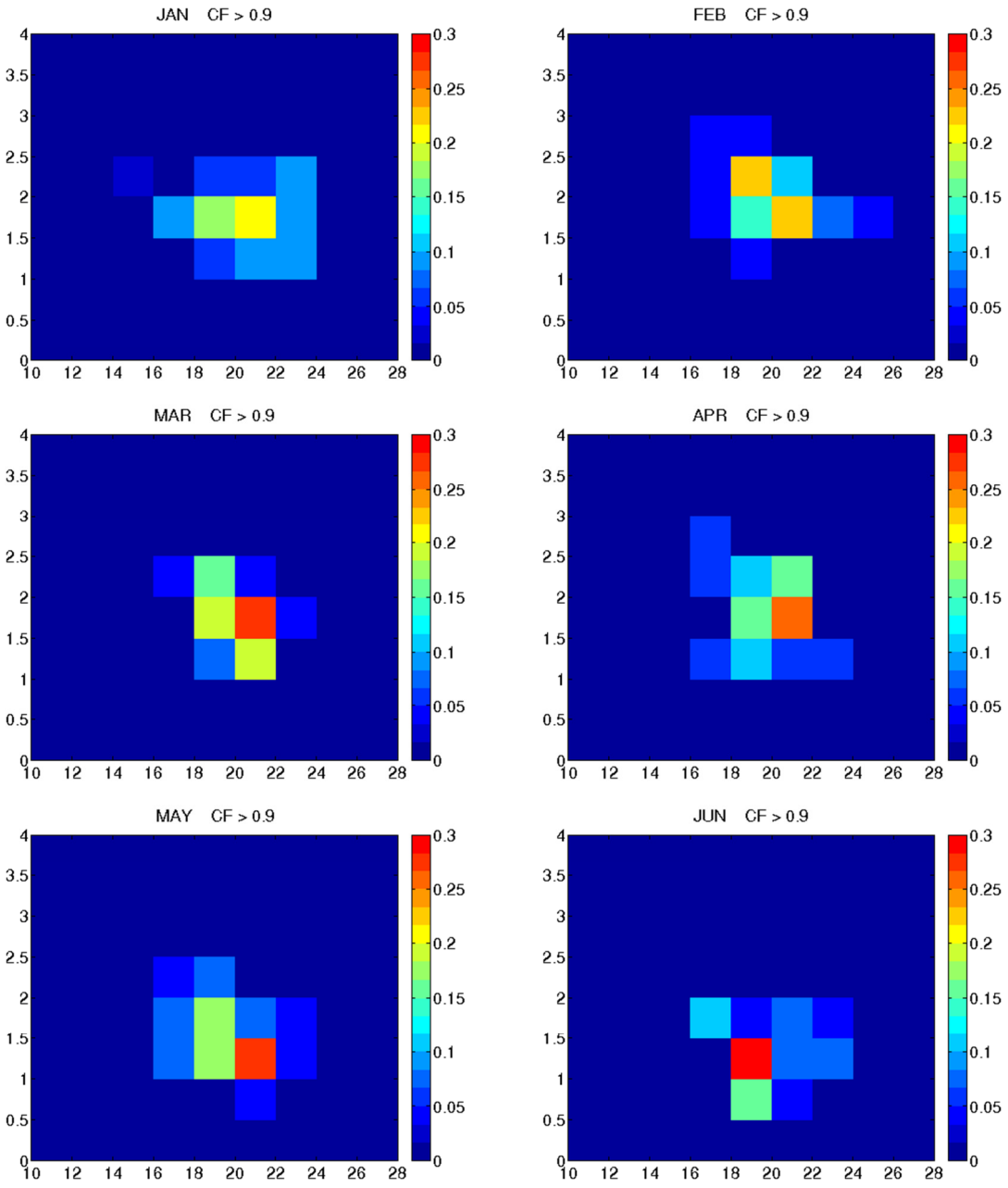
JAN CF > 0.9
FEB CF > 0.9
MAR CF > 0.9
APR CF > 0.9
MAY CF > 0.9
JUN CF > 0.9
0 0.5 1 1.5 2 2.5 3 3.5 4
10 12 14 16 18 20 22 24 26 28
0 0.05 0.1 0.15 0.2 0.25 0.3

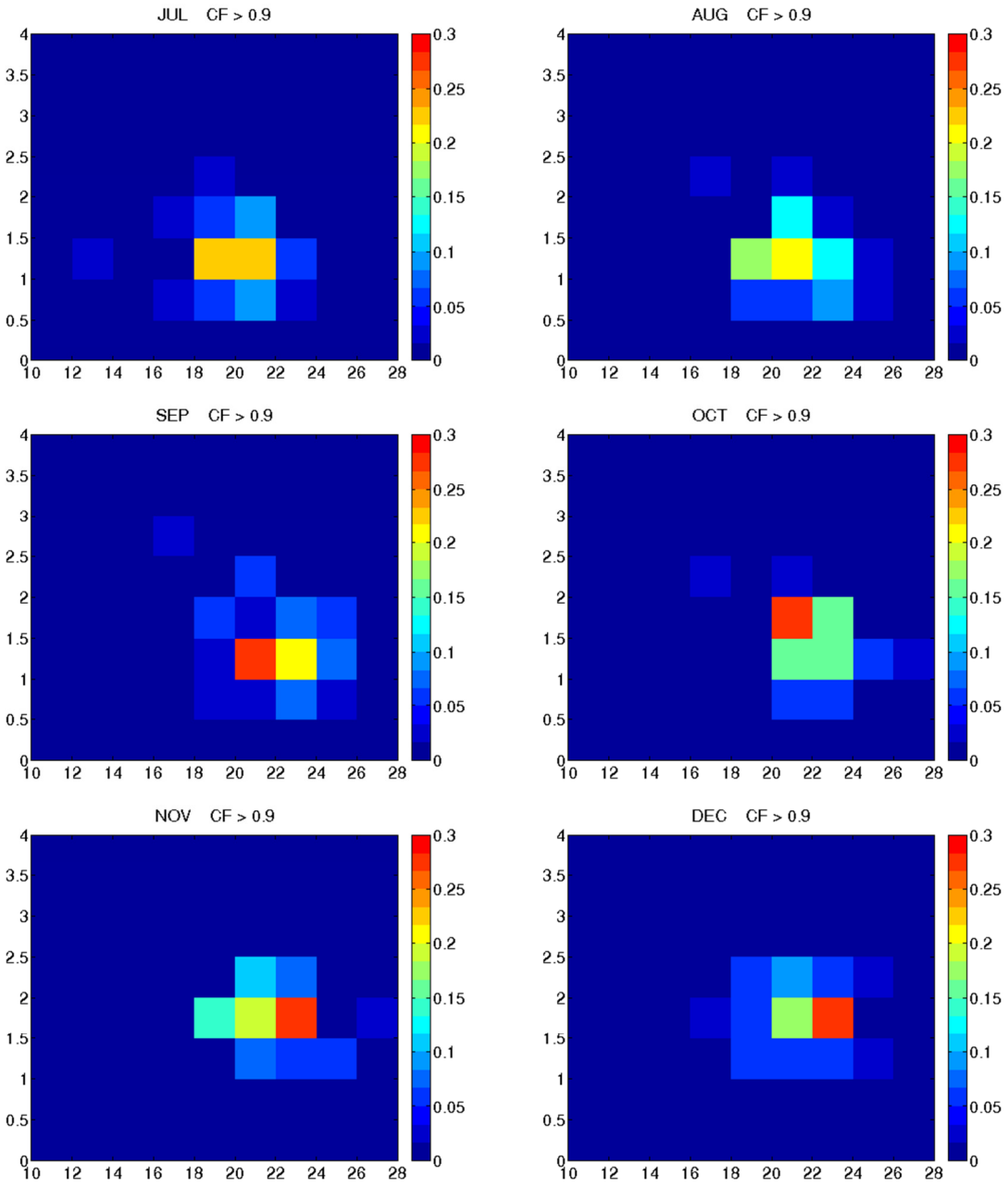
JUL CF > 0.9
AUG CF > 0.9
SEP CF > 0.9
OCT CF > 0.9
NOV CF > 0.9
DEC CF > 0.9
0 0.5 1 1.5 2 2.5 3 3.5 4
10 12 14 16 18 20 22 24 26 28
0 0.05 0.1 0.15 0.2 0.25 0.3

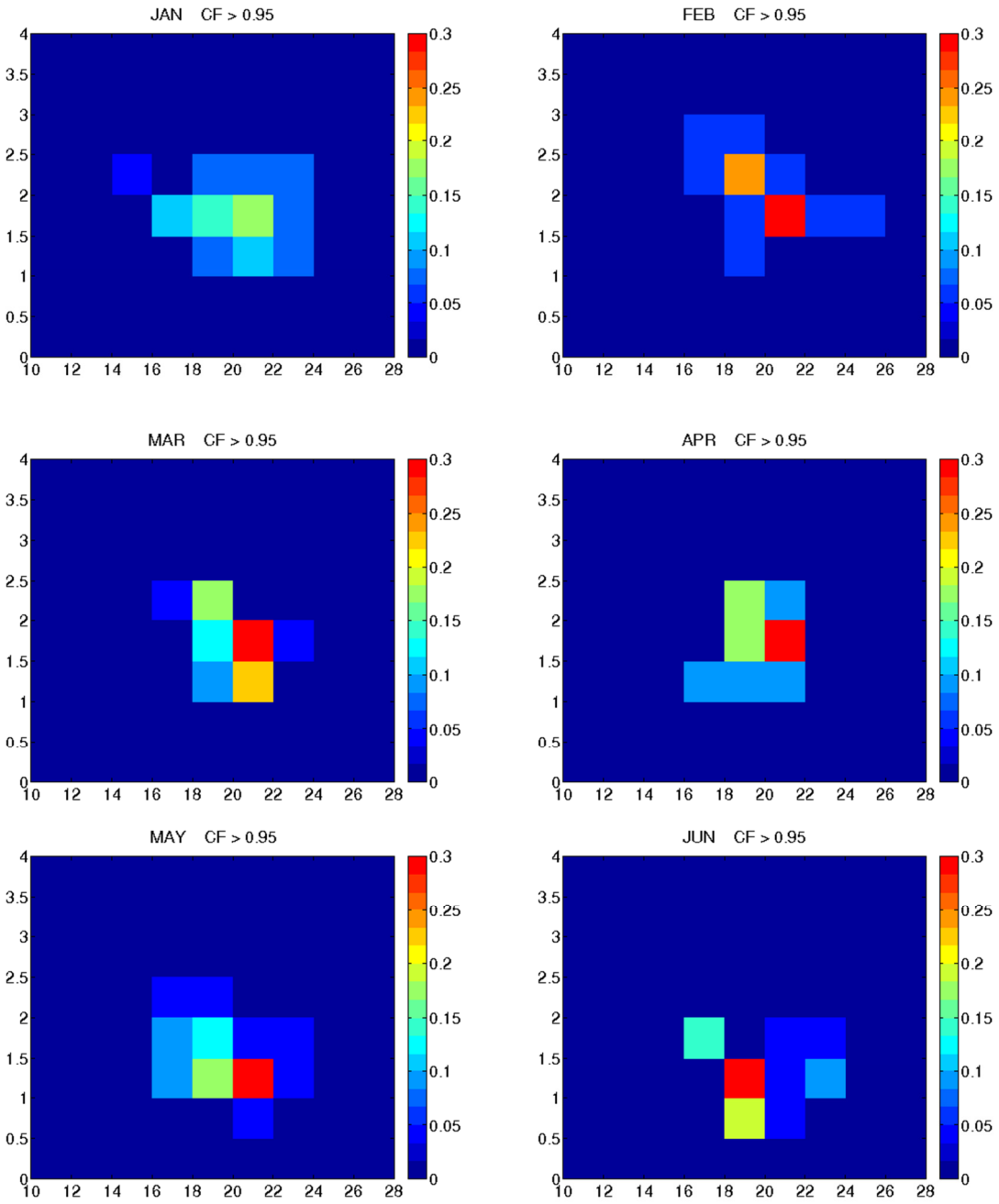
JAN CF > 0.95
FEB CF > 0.95
MAR CF > 0.95
APR CF > 0.95
MAY CF > 0.95
JUN CF > 0.95
0 0.5 1 1.5 2 2.5 3 3.5 4
10 12 14 16 18 20 22 24 26 28
0 0.05 0.1 0.15 0.2 0.25 0.3

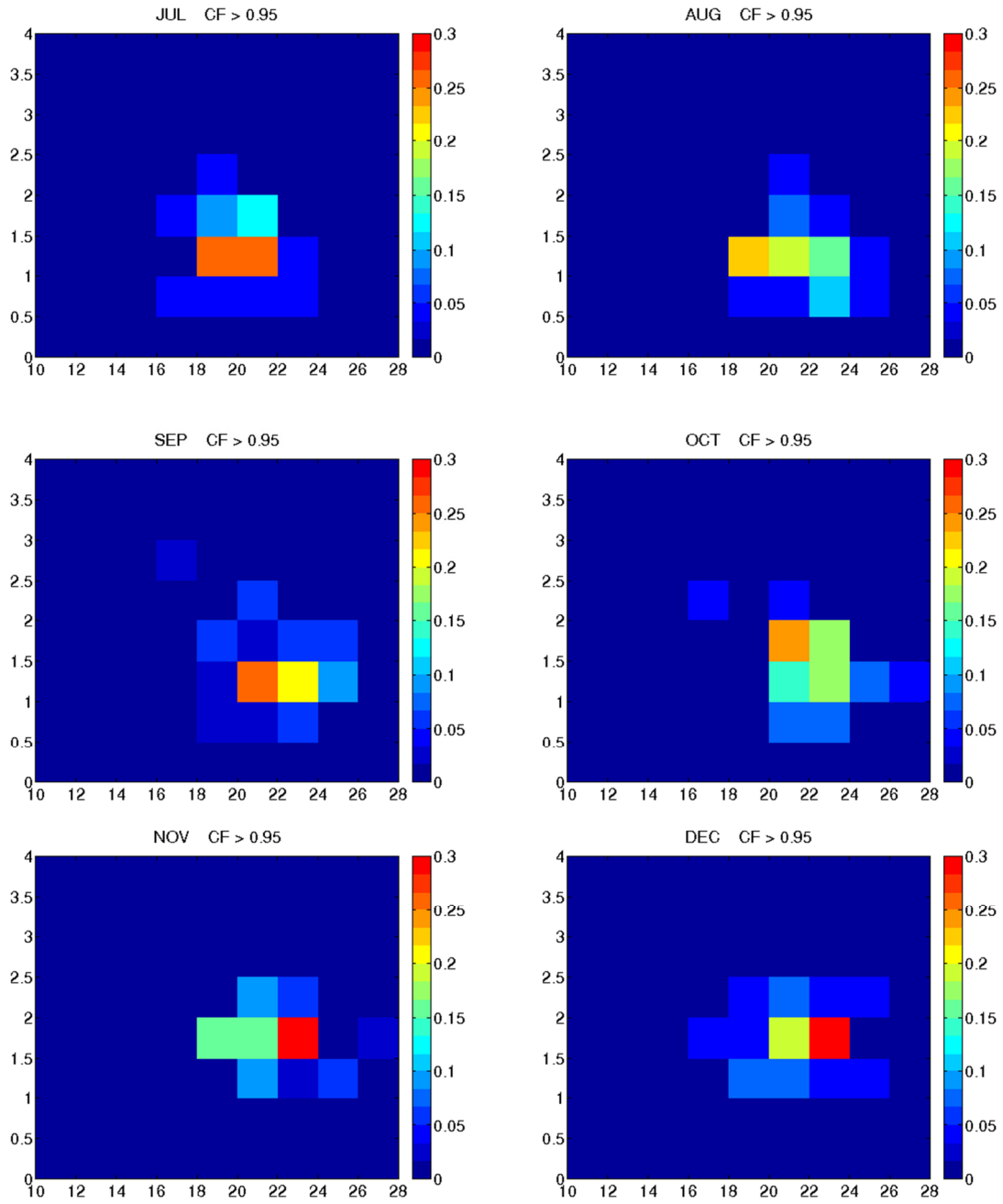
JUL CF > 0.95
AUG CF > 0.95
SEP CF > 0.95
OCT CF > 0.95
NOV CF > 0.95
DEC CF > 0.95

Appendix B

These figures show monthly normalized 2-dimensional histograms at 25°N, 125°W of cloud fraction and cloud top height with LTS within a certain range. Cloud data are from MISR and have been degraded as in Appendix A. Since some LTS ranges result in a sample size of zero, these have been excluded.

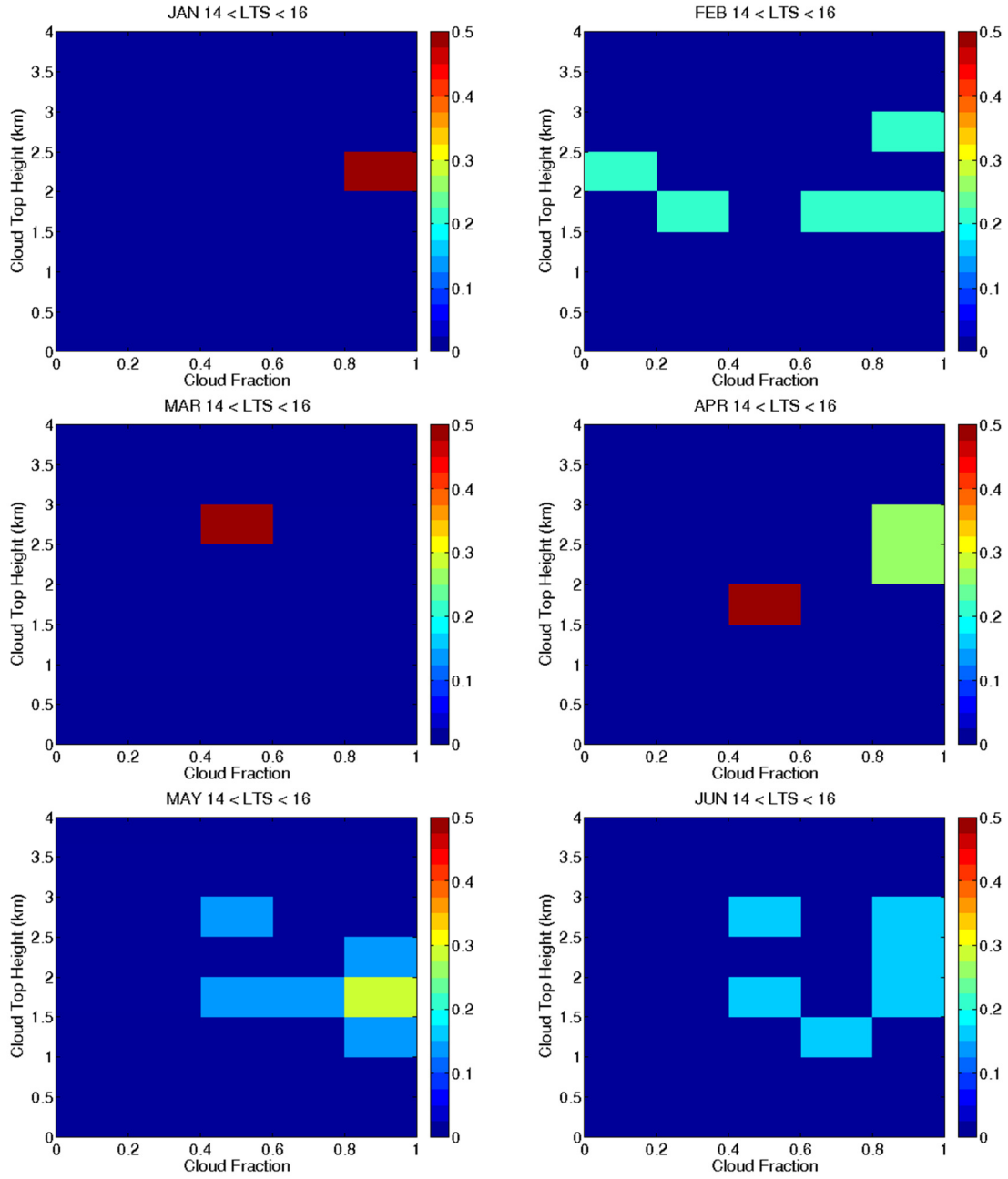

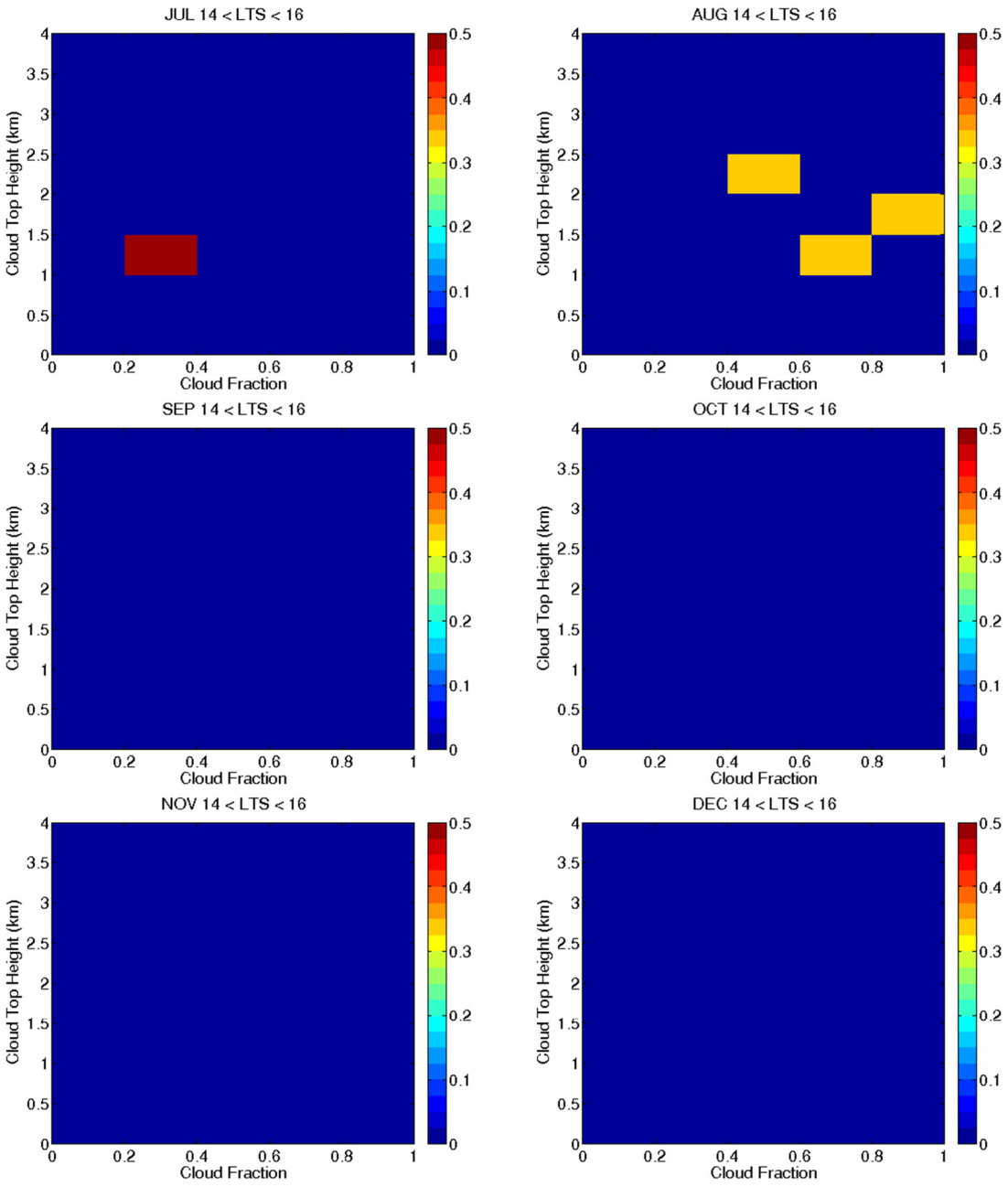
JUL 14 < LTS < 16
AUG 14 < LTS < 16
SEP 14 < LTS < 16
OCT 14 < LTS < 16
NOV 14 < LTS < 16
DEC 14 < LTS < 16
Cloud Top Height (km)
Cloud Fraction

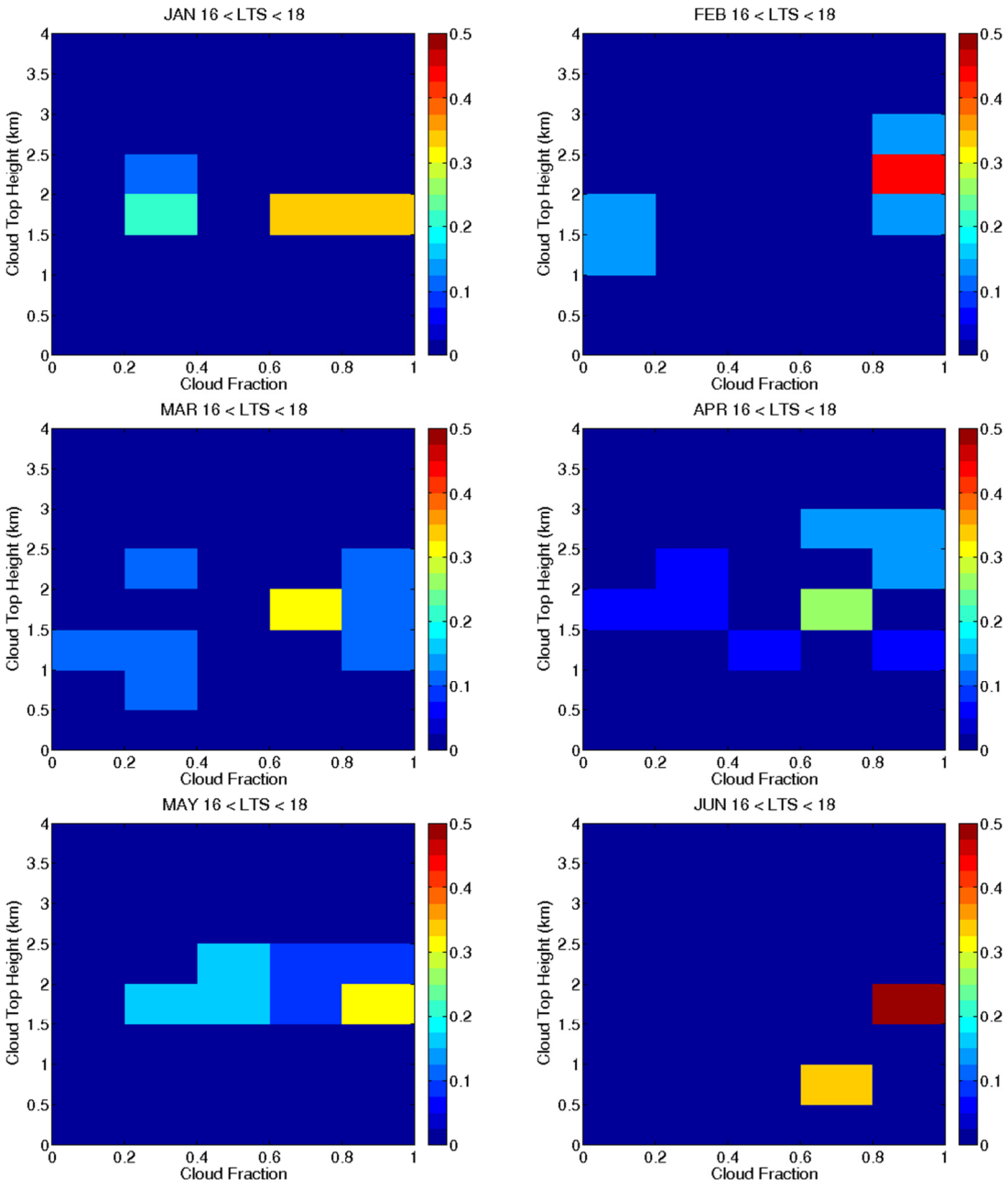
JAN 16 < LTS < 18
FEB 16 < LTS < 18
MAR 16 < LTS < 18
APR 16 < LTS < 18
MAY 16 < LTS < 18
JUN 16 < LTS < 18
Cloud Top Height (km)
Cloud Fraction
0
0.5
1
1.5
2
2.5
3
3.5
4
0.2
0.4
0.6
0.8
0.1
0.3

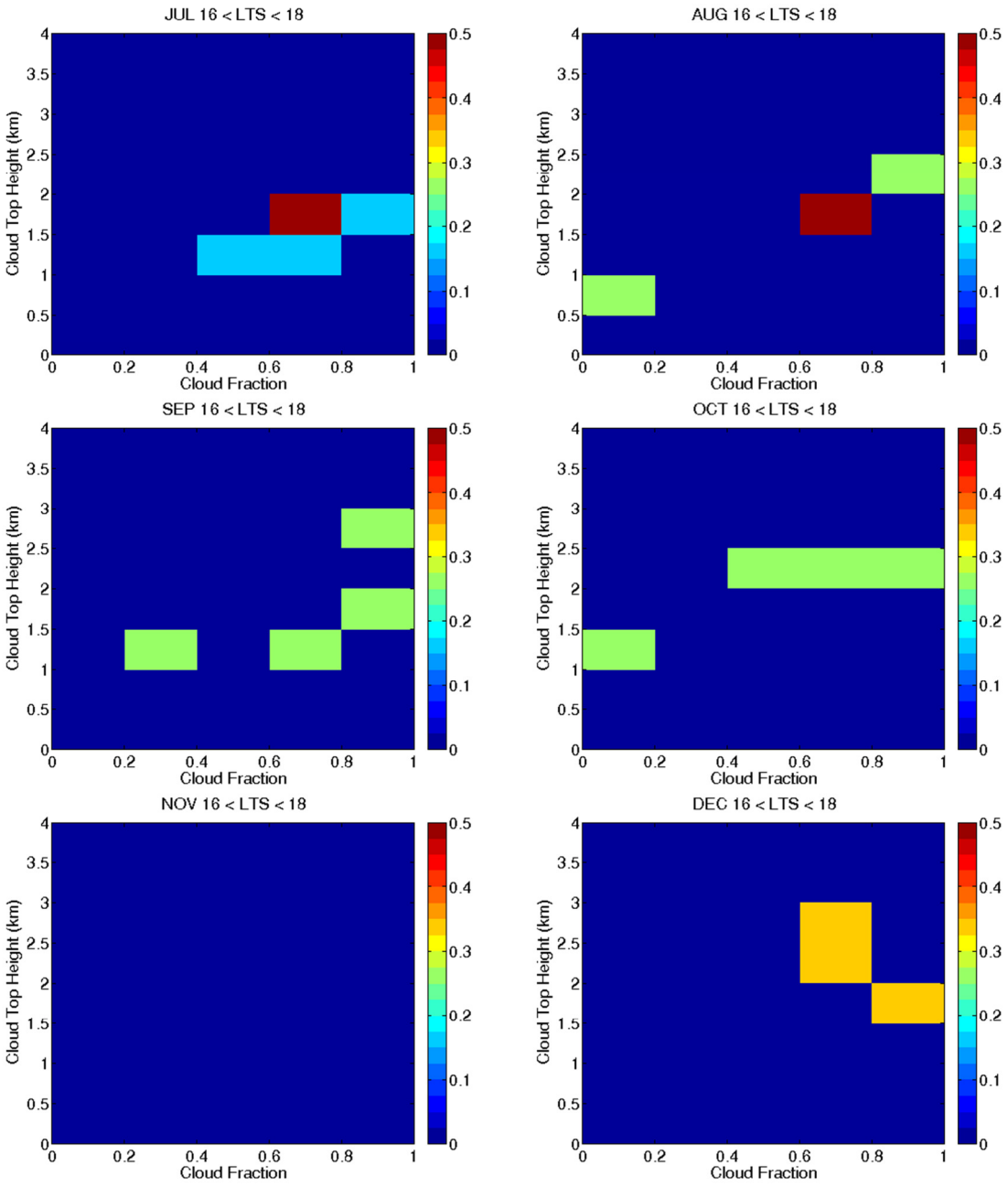
JUL 16 < LTS < 18
AUG 16 < LTS < 18
SEP 16 < LTS < 18
OCT 16 < LTS < 18
NOV 16 < LTS < 18
DEC 16 < LTS < 18
Cloud Top Height (km)
Cloud Fraction

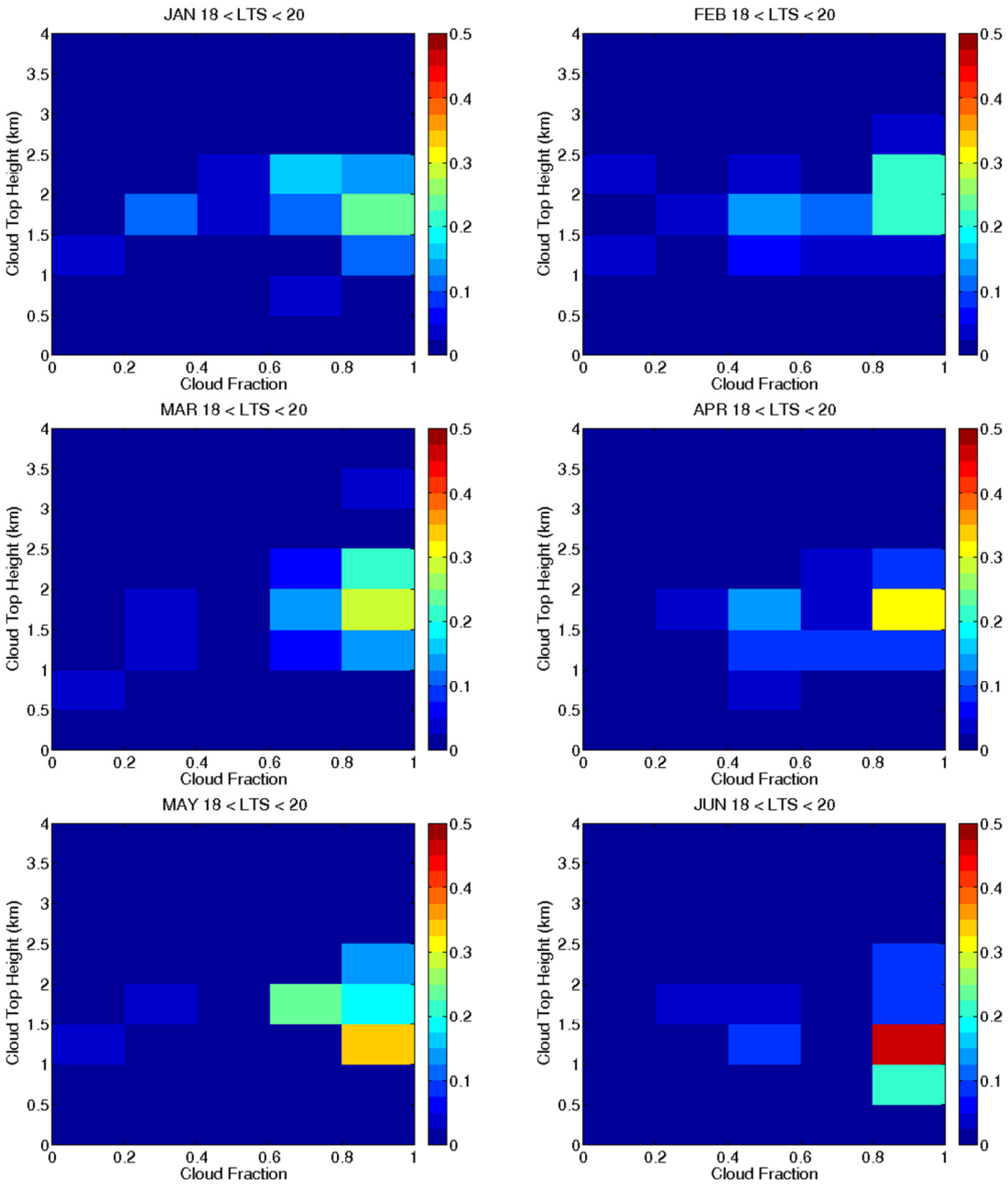
JAN 18 < LTS < 20
FEB 18 < LTS < 20
MAR 18 < LTS < 20
APR 18 < LTS < 20
MAY 18 < LTS < 20
JUN 18 < LTS < 20
Cloud Top Height (km)
Cloud Fraction

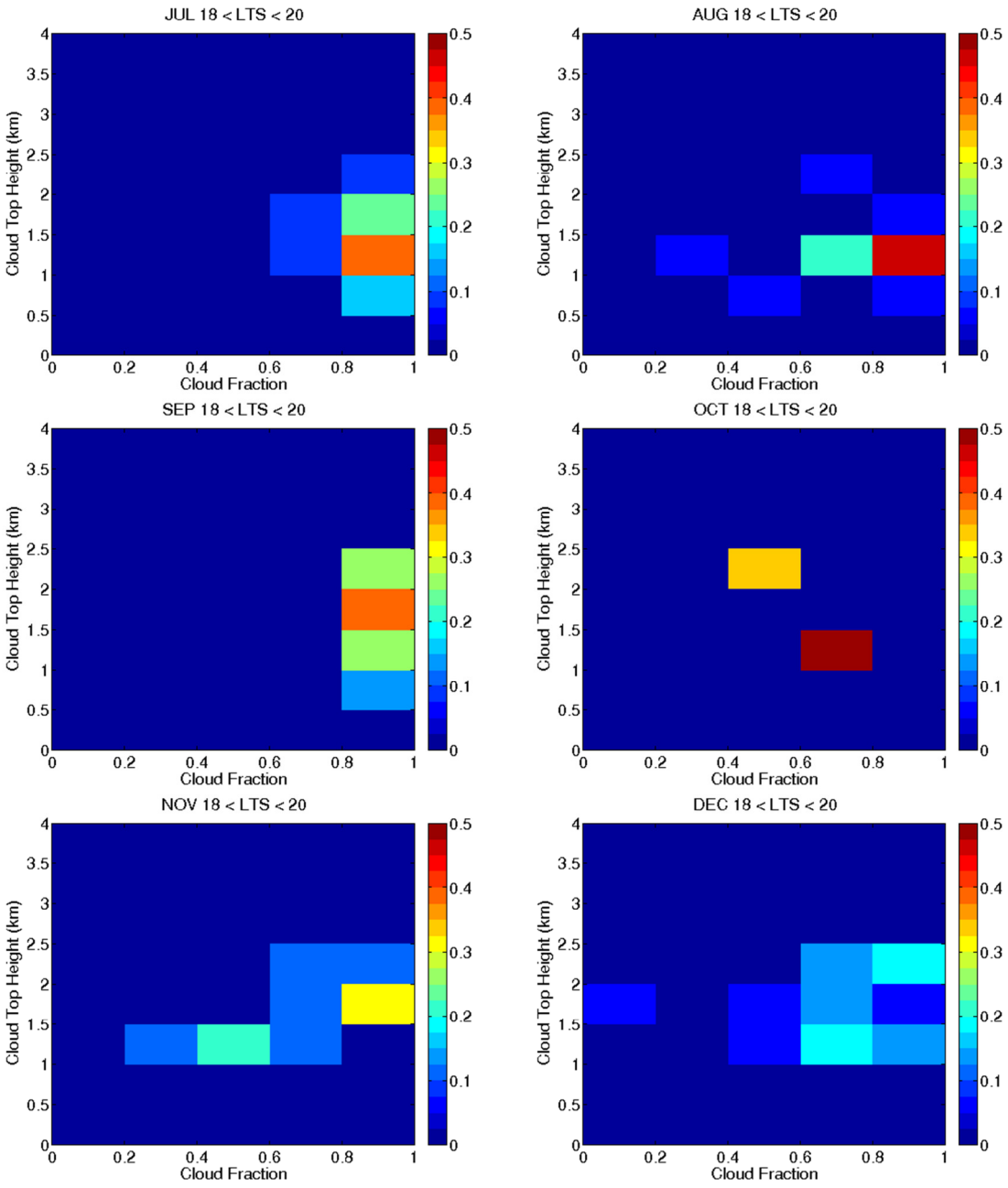
JUL 18 < LTS < 20
AUG 18 < LTS < 20
SEP 18 < LTS < 20
OCT 18 < LTS < 20
NOV 18 < LTS < 20
DEC 18 < LTS < 20
Cloud Top Height (km)
Cloud Fraction

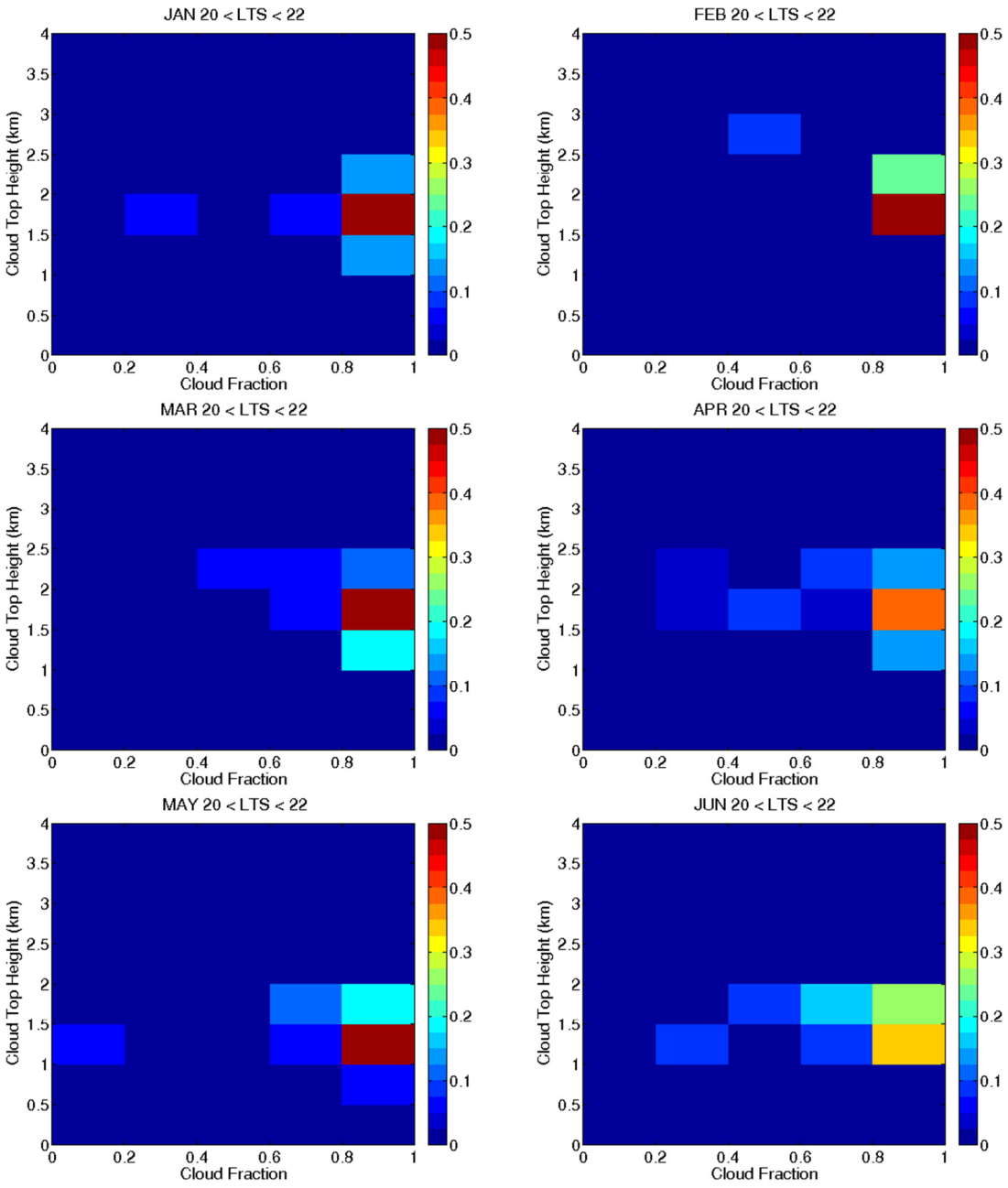
JAN 20 < LTS < 22
FEB 20 < LTS < 22
MAR 20 < LTS < 22
APR 20 < LTS < 22
MAY 20 < LTS < 22
JUN 20 < LTS < 22
Cloud Top Height (km)
Cloud Fraction
0
0.5
1
1.5
2
2.5
3
3.5
4
0.2
0.4
0.6
0.8
0.1
0.3

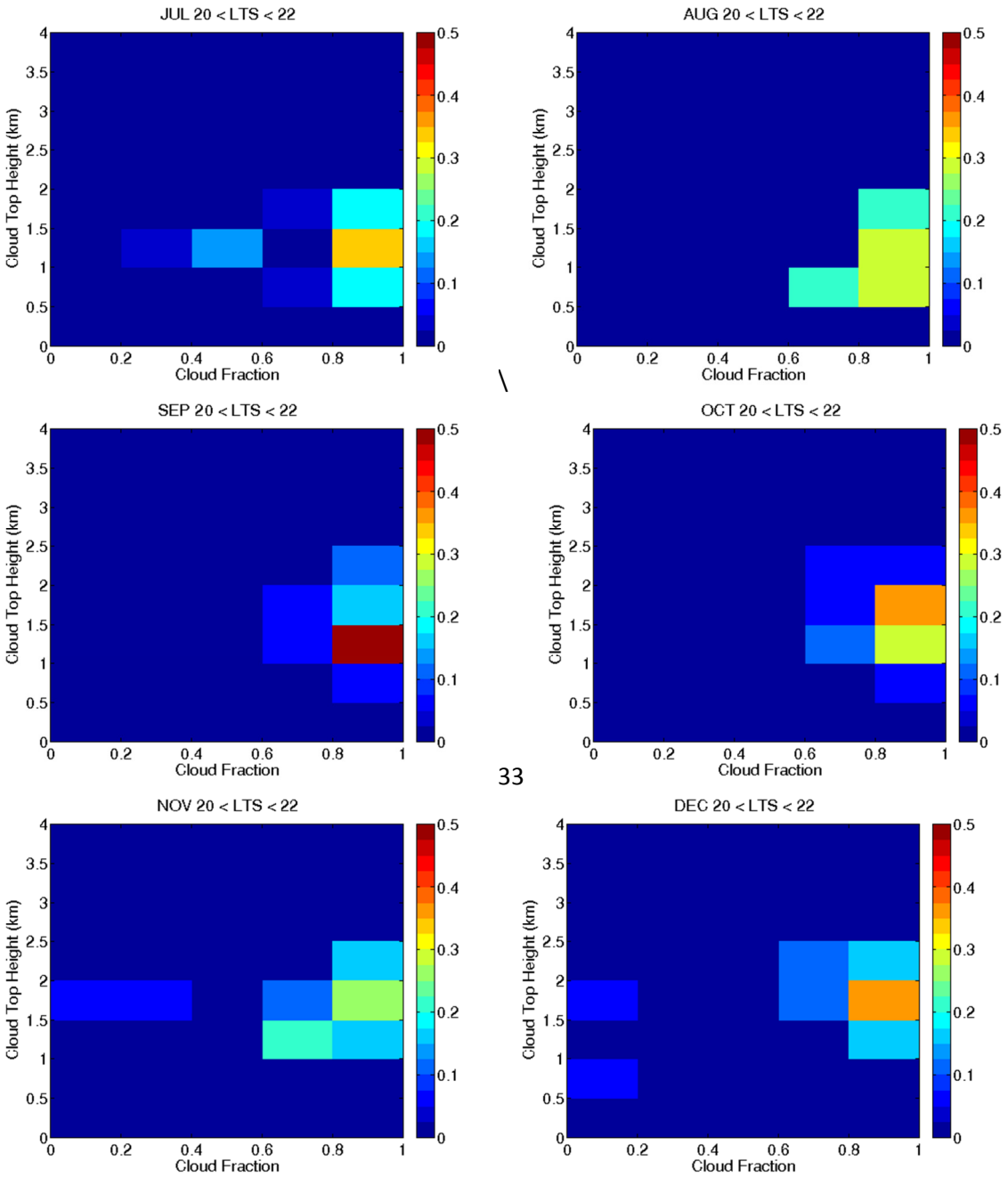
JUL 20 < LTS < 22
AUG 20 < LTS < 22
SEP 20 < LTS < 22
OCT 20 < LTS < 22
NOV 20 < LTS < 22
DEC 20 < LTS < 22
Cloud Top Height (km)
Cloud Fraction

\

33

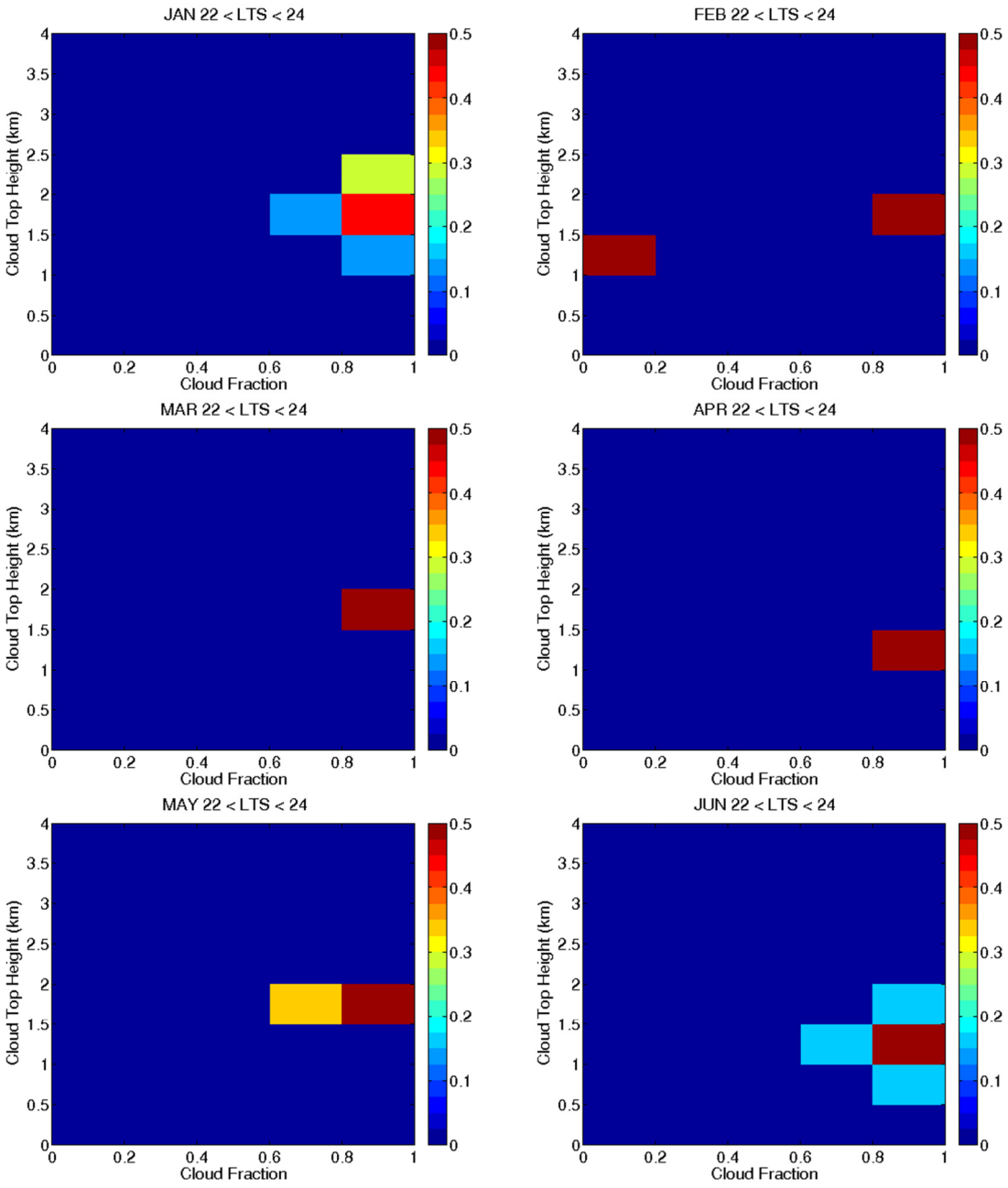
JAN 22 < LTS < 24
FEB 22 < LTS < 24
MAR 22 < LTS < 24
APR 22 < LTS < 24
MAY 22 < LTS < 24
JUN 22 < LTS < 24
Cloud Top Height (km)
Cloud Fraction

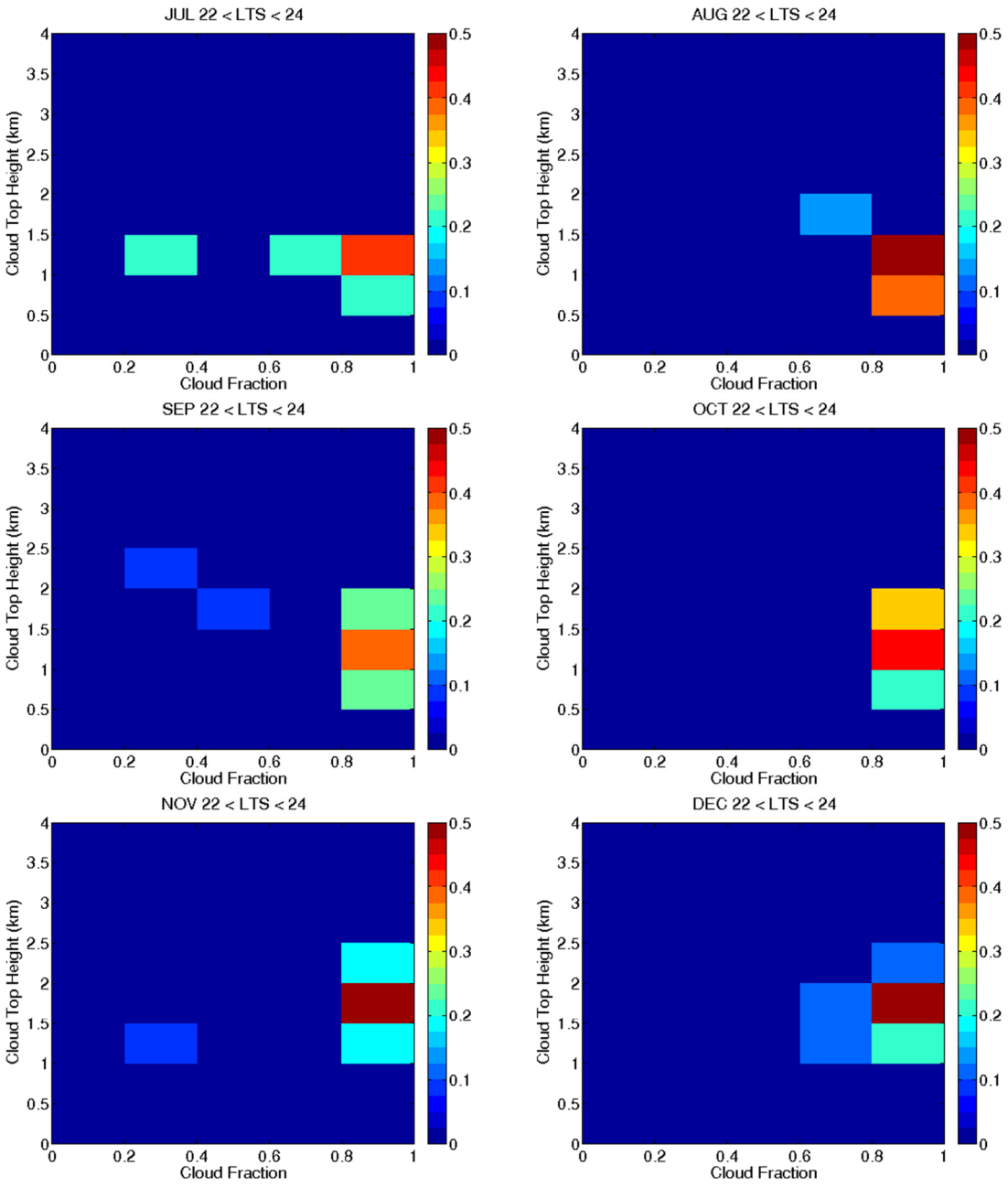
JUL 22 < LTS < 24
AUG 22 < LTS < 24
SEP 22 < LTS < 24
OCT 22 < LTS < 24
NOV 22 < LTS < 24
DEC 22 < LTS < 24
Cloud Top Height (km)
Cloud Fraction